

INTERFERENCE SUPPRESSION CAPABILITY OF FASTER THAN SYMBOL
RATE SAMPLING AND FREQUENCY DOMAIN OVERSAMPLING

A THESIS SUBMITTED TO
THE GRADUATE SCHOOL OF NATURAL AND APPLIED SCIENCES
OF
MIDDLE EAST TECHNICAL UNIVERSITY

BY

EREN BALEVI

IN PARTIAL FULFILLMENT OF THE REQUIREMENTS
FOR
THE DEGREE OF DOCTOR OF PHILOSOPHY
IN
ELECTRICAL AND ELECTRONICS ENGINEERING

JUNE 2016

Approval of the thesis:

**INTERFERENCE SUPPRESSION CAPABILITY OF FASTER THAN SYMBOL
RATE SAMPLING AND FREQUENCY DOMAIN OVERSAMPLING**

submitted by **EREN BALEVI** in partial fulfillment of the requirements for the degree
of **Doctor of Philosophy in Electrical and Electronics Engineering Department,**
Middle East Technical University by,

Prof. Dr. Gülbin Dural Ünver
Dean, Graduate School of **Natural and Applied Sciences**

Prof. Dr. Gönül Turhan Sayan
Head of Department, **Electrical and Electronics Engineering**

Prof. Dr. Ali Özgür Yılmaz
Supervisor, **Electrical and Electronics Engineering Dept.**

Examining Committee Members:

Prof. Dr. Çağatay Candan
Electrical and Electronics Engineering Dept., METU

Prof. Dr. Ali Özgür Yılmaz
Electrical and Electronics Engineering Dept., METU

Prof. Dr. Buyurman Baykal
Electrical and Electronics Engineering Dept., METU

Assoc. Prof. Dr. Sinan Gezici
Electrical and Electronics Engineering Dept., Bilkent Uni.

Assoc. Prof. Dr. Cenk Toker
Electrical and Electronics Engineering Dept, Hacettepe Uni.

Date:

I hereby declare that all information in this document has been obtained and presented in accordance with academic rules and ethical conduct. I also declare that, as required by these rules and conduct, I have fully cited and referenced all material and results that are not original to this work.

Name, Last Name: EREN BALEVI

Signature :

ABSTRACT

INTERFERENCE SUPPRESSION CAPABILITY OF FASTER THAN SYMBOL RATE SAMPLING AND FREQUENCY DOMAIN OVERSAMPLING

Balevi, Eren

Ph.D., Department of Electrical and Electronics Engineering

Supervisor : Prof. Dr. Ali Özgür Yılmaz

June 2016, 138 pages

Detection of symbols in the presence of many interference sources is a difficult task in wireless channels. It is obligatory to reduce the interference for reliable communication. In this dissertation, minimum mean square error (MMSE) detection is investigated to suppress interference. Faster Than Symbol Rate (FTSR) sampling and Frequency Domain Oversampling (FDO) methods are proposed to enhance the interference suppression level of MMSE detection for both single user and multiuser communication. The aim of single user communication is to mitigate Intersymbol Interference (ISI) by MMSE equalization with FTSR sampling or FDO, whereas ISI and Multiple Access Interference (MAI) are reduced jointly in multiuser communication by MMSE detector with FTSR sampling.

FTSR sampling is first investigated in single user communication for MMSE equalization when zeros are padded among transmission blocks. There is a performance degradation in equalization of ISI channels depending on practical conditions. In compatible with that, the performance of Zero Padding (ZP) based FTSR sampled MMSE equalization is analyzed accounting for practical channel conditions. Although FTSR sampling is generally considered as a remedy to time or phase errors, the results illustrate that the advantage of FTSR sampling on equalization is always present for a finite block length ISI channel even if perfect time information is available. Block length is the key parameter that affects the performance of FTSR sam-

pling such that there is a high Signal to Noise Ratio (SNR) improvement with smaller block lengths in comparison to the conventional Symbol Rate (SR) sampled MMSE equalization. Other parameters such as channel characteristics and excess bandwidth have influence on the performance of FTSR sampled MMSE equalization.

The concept of FTSR sampling is applied to the Cyclic Prefix (CP) based MMSE equalization as well. The performance of this equalizer is evaluated in regard to average mean square error (MSE) and bit error rate (BER). It is semi-analytically proven that FTSR sampling provides an improvement in average MSE for asynchronous communication. This motivates the fact that there is a potential gain that can be exploited by FTSR sampling for CP based MMSE equalization. In this thesis, the complexity increase due to FTSR sampling is compensated by proposing a low complexity CP based MMSE equalizer implementation. FTSR sampling exhibits superior performance for CP based MMSE equalization in the following two applications. The first one is to yield more tolerant MMSE equalization when CP is shorter than the maximum channel delay spread. The second one is to obtain a reasonable performance from 1-bit quantized MMSE equalizer for a single tap Rayleigh fading channel.

In multiuser communication, FTSR sampling is studied to exploit additional Degrees of Freedom (DoF) of excess bandwidth for the purpose of increasing simultaneous transmissions. The analysis reveals that FTSR sampling achieves extra rank proportional to any excess bandwidth being used provided that multipath channel taps are not equally spaced, which is a physical reality. The impact is further quantified by an FTSR sampled MMSE detector and a practical iterative receiver based on FTSR sampling. Spatial domain interpretation is employed as well to assess the effectiveness of FTSR sampling such that multiple receptions are considered as virtual antennas. The simulation results illustrate that interference can be greatly reduced by the FTSR sampled iterative receiver such that the number of users can be increased in a given network.

A counterpart of FTSR sampling method in frequency domain is the FDO, which is investigated to improve the error performance of MMSE Single Carrier Frequency Domain Equalization (SC-FDE) for multipath channels. The impact of FDO is analyzed in regard to the outage probability. The results show that FDO can significantly enhance the performance of MMSE SC-FDE when the ratio of block length to channel memory length is small such as in underwater acoustic channels. Its advantage is observed for moderate block length to channel memory length ratio in case of larger constellation sizes.

Keywords: Interference Mitigation, Faster Than Symbol Rate Sampling, Frequency Domain Oversampling, Linear MMSE Detector, ISI Channels

ÖZ

SEMBOL PERİYODUNDAN HIZLI ÖRNEKLEMENİN VE FREKANS ALANINDA YÜKSEK HIZDA ÖRNEKLEMENİN GİRİŞİM BASTIRMA KABİLİYETİ

Balevi, Eren

Doktora, Elektrik ve Elektronik Mühendisliği Bölümü

Tez Yöneticisi : Prof. Dr. Ali Özgür Yılmaz

Haziran 2016 , 138 sayfa

Sembollerin kablosuz kanallarda birçok girişim altında tespit edilmesi oldukça zor bir iştir. Güvenilir bir haberleşme için girişimin azaltılması zorunludur. Bu tezde girişimi bastırmak için MMSE algılayıcısı araştırılmaktadır. Sembol periyodundan hızlı örnekleme ve frekans alanında yüksek hızda örnekleme MMSE algılayıcısının girişim bastırma seviyesini iyileştirmek için tek ve çok kullanıcıli haberleşmede önerilen metotlardır. Tek kullanıcıli haberleşmede amaç sembol periyodundan hızlı örnekleme veya frekans alanında yüksek hızda örnekleme ile MMSE denkleştiricisinin semboller arası girişimi azaltmasıdır. Öbür taraftan çok kullanıcıli haberleşmede amaç sembol periyodundan hızlı örnekleme ile MMSE algılayıcısının semboller ve kullanıcılar arası girişimi azaltmasıdır.

Sembol periyodundan hızlı örnekleme ilk olarak tek kullanıcıli haberleşmede gönderilen bloklar arasına sıfırlar eklendiği durumda MMSE denkleştirici için araştırılmaktadır. Semboller arası girişim olan kanallar için uygulanan denkleştiricide pratik koşullara bağlı olarak performans bozulması olabilir. Buna uygun olarak, bloklar arasına sıfırlar eklenip sembol periyodundan hızlı örneklenen MMSE denkleştiricinin performansı pratik kanal koşullarına göre analiz edilmektedir. Sembol periyodundan hızlı örnekleme genellikle zaman veya faz hatalarına karşı kullanılmasına rağmen sonuçlar sembol periyodundan hızlı örneklemenin sonlu blok uzunluğundaki semboller

arası girişim olan bir kanalda ideal zaman bilgisinin olduğu durumda bile bir avantaj sunduğunu göstermektedir. Blok uzunluğu sembol periyodundan hızlı örnekleme performansını etkileyen en kritik parametredir. Öyle ki küçük blok uzunluklarında sembol periyodundan hızlı örnekleme MMSE denkleştirici klasik olarak kullanılan sembol periyodu ile örnekleme MMSE denkleştiriciden çok daha yüksek sinyal gürültü oranı sunmaktadır. Kanal karakteristiği ve ilave bant genişliği gibi bazı diğer parametrelerde sembol periyodundan hızlı örnekleme MMSE denkleştiricinin performansını etkilemektedir.

Sembol periyodundan hızlı örnekleme konsepti döngüsel öneke dayalı MMSE denkleştirici için de uygulanmaktadır. Bu denkleştiricinin performansı ortalama MSE ve bit hata oranı dikkate alınarak değerlendirilmektedir. Asenkron haberleşmede sembol periyodundan hızlı örnekleme ortalama MSE değerinde iyileşme sağladığı yarı-analitik olarak gösterilmektedir. Bu durum da döngüsel öneke dayalı MMSE denkleştirici için potansiyel bir kazanım olduğunu ve sembol periyodundan hızlı örneklemeyle kazanılabileceğini göstermektedir. Bu tezde sembol periyodundan hızlı örneklemeyle ilgili karmaşıklık artışını dengelemek için düşük karmaşıklıkla sahip döngüsel öneke dayalı bir MMSE denkleştirici uygulaması önerilmektedir. Sembol periyodundan hızlı örnekleme döngüsel öneke dayalı MMSE denkleştiricide aşağıdaki iki uygulama için üstün bir performans göstermektedir. Bunlardan ilki, sembol periyodundan hızlı örnekleme döngüsel öneke dayalı MMSE denkleştiricinin döngüsel önekin kanal maksimum gecikme dağılımından kısa olması durumuna karşı çok daha toleranslı olmasıdır. İkincisi, MMSE denkleştiricinin tek yönlü Rayleigh sönümlenmeli kanalda 1 bitlik nicelenmeyle kabul edilebilir bir performans sunmasıdır.

Çok kullanıcı haberleşmede sembol periyodundan hızlı örnekleme ilave bant genişliğinden gelen serbestlik derecesinden faydalanarak aynı anda gönderilen iletim sayısını artırmak amacıyla çalışılmaktadır. Analiz sembol periyodundan hızlı örnekleme tekniği ile fiziksel bir gerçek olan çok yönlü kanaldaki her bir yolun arasındaki mesafenin eşit olmamasına bağlı ilave bant genişliğiyle doğru orantılı olarak ek merite kazanıldığını göstermektedir. Bu etki sembol periyodundan hızlı örneklemeyle dayalı bir MMSE algılayıcı ve pratik bir yinelemeli alıcı için nicelenmektedir. Sembol periyodundan hızlı örnekleme verimliliğini değerlendirmek için uzaysal alan da kullanılmaktadır. Buna göre çoklu almalar sanal anten olarak düşünülmektedir. Simülasyon sonuçları sembol periyodundan hızlı örnekleme yinelemeli alıcının girişimi önemli ölçüde azaltabildiğini göstermektedir. Bu durum herhangi bir ağda kullanıcı sayısının artmasını sağlayabilir.

Sembol periyodundan hızlı örnekleme frekansdaki emsali frekans alanında yüksek hızda örnekleme. Frekans alanlı yüksek hızda örnekleme çok yönlü kanallarda tek taşıyıcı frekans alanlı MMSE denkleştiricinin hata performansını geliştirme amaçlı araştırılmaktadır. Frekans alanlı yüksek hızda örnekleme etkisi kesinti olasılığı göz önüne alınarak analiz edilmektedir. Sonuçlar frekans alanlı yüksek hızda örnekleme sualtı akustik kanallarında olduğu gibi blok uzunluğunun kanal hafıza uzunluğuna

göre düşük oranlı olduđu tek taşıyıcılı frekans alanlı MMSE denkleştiricide önemli miktarda bir iyileşme sağladığını göstermektedir. Bu tekniğin orta ölçekli blok uzunluğunun kanal hafıza uzunluğuna oranında da geniş alfabeler için avantaj sağladığı gözlemlenmektedir.

Anahtar Kelimeler: Girişim Bastırma, Sembol Periyodundan Hızlı Örnekleme, Frekans Alanında Yüksek Hızda Örnekleme, Lineer MMSE Algılayıcı, Semboller Arası Girişimli Kanallar

To the memory of my mother Necla Balevi,

ACKNOWLEDGMENTS

I would like to express my respect to my advisor, Prof. Dr. Ali Özgür Yılmaz for his continuous support. His encouragement always motivated me throughout the research.

I would like to thank Prof. Dr. Mehmet Şafak, Prof. Dr. Çağatay Candan and Assoc. Prof. Dr. Sinan Gezici for their advices and invaluable comments during my studies as Thesis committee. I would also like to thank Prof. Dr. Özgür Barış Akan who has taught me to never forget that success comes with persistence and hard work. It is a pleasure to acknowledge the kind interest and helpful discussions of Dr. Muzaffer Gökhan Güvensen.

I would like to thank ASELSAN Inc. for the facilities provided during my Ph.D. degree. I am also grateful to The Scientific and Technological Research Council of Turkey (TÜBİTAK) for its financial support to scientific research.

Finally, I would like to pay my sincere thanks to my family for their support, patience and faith to me in every aspect of life.

TABLE OF CONTENTS

ABSTRACT	v
ÖZ	vii
ACKNOWLEDGMENTS	xi
TABLE OF CONTENTS	xii
LIST OF TABLES	xvi
LIST OF FIGURES	xvii
LIST OF ABBREVIATIONS	xxi
CHAPTERS	
1 INTRODUCTION	1
1.1 Motivation	2
1.2 Related Works	3
1.2.1 Recent Studies in FTSR Sampling	3
1.2.2 Recent Studies in FDO	4
1.3 Overview of This Work	5
2 FUNDAMENTALS OF FASTER THAN SYMBOL RATE SAMPLING AND FREQUENCY DOMAIN OVERSAMPLING	9
2.1 FTSR Sampling Method	9

2.2	FDO Method	12
3	FASTER THAN SYMBOL RATE SAMPLING IN SINGLE USER COMMUNICATION: ZP BASED TRANSMISSION	15
3.1	ZP Based Transmission for FTSR Sampled MMSE Equal- ization	15
3.2	Time Domain Interpretation of FTSR Sampling	17
3.3	Frequency Domain Interpretation of FTSR Sampling	20
3.4	FTSR Sampling for ZP based MMSE Equalization	23
3.4.1	Time Domain Analysis	23
3.4.2	Frequency Domain Analysis	27
3.5	FTSR Sampled ZP Based MMSE Equalization: Equally Spaced Channel Taps	29
3.6	FTSR Sampled ZP Based MMSE Equalization: Unequally Spaced Channel Taps	33
3.7	Conclusions	37
4	FASTER THAN SYMBOL RATE SAMPLING IN SINGLE USER COMMUNICATION: CP BASED TRANSMISSION	39
4.1	CP Based Transmission for FTSR sampled MMSE Equal- ization	39
4.2	System Model for FTSR Sampled CP based MMSE Equal- ization	42
4.3	Analysis of FTSR Sampled CP Based MMSE Equalization	44
4.4	A Novel CP Based MMSE Equalization Implementation	52
4.5	CP Reduction	57
4.6	1-bit Quantization	62

4.7	Conclusions	64
5	FASTER THAN SYMBOL RATE SAMPLING IN MULTIUSER COMMUNICATION	67
5.1	Interference Mitigation in Multiuser Communication by FTSR Sampling	67
5.2	Analysis of FTSR Sampling in Multiuser Communication	69
5.2.1	DoF Analysis	70
5.2.2	Rank Analysis	72
5.2.3	Comparison with FTN Signaling	82
5.3	Applications of FTSR Sampling	83
5.3.1	FTSR Sampled MMSE Multiuser Detector	84
5.3.2	An Iterative Receiver Based on FTSR Sampling	89
5.4	Conclusions	96
6	FREQUENCY DOMAIN OVERSAMPLING	99
6.1	Frequency Domain Oversampled MMSE SC-FDE	99
6.2	System Model	101
6.3	Outage Analysis	102
6.3.1	Outage Probability Analysis with Lower Bounds	103
6.3.2	Direct Outage Probability Analysis	105
6.4	Simulations	108
6.5	Conclusions	115
7	CONCLUSIONS AND FUTURE WORKS	117

REFERENCES	121
APPENDICES	
A POTENTIAL OF EXCESS BANDWIDTH IN SINGLE USER COMMUNICATION	129
B MMSE FILTERING COMPARISON FOR TIME AND FREQUENCY DOMAIN	131
C CIRCULANT MATRIX INTERPRETATION OF \mathbf{H}_{ZP}	133
D AN ILLUSTRATIVE MATRIX EXAMPLE FOR OUTAGE PROBABILITY ANALYSIS	135
CURRICULUM VITAE	137

LIST OF TABLES

TABLES

Table 5.1	Example channels of both users	78
-----------	--	----

LIST OF FIGURES

FIGURES

Figure 2.1 SR sampling of the received signal	11
Figure 2.2 FTSR sampling of the received signal	11
Figure 2.3 General structure of an MMSE based detector	11
Figure 2.4 An illustration of FDO method on the DTFT of the received signal	13
Figure 2.5 FDO method in a general MMSE based detector	13
Figure 3.1 Conventional front-end model	18
Figure 3.2 Alternative front-end model	18
Figure 3.3 Allocated frequency band for a communication system	21
Figure 3.4 Low pass equivalent of a bandpass communication system	21
Figure 3.5 Spectrum of the sampled signal with sampling period of $T/2$	22
Figure 3.6 Spectrum of the sampled signal with sampling period of $T/(1+r)$	22
Figure 3.7 FTSR sampled ZP based MMSE equalization with pulse matched filtering	23
Figure 3.8 Discrete time representation of FTSR sampled ZP based MMSE equalization with pulse matched filtering	27
Figure 3.9 Spectrum of the MMSE equalized signal with sampling period of $T/2$	29
Figure 3.10 The comparison of FTSR and SR sampled MMSE equalization for a pulse shape without excess bandwidth	30
Figure 3.11 The impact of FTSR sampling for 10 equally spaced channel taps and a block length of 50	31

Figure 3.12 The impact of FTSR sampling for 10 equally spaced channel taps and a block length of 500	33
Figure 3.13 Excess bandwidth effect on FTSR sampled MMSE equalizer	34
Figure 3.14 The effect of FTSR sampling for 10 unequally spaced channel taps and a block length of 50	35
Figure 3.15 The effect of FTSR sampling for 10 unequally spaced channel taps and a block length of 500	35
Figure 3.16 The comparison of faster sampling rates for 10 unequally spaced channel taps and a block length of 500	36
Figure 4.1 FTSR sampled CP based MMSE equalization with pulse matched filtering	42
Figure 4.2 The performance of CP based MMSE equalization depending on sampling rate for 8 equally spaced channel taps and 30% excess bandwidth	46
Figure 4.3 The performance of CP based MMSE equalization depending on sampling rate for 8 unequally spaced channel taps and 30% excess bandwidth	48
Figure 4.4 The performance of CP based MMSE equalization depending on sampling rate for 8 unequally spaced channel taps without excess bandwidth	49
Figure 4.5 The impact of excess bandwidth for CP based MMSE equalization depending on sampling rate for 8 unequally spaced channel taps	50
Figure 4.6 Block length effect for CP based MMSE equalization depending on sampling rate for 8 unequally spaced channel taps	51
Figure 4.7 The performance of CP based MMSE equalization for different modulation formats depending on sampling rate for 8 unequally spaced channel taps	52
Figure 4.8 The error rate of the proposed FTSR sampled CP based MMSE equalization structure with complexity $O(N)$ for QPSK	55
Figure 4.9 The error rate of the proposed FTSR sampled CP based MMSE equalization structure with complexity $O(N)$ for 16-QAM	56
Figure 4.10 The error rate of the proposed FTSR sampled CP based MMSE equalization structure with complexity $O(N)$ for 64-QAM	56
Figure 4.11 The effect of 20% reduced CP on the FTSR and SR sampled MMSE equalization	61

Figure 4.12 The effect of 40% reduced CP on the FTSR and SR sampled MMSE equalization	61
Figure 4.13 The receiver model for 1-bit quantization	63
Figure 4.14 The performance of CP based MMSE equalization with 1-bit quantization for single tap Rayleigh fading channel	64
Figure 5.1 The cdf of FTSR sampled channel matrix rank for 10 equally spaced taps and 0.3 excess bandwidth for 2 users	77
Figure 5.2 The cdf of FTSR sampled channel matrix rank for 10 unequally spaced taps and 0.3 excess bandwidth for 2 users	80
Figure 5.3 The cdf of FTSR sampled channel matrix rank for 10 unequally spaced taps and 0.3 excess bandwidth for 5 users	81
Figure 5.4 The cdf of FTSR sampled channel's matrix rank for 10 unequally spaced taps and 0.3 excess bandwidth when the user's channels are identical	82
Figure 5.5 Conventional MMSE multiuser detector	84
Figure 5.6 Low complexity MMSE multiuser detector	84
Figure 5.7 Excess bandwidth effect on the FTSR sampled MMSE detector for 10 unequally spaced complex Gaussian channel taps	86
Figure 5.8 The effect of 10 equally spaced complex Gaussian channel taps on the FTSR sampled MMSE detector when roll off factor is 0.6	87
Figure 5.9 The effect of sampling rate for 10 unequally spaced complex Gaussian channel taps with a roll off factor 0.3 on the FTSR sampled MMSE detector	88
Figure 5.10 An iterative receiver based on FTSR sampling for multiple users	89
Figure 5.11 There are 2 transmitters and channel has 2 taps (a) Performance of the SR sampled iterative receiver (b) Performance of the FTSR sampled iterative receiver with $G = 2$	93
Figure 5.12 There are 2 transmitters and channel has 5 taps (a) Performance of the SR sampled iterative receiver (b) Performance of the FTSR sampled iterative receiver with $G = 2$	95
Figure 5.13 The performance of the FTSR sampled iterative receiver with $G = 3$ for 3 transmitters and a single receiver for 2 channel taps	96

Figure 6.1	The implementation of MMSE SC-FDE with ZP	101
Figure 6.2	The performance specification of padding zero mean unit variance i.i.d. Gaussian random variables instead of zeros for the implementation of SC-FDE	102
Figure 6.3	Outage probability comparison of SC-FDE for CP and ZP with FDO implementations	109
Figure 6.4	MMSE SC-FDE error performance for QPSK when the block length to channel memory length ratio is 5	110
Figure 6.5	MMSE SC-FDE error performance for QPSK when the block length to channel memory length ratio is 2	111
Figure 6.6	MMSE SC-FDE error performance for 16-QAM when the block length to channel memory length ratio is 5	112
Figure 6.7	MMSE SC-FDE error performance for 16-QAM when the block length to channel memory length ratio is 2	113
Figure 6.8	MMSE SC-FDE error performance for QPSK when the block length to channel memory length ratio is 5 and there are unequally spaced chan- nel taps	114
Figure 6.9	MMSE SC-FDE error performance for QPSK when the block length to channel memory length ratio is 2 and there are unequally spaced chan- nel taps	115

LIST OF ABBREVIATIONS

ADC	Analog-to-Digital Converter
AMOUR	A Mutually Orthogonal Usercode-Receiver
AWGN	Additive White Gaussian Noise
BER	Bit Error Rate
bpcu	bit per channel use
BPSK	Binary Phase Shift Keying
cdf	cumulative distribution function
CDMA	Code Division Multiple Access
CP	Cyclic Prefix
DFT	Discrete Fourier Transform
DTFT	Discrete Time Fourier Transform
DoF	Degrees of Freedom
FDO	Frequency Domain Oversampling
FIR	Finite Impulse Response
FSE	Fractionally Spaced Equalization
FTN	Faster Than Nyquist
FTSR	Faster Than Symbol Rate
IDFT	Inverse Discrete Fourier Transform
IBI	Interblock Interference
i.i.d.	independent and identically distributed
ISI	Intersymbol Interference
LTE	Long Term Evaluation
NBI	Narrowband Interference
MAI	Multiple Access Interference
MC	multicarrier
MIMO	Multiple Input Multiple Output
ML	Maximum Likelihood
MMSE	Minimum Mean Square Error

MSE	Mean Square Error
OFDM	Orthogonal Frequency Division Multiplexing
OQPSK	Offset Quadrature Phase Shift Keying
pdf	probability density function
QAM	Quadrature Amplitude Modulation
QPSK	Quadrature Phase Shift Keying
SC-FDE	Single Carrier Frequency Domain Equalization
SER	Symbol Error Rate
SINR	Signal to Interference plus Noise Ratio
SNR	Signal to Noise Ratio
SR	Symbol Rate
ZF	Zero Forcing
ZP	Zero Padding
3GPP	3 th Generation Partnership Project

CHAPTER 1

INTRODUCTION

Wireless channels have many interference sources. Among them, one symbol can interfere with subsequent symbols, which is called Intersymbol Interference (ISI). Indeed, ISI is one of the primary impediments in the channel limiting the system performance. There are many proposed methods to mitigate ISI including multicarrier (MC) modulation, spread spectrum and equalization. Another source of interference surfaces due to simultaneous transmission of multiple users denoted as Multiple Access Interference (MAI). Multiuser detectors, using multiple antennas, beamforming are some methods to suppress MAI. Moreover, a user can be exposed to an interference from users belonging to another network, which is called cochannel interference. There can be many reasons for cochannel interference, e.g., the users in neighboring cells can interfere with the intended signal in cellular communication.

Interference mitigation is a difficult problem. However, ensuring a reliable wireless communication is obligatory despite many types of interference sources and efficient techniques are highly needed. We seek an implementable low complexity approach for interference mitigation. At this point, minimum mean square error (MMSE) detection is utilized to alleviate the interference problem. MMSE based detection has been utilized in various fields, e.g., 3th Generation Partnership Project (3GPP), 802.11n, 802.16e, etc. Therefore, enhancing the performance of MMSE detection by additional operations is crucial and worth of studying, since it can affect many currently used communication systems. Preserving the incoming channel information into the discrete time signal is critical for MMSE detection. Within this scope, oversampling in time domain and its counterpart in frequency domain are investigated in

this dissertation to improve the interference suppression level of MMSE detection.

1.1 Motivation

The main aim in this thesis is to increase the interference mitigation level of MMSE detection which refers to the linear MMSE detection throughout the study. The optimum MMSE detection in nonlinear settings is out of the scope, because it requires the computation of conditional mean, and thus a joint probability density function (pdf) has to be found that contradicts the goal of reaching a low complexity interference suppression method. The classical MMSE detection model consists of adaptive analog filter due to channel matched filtering which matches to the signal in the channel and adaptive digital transversal filter stemming from MMSE filtering. The major challenge of this model is the difficulty of implementing adaptive analog filter. Analog filters require the calculation of values belonging to resistors, capacitors and inductors instead of filter coefficients in digital filters, therefore, modifying the values of these resistors, capacitors and inductors for varying conditions is not as easy as changing filter coefficients in digital filters. From this point of view, we prefer a model composed of non-adaptive analog filter and adaptive digital transversal filter for MMSE detection. Notice that implementation of adaptive digital filters is not so problematic unlike adaptive analog filters.

Symbol Rate (SR) sampling with channel matched filtering constitutes sufficient statistics for detecting the symbols despite excess bandwidth in which SR sampling remains below the Nyquist sampling rate [1], [2]. This condition is violated when pulse matched filtering, which matches to the transmitted pulse instead of the channel, is used instead of channel matched filtering. In particular, pulse matched filters are used in practical systems, because channel is not known at the time of chip fabrication, and hence the front-end filters are matched to the pulse instead of the channel. Therefore, it is worth to investigate faster sampling rates for pulse matched filtering in which SR sampling ensures neither the Nyquist sampling rate in case of excess bandwidth nor the sufficient statistics condition in [1], [2].

Our focus is primarily on frequency selective wireless channels implying wideband

communication throughout the thesis. Therefore, excess bandwidth refers to significant amount of bandwidth, however, it disappears in case of SR sampling due to aliasing. Faster Than Symbol Rate (FTSR) sampling is proposed to exploit the additional bandwidth for improving system performance as well as solving practical problems. In fact, the ultimate goal of FTSR sampling is to pack more than one user for a given bandwidth by taking the advantage of excess bandwidth.

A counterpart of FTSR sampling method in frequency domain is the Frequency Domain Oversampling (FDO). It is the other proposed method based on the motivation of obtaining more efficient interference suppression scheme from an MMSE detection. The rationale behind FDO is to exploit the available information in the channel more efficiently by appending zeros at the receiver.

1.2 Related Works

The methods of FTSR sampling and FDO are investigated for different purposes in the literature. We summarize these studies first with FTSR sampling in Section 1.2.1. Subsequently, the studies in the field of FDO are presented in Section 1.2.2.

1.2.1 Recent Studies in FTSR Sampling

Excess bandwidth leads to aliasing in the received signal in case of SR sampling. On the other hand, aliasing can be avoided by FTSR sampling. It is the main motivation of Fractionally Spaced Equalization (FSE), because any spectral null in the roll off portion of the signal due to timing errors can easily be compensated which can tolerate the timing errors more efficiently with respect to SR spaced equalization [1], [3], [4], [5], [6], [7]. In an analogous manner, it is shown in one digital receiver architecture that faster sampling rates do not have to synchronize with the transmitter clock [8]. The impact of FTSR sampling is studied for Cyclic Prefix (CP) based systems as well to better equalize the channel [9], [10], [11], [12]. More specifically, it is adopted to Single Carrier Frequency Domain Equalization (SC-FDE) to avoid aliasing in [13] and compensate the sampling time errors in [14], [15]. Moreover, FTSR sampling is implemented for SC-FDE in case of Offset Quadrature Phase Shift Keying (OQPSK)

modulation to enhance performance [16]. In addition to linear equalization, FTSR sampling is investigated for optimum Maximum Likelihood (ML) receiver in [17]. FTSR sampling can provide gains far beyond them such that [18] points out that the loss of multipath diversity in uncoded Orthogonal Frequency Division Multiplexing (OFDM) can be regained by FTSR sampling.

In case of multiuser communication, FTSR sampling is used to obtain more efficient performance from Code Division Multiple Access (CDMA) systems in [19], [20]. In particular, [20] suppresses the interference in CDMA systems by an MMSE detector such that the output of matched filter is oversampled at each symbol interval and processed by a finite impulse response (FIR) MMSE filter. Similarly, faster sampling rates improve the performance of asynchronous CDMA systems by suppressing the Narrowband Interference (NBI) and MAI in a frequency selective wireless channel [21], [22], [23]. MAI and ISI are successfully suppressed in a special receiver design called A Mutually Orthogonal Usercode-Receiver (AMOUR) proposed in [24]. Sampling the received signal with faster than transmission rate is studied to improve the AMOUR performance by [25].

1.2.2 Recent Studies in FDO

FDO is used against the carrier frequency offset problem analogous to time compensation behavior of FTSR sampling. Accordingly, a blind frequency offset recovery algorithm for OFDM systems is proposed based on FDO [26]. Furthermore, FDO is investigated to obtain better diversity gain from OFDM systems in [27], which projects the received signal into a higher dimensional signal space and filters the signal through a linear MMSE filter. [27] shows that the multipath diversity gain inherent in the channel is better exploited by the proposed method. [28] aims to increase the OFDM performance for underwater acoustic channel by FDO. Their results suggest that error rate heavily deteriorates the OFDM performance in direct relation with increasing Doppler spread, whereas the receiver with FDO is not affected much by the Doppler spread increase. In addition to compensating carrier frequency offset, obtaining better diversity gain and becoming more robust to Doppler spread, the FDO technique is utilized to suppress MAI in MC CDMA [29]. FDO is proposed for the

implementation of SC-FDE as well in [30]. More specifically, [30] implements the SC-FDE with Zero Padding (ZP) rather than CP and shows that FDO produces more accurate channel estimation and better error rate performance for SC-FDE. Furthermore, [31] proves the superiority of FDO for MMSE SC-FDE in terms of outage probability and quantifies the improvement in regard to transmission block length to channel memory length for different modulation formats.

1.3 Overview of This Work

The benefit of FTSR sampling is investigated beginning with single user frequency selective wireless channels resulting in Interblock Interference (IBI) and ISI. We firstly study the impact of FTSR sampling when zeros are padded among blocks to prevent IBI and MMSE equalization is employed for ISI suppression. In such a scenario, the performance of FTSR and SR sampled MMSE equalization are directly compared by taking into account the practical channel conditions and the impact of correlated noise stemming from the usage of pulse matched filtering and FTSR sampling. It is shown that the characteristics of channel taps, i.e., being equally spaced or unequally spaced play a crucial role in the performance of equalization. We observe that FTSR sampled MMSE equalization brings some gain even if there are no timing errors, i.e., channel taps are equally spaced and receiver sampling time is perfectly aligned relative to the symbol period contrary to widespread usage of FTSR sampling which is proposed for timing errors. One important loss in equalization stems from discarding the guard interval. Here, guard interval refers to ZP region at the end of each data block at transmitter. Indeed, it is obligatory to remove the guard interval for unequally spaced channel taps unless very large guard interval is used which is not desired due to spectral efficiency. FTSR sampling is proposed as a remedy to compensate the performance loss due to discarding the guard interval. Performance improvement limits depending on transmission block length, excess bandwidth and sampling rate are determined as well under this condition.

Secondly, FTSR sampled MMSE equalization is studied in case of appending CP among blocks at the transmitter instead of ZP. We derive an average mean square error (MSE) expression in terms of the eigenvalues of the channel and the noise auto-

correlation matrix and use this expression to compare the FTSR and SR sampled CP based MMSE equalization. Although CP prevents matrix inversion operation within MMSE equalization if it is implemented in frequency domain, FTSR sampling causes matrix inversion for equalization even if CP is employed. That's why, we propose a lower complexity equalization implementation to avoid the high complexity matrix inversion. Our results show that there is a significant gain for our proposed equalization structure based on FTSR sampling which is quite revolutionary for current communication systems. Furthermore, we indicate two superior behavior of FTSR sampling on CP based MMSE equalization. These are, more robust MMSE equalization once CP is shorter than the maximum channel delay spread and a reasonable performance when 1-bit Analog-to-Digital Converter (ADC) is employed at the receiver for single tap Rayleigh fading channels.

Lastly, FTSR sampling is investigated for multiuser communication with the ultimate aim of packing more than one user for a given bandwidth by exploiting excess bandwidth which can increase the total number of users in a network. At this point, it is proven that there is a gain in Degrees of Freedom (DoF) due to excess bandwidth which can be exploited by FTSR sampling. Following that, a rank analysis is given which directly indicates that rank can increase in direct proportion to excess bandwidth due to FTSR sampling once channel taps are unequally spaced which facilitates interference suppression. With the help of an iterative FTSR sampled MMSE multiuser receiver, the excess bandwidth advantage enables the separation of two users' signals from each other which share the same resources with different channels. This result implies that one can double the number of users in a TDMA or FDMA network.

Another important point of this thesis is to improve the interference suppression capability of MMSE equalization by FDO. Within this scope, we propose to implement MMSE SC-FDE by ZP at the transmitter and FDO at the receiver without appending CP. A quick advantage of this method is to prevent CP usage which brings power consumption saving. We will prove that the proposed implementation has better outage probability than the conventional one. Our results illustrate that FDO can considerably improve the performance of MMSE SC-FDE when the block length to channel memory length ratio is small. The benefit continues for moderate ratios of block length to channel memory length in case of modulation formats with larger constel-

lation sizes.

The thesis is organized as follows. Background information is provided for the proposed methods in Chapter 2. In Chapter 3 and 4, FTSR sampling is studied for single user communication for ZP based and CP based block transmission respectively. Then, FTSR sampling is generalized for multiuser communication in Chapter 5. Following that, FDO is employed to enhance the performance of MMSE SC-FDE in Chapter 6. The thesis is finalized with the concluding remarks and future research in Chapter 7.

CHAPTER 2

FUNDAMENTALS OF FASTER THAN SYMBOL RATE SAMPLING AND FREQUENCY DOMAIN OVERSAMPLING

The proposed FTSR sampling and FDO methods are discussed in detail in this chapter. MMSE detection is the main application of the proposed methods. More specifically, FTSR sampling and FDO are studied to enhance the interference suppression capability of MMSE detection. Within this scope, FTSR sampling is elaborated in Section 2.1 and FDO method is detailed in Section 2.2.

2.1 FTSR Sampling Method

Representation of a continuous time signal as a finite dimensional vector without any information loss is one of the crucial point in detection problem. The Nyquist sampling theorem can ensure information lossless transformation for bandlimited signals such that continuous time signals can be fully recovered from its samples provided that the Nyquist sampling rate is satisfied. One can argue that detection and reconstruction of the original signal from its samples are different processes and the Nyquist sampling rate may not be needed to make a perfect detection. At this point, the concept of sufficient statistics can be used to produce the sufficient information. To illustrate, SR sampling constitutes sufficient statistics when channel matched filtering is performed at the receiver despite the fact that SR sampling remains below the Nyquist sampling rate in case of excess bandwidth [1], [2]. However, this is an impractical special case that requires the full knowledge of the channel impulse response with the assumption of no synchronization error between transmitter and receiver.

In practice, pulse matched filtering is employed instead of channel matched filtering, and hence the general sufficient statistics condition is not valid including MMSE detection [1], [2]. Note that if there is not any sufficient statistics condition for one detection model, it will be mandatory to satisfy the Nyquist sampling rate to preserve all the incoming continuous time information. Since SR sampling remains below the Nyquist sampling rate when excess bandwidth exists, FTSR sampling seems as a necessity for this case. Notice that time domain support of transmitted signals is not infinite in practice referring that the received signals are not bandlimited and the Nyquist sampling rate criterion is no more valid to preserve the signal information. Although this fact does not have a considerable impact for fast decaying pulse shapes, it can affect slowly decaying pulse shapes. This further increases the interest to the FTSR sampling.

One outstanding property of FTSR sampling is to prevent aliasing in case of excess bandwidth. SR sampling leads to aliasing when pulse shape filter has excess bandwidth. More rigorously, assume that $r(t)$ is the received signal which is sampled at SR yielding

$$r_s(t) = r(t) \sum_k \delta(t - kT) \quad (2.1)$$

where $\delta(t)$ is the Dirac delta function and T is the sampling period. Eqn. (2.1) can be written in frequency domain as

$$R_s(f) = R(f) * 1/T \sum_k \delta(f - k/T) \quad (2.2)$$

where $R_s(f)$ and $R(f)$ are the Fourier transform of $r_s(t)$ and $r(t)$, and $*$ denotes linear convolution operator. Eqn. (2.2) is equivalent to

$$R_s(f) = 1/T \sum_k R(f - k/T). \quad (2.3)$$

An example plot corresponding to Eqn. (2.3) is drawn in Figure 2.1. As can be observed, SR sampling leads to aliasing in case of excess bandwidth which is denoted by r .

On the other hand, FTSR sampling produces

$$r_s(t) = r(t) \sum_k \delta(t - kT') \quad (2.4)$$

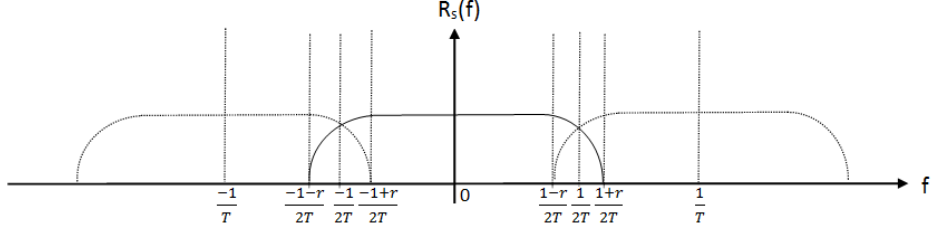


Figure 2.1: SR sampling of the received signal

in which $T' < T$. Eqn. (2.4) can be written in frequency domain as

$$R_s(f) = R(f) * 1/T' \sum_k \delta(f - k/T') \quad (2.5)$$

which yields

$$R_s(f) = 1/T' \sum_k R(f - k/T'). \quad (2.6)$$

Aliasing is avoided in FTSR sampling as given in Eqn. (2.6) if $T/T' > (1 + r)$ and illustrated in Figure 2.2 for $T' = T/2$.

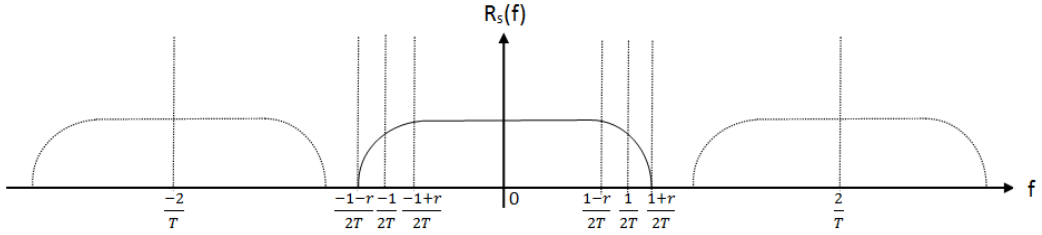


Figure 2.2: FTSR sampling of the received signal

Our aim is to use the benefit of FTSR sampling for MMSE detectors. Although the optimum detection rule is derived based on ML criterion [2], [32], [33], ML detection requires trellis based detection, and hence the algorithms devised for them necessitate exponential complexity that favors MMSE detection, which has relatively lower complexity with respect to ML detection. We investigate the effect of FTSR sampling in a canonical MMSE based detector given in Figure 2.3, which is mainly composed of a front-end filter prior to FTSR sampling and an MMSE detector.

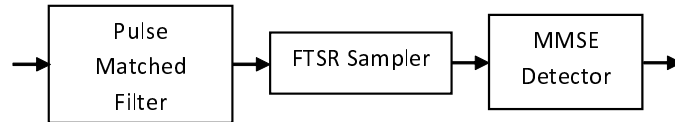


Figure 2.3: General structure of an MMSE based detector

Analog pulse matched filtering is chosen as the front-end filter instead of channel matched filtering due to the fact that it is rather difficult to implement a channel

matched filter, since it requires an adaptive analog filter. The main function of a pulse matched filter is to reduce the channel noise and suppress out of band interference. We adopt FTSR sampling following the pulse matched filter to satisfy the Nyquist sampling rate in case of excess bandwidth if the signal is bandlimited and to reduce the information loss as much as possible if the signal is not bandlimited or almost bandlimited. The basic principle of MMSE detector is to minimize the MSE between the actual and estimated symbols. MMSE detection has been comfortably implemented such that the estimation of the channel in addition to the first and second order statistics of the input and noise are sufficient. Moreover, MMSE detection is convenient to blind adaptation making the detector more important regarding practicality [34].

2.2 FDO Method

A counterpart method of FTSR sampling in frequency domain is the FDO. Although both methods have analogous purposes, their implementations are quite different. FDO is based on the method of ZP before taking Discrete Fourier Transform (DFT). Although ZP does not carry any information, it can prevent the potential information loss in the channel. A simple graph can better explain this idea, which is given in Figure 2.4. ZP before DFT corresponds to the taking closer samples from the Discrete Time Fourier Transform (DTFT) of the received signal, which is represented as $R(\Omega)$ in Figure 2.4. Then, it is more likely to sample the signal closer to its peaks and take more information from the channel by FDO.

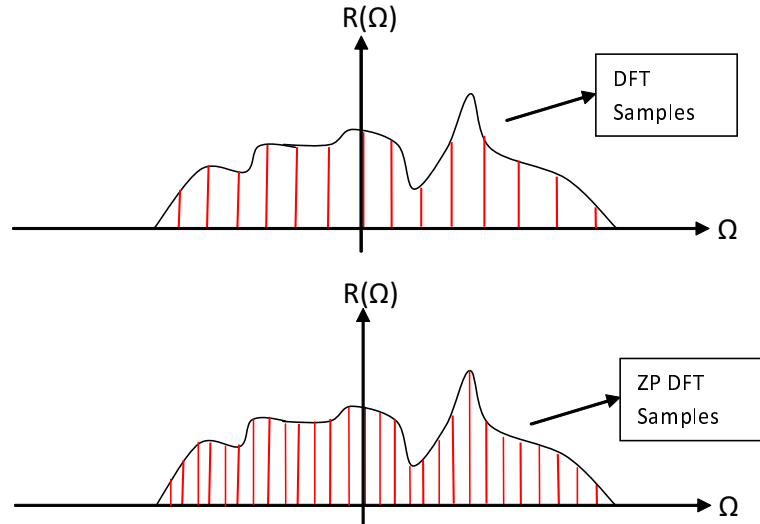


Figure 2.4: An illustration of FDO method on the DTFT of the received signal

FDO method is studied in a generic MMSE detector structure given in Figure 2.5. Accordingly, there is a pulse matched filter whose outputs are sampled at SR. Following that, zeros are inserted and DFT is performed before MMSE detector. Lastly, Inverse Discrete Fourier Transform (IDFT) takes place and decision is made from the processed samples.

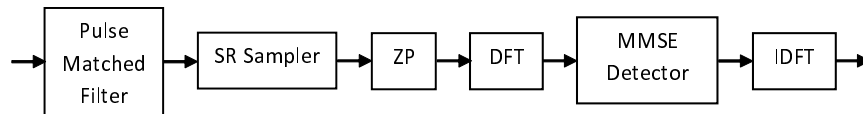


Figure 2.5: FDO method in a general MMSE based detector

The highlighted detector architecture in Figure 2.5 is studied for the sake of SC-FDE, which is one of the primary alternative to the OFDM systems. Notice that SC-FDE has superiority over OFDM systems regarding practical concerns and it is highly likely to be employed in practical communication systems. That's why, it is quite important to make any performance improvement in SC-FDE with FDO that can affect the reliability and efficiency of the communication among users.

CHAPTER 3

FASTER THAN SYMBOL RATE SAMPLING IN SINGLE USER COMMUNICATION: ZP BASED TRANSMISSION

SR sampling constitutes sufficient statistics when channel matched filtering is performed at the front-end of receiver and there is no sampling time errors even if excess bandwidth exists in which SR sampling remains below the Nyquist sampling rate. However, channel matched filters are highly undesirable in practical applications, since it requires an adaptive analog filter implementation. This refers to the fact that SR sampling may not be sufficient statistics when non-adaptive analog filter is preferred instead of channel matched filtering which emphasizes the importance of FTSR sampling. The main concepts of FTSR sampling are served in time and frequency domain in this chapter when linearly modulated symbols are transmitted as blocks over a single user frequency selective wireless channel resulting in both IBI and ISI. In this chapter, ZP occurs among blocks at the transmitter to prevent IBI and MMSE equalization is employed to eliminate ISI. Eventually, we observe the efficiency of FTSR sampling while mitigating ISI by MMSE equalization when zeros are padded among blocks at the transmitter and pulse matched filtering is used at the receiver.

3.1 ZP Based Transmission for FTSR Sampled MMSE Equalization

A channel matched filter whose output is sampled at SR captures all available information in the received continuous time signal and constitutes sufficient statistics when there is no sampling time errors [1], [2]. However, a channel matched filter must adapt to changing channel conditions which requires an analog adaptive filter

design that is highly undesirable for practical systems. Therefore, practical receivers avoid channel matched filtering and utilize a non-adaptive analog filter which matches to the transmitted pulse instead of the channel called pulse matched filter. Note that there is not any general theorem stating that SR sampling will also produce sufficient statistics for pulse matched filtering when excess bandwidth exists. That's why, it is worth to investigate FTSR sampling in detail in case of pulse matched filtering.

The inherent multipath propagation for single user frequency selective wireless channels leads to ISI. MMSE equalization is an appealing method to mitigate ISI due to their lower complexity and relatively good performance despite their non-optimality with respect to non-linear ML detection. In this chapter, MMSE equalization with faster sampling rates is investigated when high complexity channel matched filtering is replaced with low complexity pulse matched filtering. Recall that zeros are padded among blocks at the transmitter which is called guard interval to prevent IBI. This interval can be used to equalize the channel when ISI channel taps are synchronous or equally spaced with symbol period, since the channel samples at the guard interval do not interfere with the next block. On the other hand, guard interval cannot be utilized for asynchronous or unequally spaced ISI channel taps due to interference among blocks unless a very large guard interval is used involving the maximum channel delay spread and all the tails of pulse shape. It is critical to keep the number of padded zeros minimum for the sake of spectral efficiency.

In real life, multipath channel taps are unequally spaced such that each taps' propagation delay is randomly distributed between 0 and a maximum channel delay spread. When the length of guard interval is restricted to the maximum channel delay spread excluding the pulse shape length to obtain better transmission efficiency, interference surfaces within the guard interval between the multipath echos of the symbols in the end of a block and the precursors of pulse shape belonging to the symbols in the beginning of the next block. Eventually, MMSE equalization disregards the samples in the guard interval in case of unequally spaced channel taps, which is ordinarily a loss [35]. FTSR sampling can compensate this loss, because some energy of removed symbols can be taken with FTSR sampling coming from the tails of pulse shape.

Faster sampling rates for MMSE equalization have been studied under the concept

of FSE for a long time. The main focus of FSE has been restricted to timing error compensation such that existing FSE works did not analyze the sufficient statistics condition of SR sampling in terms of equally or unequally spaced channel taps and did not consider to compensate the performance loss in MMSE equalization stemming from not using the guard interval [1], [3], [4], [5], [6], [7]. Moreover, some of FSE studies consider larger front-end filter bandwidth than the transmitted signal prior to sampling or do not have any filter preceding FSE [1], [3], [4], [5], [6], [9]. We criticize these studies, since spectrum is highly crowded such that all frequency bands are assigned for different systems and it is not reasonable to employ a low pass filter with larger bandwidth that leads to cochannel interference and extra noise.

The contributions of this chapter are two-fold. Firstly, the concept of FTSR sampling is analyzed in time and frequency domain separately. Secondly, FTSR sampling is studied for the sake of MMSE equalization and proposed as a remedy to compensate the performance loss when pulse matched filtering is employed and guard interval is removed. Moreover, FTSR sampled MMSE equalization is quantified depending on the properties of channel taps, excess bandwidth and block length. We explicitly investigate the different faster sampling rates as well including a sampling rate which is 2 times of SR sampling exceeding the Nyquist sampling rate unless there is 100% excess bandwidth and the minimum one that equals the Nyquist sampling rate.

This chapter is organized as follows. Time and frequency domain interpretation of FTSR sampling are studied in Section 3.2 and Section 3.3 respectively. Our system model is given in Section 3.4. The analysis of FTSR sampled MMSE equalization in case of equally and unequally spaced channel taps are covered in Section 3.5 and Section 3.6 respectively. The chapter is finalized with concluding remarks in Section 3.7.

3.2 Time Domain Interpretation of FTSR Sampling

Conventional receiver front-end consists of a channel matched filter whose output is sampled at SR. A simple sketch is depicted in Figure 3.1. Herein, $p(t)$ is a real pulse shape without loss of generality, $c(t)$ is the channel, $w(t)$ is the additive noise,

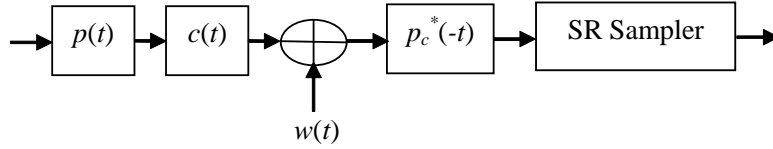


Figure 3.1: Conventional front-end model

$p_c(t) = p(t) * c(t)$ which is complex, because $c(t)$ is complex and $p_c^*(-t)$ is the channel matched filter so that $(.)^*$ represents conjugate operation. Note that causality does not affect the FTSR sampling analysis, therefore it is disregarded. Assuming that $r(t)$ is the received signal, $\{p_c^*(t - nT)\}$ is the finite set of square-integrable basis functions, and T is the symbol period, it is well known that $\langle r(t), p_c(t - nT) \rangle$ forms sufficient statistics [1], [2], where $\langle ., . \rangle$ represents inner product. Since channel matched filtering with SR sampling corresponds to the inner product of the received signal with $p_c(t - nT)$ such as

$$\langle r(t), p_c(t - nT) \rangle = r(t) * p_c^*(-t)|_{t=nT}, \quad (3.1)$$

channel matched filtering with SR sampling will also yield sufficient statistics. Eventually, SR sampled channel matched filter output provides sufficient statistics with the assumption of full channel knowledge at the receiver and the sampling time of receiver is perfectly aligned relative to the symbol interval. The primary difficulty of this structure is to implement adaptive analog filter due to channel matched filter $p_c^*(-t)$.

An alternative low complexity implementation of this front-end model is to replace the adaptive analog filter with a simple non-adaptive low pass filter. That is, utilize pulse matched filter $p(-t)$ instead of $p_c^*(-t)$ as illustrated in Figure 3.2. Then, it is

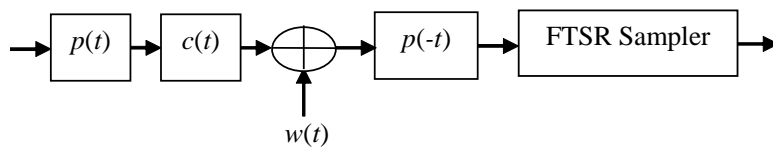


Figure 3.2: Alternative front-end model

questionable whether SR sampling becomes sufficient statistics or not in response to transmission of linearly modulated symbols over frequency selective wireless channels when excess bandwidth exists and is analyzed in more detail. Notice that SR sampling becomes sufficient statistics without excess bandwidth, since it has already satisfied the Nyquist sampling rate.

Assume that transmitted symbols x_n are independent and identically distributed (i.i.d.) and transmitted as blocks with block length N and zeros are padded at the end of each block to prevent IBI due to the frequency selective wireless channel. The transmitted signal for one block is equal to

$$s(t) = \sum_{n=0}^{N-1} x_n p(t - nT). \quad (3.2)$$

The frequency selective wireless channel leads to ISI which can be modeled as having $(L + 1)$ multipath components such that $(L + 1) < N$ and

$$c(t) = \sum_{k=0}^L \alpha_k \delta(t - \tau_k) \quad (3.3)$$

where α_k represents the complex Gaussian path coefficient and τ_k is the propagation delay belonging to the k^{th} path. The channel is taken to be static during each block, and changes independently among blocks [35]. The signal after passing through the channel is written as

$$r(t) = \sum_{n=0}^{N-1} x_n p_c(t - nT) + w(t) \quad (3.4)$$

where $p_c(t) = \sum_{k=0}^L \alpha_k p(t - \tau_k)$ and $w(t)$ is the circularly symmetric complex white Gaussian noise process with zero mean and power spectral density N_0 . A non-causal pulse matched filter $p(-t)$ is chosen to simplify discussion and applied to the received signal which leads to

$$y(t) = \sum_{n=0}^{N-1} x_n h(t - nT) + z(t) \quad (3.5)$$

where $h(t) = p(t) * c(t) * p(-t)$ and $z(t) = w(t) * p(-t)$.

Lemma 3.2.1 *Pulse matched filtering with SR sampling at $\{0, T, \dots, (N + L - 1)T\}$ constitutes sufficient statistics for estimating $\{x_n\}$ when ISI channel taps are equally spaced, i.e., $\tau_k = kT$ and excess bandwidth exists in case of ZP based block transmission.*

Proof 3.2.2 *The desired signal component can be written with the help of Eqn. (3.4)*

as

$$\begin{aligned}
d(t) = & x_0[\alpha_0 p(t) + \alpha_1 p(t - T) + \cdots + \alpha_L p(t - LT)] + \\
& x_1[\alpha_0 p(t - T) + \alpha_1 p(t - 2T) + \cdots + \alpha_L p(t - (L + 1)T)] + \\
& \vdots \\
& x_{N-1}[\alpha_0 p(t - (N - 1)T) + \alpha_1 p(t - NT) + \cdots + \alpha_L p(t - (N + L - 1)T)].
\end{aligned} \tag{3.6}$$

It is straightforward to express that $\{p(t - nT)\}$ for $n = 0, 1, \dots, (N + L - 1)$ constitute complete orthogonal basis for Eqn. (3.6). It is orthogonal due to the fact that symbols are sent orthogonally with transmitter filter $p(t)$ and it is complete basis, since every signal in Eqn. (3.6) can be spanned by $\{p(t - nT)\}$ for $n = 0, 1, \dots, (N + L - 1)$. Since orthogonal expansion of received signal with $\{p(t - nT)\}$ equals

$$\langle r(t), p(t - nT) \rangle = \int_{-\infty}^{\infty} r(t)p(t - nT)dt, n = 0, 1, \dots, (N + L - 1), \tag{3.7}$$

pulse matched filtering with SR sampling yields sufficient statistics.

Lemma 3.2.3 *Pulse matched filtering with SR sampling does not cover all the continuous time signal information when ISI channel taps are unequally spaced, i.e., $\tau_k \neq kT$ and excess bandwidth exists in case of ZP based block transmission.*

Proof 3.2.4 *When ISI channel taps are unequally spaced, the received signal cannot be written by using the orthogonal set $\{p(t - nT)\}$ for $n = 0, 1, \dots, (N + L - 1)$. This can be proved by a counter example. Assume that the k^{th} echo of n^{th} transmitted signal is shifted by $t_n \neq 0$ and it becomes $x_n \alpha_k p(t - nT - t_n)$ which cannot be written in terms of the linear combination of $\{p(t - nT)\}$. Therefore, it is clear that $\{p(t - nT)\}$ is not a complete orthogonal basis for unequally spaced ISI channel taps, and hence pulse matched filtering with SR sampling does not cover all the incoming information.*

3.3 Frequency Domain Interpretation of FTSSR Sampling

Many frequency bands are used by different systems making the spectrum crowded. Therefore, it is obligatory for one receiver front-end to filter only the given frequency

band to prevent cochannel interference due to neighboring systems on the spectrum and extra noise. Communication system design, i.e., the extent of excess bandwidth and data rate are determined in accordance with the pre-allocated frequency band. Notice that excess bandwidth has been employed in current communication systems, because implementing a pulse shaping filter without excess bandwidth is pretty difficult. Indeed, one of the primary intent of FTSR sampling is to exploit excess bandwidth which disappears in SR sampling due to aliasing, while FTSR sampling avoids aliasing and preserves additional bandwidth.

A simple sketch of communication system in frequency domain for root raised cosine transmitter filter and ideal channel is illustrated in Figure 3.3 with center frequency f_c and bandwidth W . Its low pass equivalent is given in Figure 3.4 as well. To

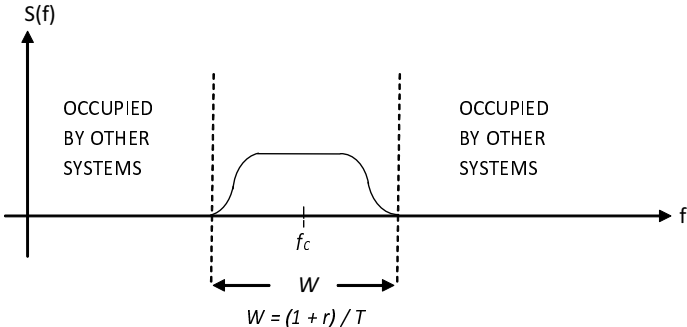


Figure 3.3: Allocated frequency band for a communication system

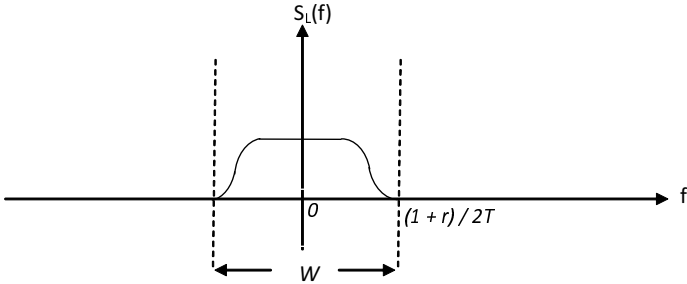


Figure 3.4: Low pass equivalent of a bandpass communication system

avoid cochannel interference and remove out of band noise, front-end filter must be designed according to

$$P(f) = \begin{cases} \text{nonzero}, & |f| \leq (1+r)/2T \\ 0, & \text{otherwise} \end{cases} \quad (3.8)$$

Pulse matched filter can be an appropriate choice for Eqn. (3.8). Following filtering, the signal has to be sampled at least at the Nyquist sampling rate to prevent information loss. There can be two alternatives for sampling rate selection that affects the received signal spectrum. One is simply doubling the SR sampling which yields a sampling period of $T/2$ and exceeds the Nyquist sampling rate unless 100% excess bandwidth exists or $r = 1$. The spectrum of sampled signal for this case is shown in Figure 3.5. Here, Ω represents the frequency for DTFT.

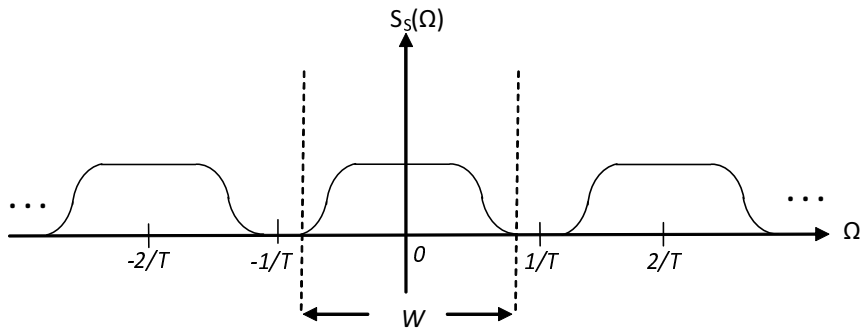


Figure 3.5: Spectrum of the sampled signal with sampling period of $T/2$

The other choice is to select a sampling rate whose period is $T/(1+r)$ which satisfies the Nyquist sampling rate exactly. This case is illustrated in Figure 3.6. Note that a sampling period of $T/2$ has been usually preferred for FTSR sampling in the literature [1].

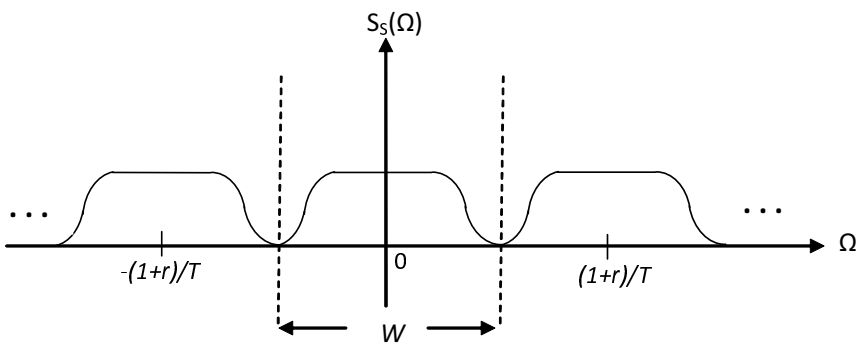


Figure 3.6: Spectrum of the sampled signal with sampling period of $T/(1+r)$

3.4 FTSR Sampling for ZP based MMSE Equalization

Frequency selective wireless channels result in IBI and ISI for a block transmission. We prevent IBI by ZP among blocks at the transmitter and ISI is removed by FTSR sampled MMSE equalization. In particular, the influence of FTSR sampling is studied for a single user receiver consisting of a pulse matched filter whose output is sampled by FTSR sampler and an MMSE equalizer as depicted in Figure 3.7. To prevent

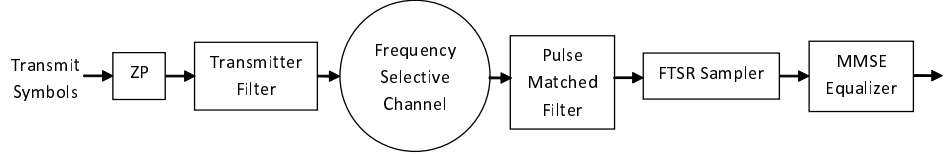


Figure 3.7: FTSR sampled ZP based MMSE equalization with pulse matched filtering

adaptive analog filtering, pulse matched filtering is chosen instead of channel matched filtering. Note that the front-end of this model is used to analyze FTSR sampling for maximal ratio combining receivers as well in [18].

3.4.1 Time Domain Analysis

Sampling a continuous time signal with a period of $T/(1+r)$ has not been preferred and usually $T/2$ has been employed as a sampling period in the literature [1]. Throughout the analysis, we prefer a sampling period of $T/2$ as well for ease of explanation such that sampling the Eqn. (3.5) and removing the guard interval produce the following vector-matrix representation

$$\mathbf{y}_{ftsr} = \mathbf{H}_{ftsr}\mathbf{x} + \mathbf{z}_{ftsr} \quad (3.9)$$

where $\mathbf{y}_{ftsr} = [y_0 \ y_1 \ \cdots \ y_{2N-1}]^T$ such that $y_n = y(nT/2)$ and $[\cdot]^T$ denotes transpose operation, \mathbf{H}_{ftsr} is a $2N \times N$ channel matrix, $\mathbf{x} = [x_0 \ x_1 \ \cdots \ x_{N-1}]^T$ and x_n is the n^{th} transmitted symbol, and $\mathbf{z}_{ftsr} = [z_0 \ z_1 \ \cdots \ z_{2N-1}]^T$ in which $z_n = z(nT/2)$.

Notice that

$$z(t) = \int_{-\infty}^{\infty} p(-\tau)w(t-\tau)d\tau \quad (3.10)$$

and the noise auto-correlation function becomes

$$E[z(t)z^*(t')] = E \left[\int_{-\infty}^{\infty} p(-\tau)w(t-\tau)d\tau \int_{-\infty}^{\infty} p(-\tau')w^*(t'-\tau')d\tau' \right] \quad (3.11)$$

where $E[.]$ denotes expectation and

$$E[z(t)z^*(t')] = \int_{-\infty}^{\infty} \int_{-\infty}^{\infty} p(-\tau)p(-\tau')E[w(t-\tau)w^*(t'-\tau')]d\tau d\tau' \quad (3.12)$$

which is equal to

$$E[z(t)z^*(t')] = \sigma^2 \int_{-\infty}^{\infty} p(-\tau)p(t-\tau-t')d\tau \quad (3.13)$$

where σ^2 is the variance of $z(t)$. Defining $\tilde{p}(t) = p(t) * p(-t)$ yields

$$E[z(t)z^*(t')] = \sigma^2 \tilde{p}(t-t') \quad (3.14)$$

such that pulse shape energy is normalized to one, i.e., $\tilde{p}(0) = 1$. Therefore, noise becomes correlated due to Eqn. (3.14) when sampling rate is $2/T$. In fact, noise becomes uncorrelated only if $t-t' = kT$ for integer k in case of pulses that obey the Nyquist criterion, otherwise the noise becomes correlated.

MMSE equalization requires the multiplication of Eqn. (3.9) with the following matrix

$$\mathbf{W}_{mmse} = \mathbf{H}_{f_{tsr}}^H (\mathbf{H}_{f_{tsr}} \mathbf{H}_{f_{tsr}}^H + \mathbf{R}_z)^{-1} \quad (3.15)$$

where $(.)^H$ is the Hermitian operation and \mathbf{R}_z is the $2N \times 2N$ noise auto-correlation matrix, which is equal to

$$\mathbf{R}_z = \sigma^2 \begin{pmatrix} \tilde{p}(0) & \tilde{p}(-T/2) & 0 & \tilde{p}(-3T/2) & \cdots & 0 & \cdots & 0 \\ \tilde{p}(T/2) & \tilde{p}(0) & \tilde{p}(-T/2) & 0 & \cdots & \cdots & \ddots & 0 \\ \vdots & \ddots & \ddots & \vdots & \vdots & \vdots & \vdots & 0 \\ \vdots & \vdots & \ddots & \ddots & \vdots & \vdots & \vdots & \vdots \\ \vdots & \vdots & \vdots & \ddots & \ddots & \vdots & \vdots & \vdots \\ 0 & \vdots & \vdots & \vdots & \ddots & \ddots & \vdots & \vdots \\ \vdots & \ddots & \vdots & \vdots & \vdots & \ddots & \ddots & \vdots \\ 0 & 0 & 0 & \cdots & \cdots & \cdots & \tilde{p}(T/2) & \tilde{p}(0) \end{pmatrix}.$$

Lemma 3.4.1 *The matrix $\mathbf{H}_{f_{tsr}} \mathbf{H}_{f_{tsr}}^H + \mathbf{R}_z$ is invertible.*

Proof 3.4.2 *Consider the raised cosine filter $\tilde{p}(t)$ which is equal to*

$$\tilde{p}(t) = \text{sinc}\left(\frac{t}{T}\right) \left(\frac{\cos\left(\frac{\pi r t}{T}\right)}{1 - \frac{4r^2 t^2}{T^2}} \right). \quad (3.16)$$

Note that the tails of $\tilde{p}(t)$ decays with $1/t^3$ for $r > 0$. Hence, the \mathbf{R}_z derived from a $2N$ length sequence $\tilde{\mathbf{p}} = [\tilde{p}_0 \tilde{p}_1 \cdots \tilde{p}_{2N-1}]$ with

$$\tilde{p}_n = \tilde{p}(t)|_{t=nT/2}, n = 0, 1, \dots, 2N - 1 \quad (3.17)$$

becomes

$$|\mathbf{R}_{z,ii}| > \sum_{i \neq j} |\mathbf{R}_{z,ij}|, i = 1, 2, \dots, 2N. \quad (3.18)$$

Eqn. (3.18) refers that \mathbf{R}_z is strictly diagonally dominant matrix. Since strictly diagonally dominant matrices are always invertible due to Gershgorin's theorem for finite matrix dimension [36], \mathbf{R}_z is invertible, and hence positive definite. On the other hand, it is clear that $\mathbf{H}_{ftsr} \mathbf{H}_{ftsr}^H$ is positive semidefinite. Then, defining

$$\mathbf{A} = \mathbf{H}_{ftsr} \mathbf{H}_{ftsr}^H \quad (3.19)$$

and

$$\mathbf{B} = \mathbf{R}_z, \quad (3.20)$$

$\mathbf{A} + \mathbf{B}$ is positive definite by definition, because multiplying both right and left hand side with a non-zero vector \mathbf{v} and its conjugate \mathbf{v}^* respectively yields

$$\mathbf{v}^*(\mathbf{A} + \mathbf{B})\mathbf{v} > 0 \quad (3.21)$$

relying on the fact that

$$\mathbf{v}^* \mathbf{A} \mathbf{v} \geq 0 \quad (3.22)$$

and

$$\mathbf{v}^* \mathbf{B} \mathbf{v} > 0. \quad (3.23)$$

As a result, $\mathbf{H}_{ftsr} \mathbf{H}_{ftsr}^H + \mathbf{R}_z$ is positive definite, and hence invertible, which completes the proof.

It can be inferred from Lemma 3.4.1 that a unique MSE solution exists for our MMSE equalization model. Note that although it is known from Toeplitz theory that a signal with a power spectral density $S(\Omega)$ has bounded eigenvalues for auto-correlation matrix such that [37]

$$\min_{0 \leq \omega \leq 2\pi} S(\Omega) < \lambda_k < \max_{0 \leq \omega \leq 2\pi} S(\Omega) \quad (3.24)$$

and when the dimension of auto-correlation matrix goes to infinity [37]

$$\lambda_{min} \rightarrow \min_{0 \leq \omega \leq 2\pi} S(\Omega), \quad (3.25)$$

$\mathbf{H}_{f_{tsr}} \mathbf{H}_{f_{tsr}}^H + \mathbf{R}_z$ is neither a Toeplitz matrix nor it has infinite dimension in our case. For the sake of completeness, we provide the following corollary.

Corollary 3.4.3 *Strictly diagonally dominant matrices are not always invertible for infinite N .*

Proof 3.4.4 *We prove this with a counter example. Consider a strictly diagonally dominant matrix \mathbf{R}_z in response to $\tilde{p}(t)$ when $N \rightarrow \infty$. Then, the continuous time Fourier transform of $\tilde{p}(t)$ sampled with a period of $T/2$ has null regions for $-1/T \leq \omega < -(1+r)/2T$ and $(1+r)/2T < \omega \leq 1/T$. This implies that the DTFT of infinite length sequence due to sampling of $\tilde{p}(t)$ which is denoted as $\tilde{P}(\Omega)$ has spectral nulls as well in between $[0, 2\pi]$. Since there are null roots on the unit circle, \mathbf{R}_z cannot be invertible which completes the proof.*

Corollary 3.4.3 implies that the studied MMSE equalization implementation has many MSE solutions for infinite length equalizer though all of them gives the same MSE value.

After MMSE filtering, the error matrix becomes

$$\mathbf{M} = E[(\mathbf{W}_{mmse} \mathbf{y}_{f_{tsr}} - \mathbf{x})(\mathbf{W}_{mmse} \mathbf{y}_{f_{tsr}} - \mathbf{x})^H] \quad (3.26)$$

which can be expressed as

$$\mathbf{M} = E[\mathbf{x}\mathbf{x}^H - \mathbf{W}_{mmse} \mathbf{y}_{f_{tsr}} \mathbf{x}^H - \mathbf{x} \mathbf{y}_{f_{tsr}}^H \mathbf{W}_{mmse}^H + \mathbf{W}_{mmse} \mathbf{y}_{f_{tsr}} \mathbf{y}_{f_{tsr}}^H \mathbf{W}_{mmse}^H]. \quad (3.27)$$

More simply,

$$\mathbf{M} = E[\mathbf{x}\mathbf{x}^H] - \mathbf{W}_{mmse} \mathbf{H}_{f_{tsr}} - \mathbf{H}_{f_{tsr}}^H \mathbf{W}_{mmse}^H + \mathbf{W}_{mmse} (\mathbf{H}_{f_{tsr}} \mathbf{H}_{f_{tsr}}^H + \mathbf{R}_z) \mathbf{W}_{mmse}^H. \quad (3.28)$$

When symbols energy are normalized to unity, the auto-correlation of i.i.d. symbols become

$$E[\mathbf{x}\mathbf{x}^H] = \mathbf{I}_N \quad (3.29)$$

with \mathbf{I}_N being the $N \times N$ identity matrix. Then,

$$\mathbf{M} = \mathbf{I}_N - \mathbf{H}_{f_{tsr}}^H (\mathbf{H}_{f_{tsr}} \mathbf{H}_{f_{tsr}}^H + \mathbf{R}_z)^{-1} \mathbf{H}_{f_{tsr}}. \quad (3.30)$$

From the trace of matrix \mathbf{M} , the average MSE value can be found as

$$MSE_{av} = \frac{tr\{\mathbf{M}\}}{N} \quad (3.31)$$

where $tr\{\cdot\}$ is the trace operation of a square matrix and average Signal to Interference plus Noise Ratio (SINR) becomes

$$SINR_{av} = \frac{1}{MSE_{av}} - 1. \quad (3.32)$$

3.4.2 Frequency Domain Analysis

Discrete time representation of Figure 3.7 for a sampling period of $T/2$ is presented in Figure 3.8 similar to the model given in [38] so that p_n , c_n , w_n , p_{-n} and ω_n are transmitter filter, channel, noise, receiver filter and coefficients of MMSE equalizer in discrete time respectively. Transmission blocks are upsampled with 2 and pass

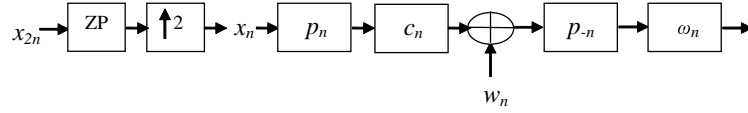


Figure 3.8: Discrete time representation of FTSR sampled ZP based MMSE equalization with pulse matched filtering

through the channel which can be modeled as a tapped delay line with a proper spacing among taps [39] such that the sufficient tap spacing is the one that satisfies the Nyquist sampling rate [7]. Therefore, the sufficient channel in discrete time can be derived as

$$c_n = c(t)|_{t=nT/2} \quad (3.33)$$

for $n = 0, 1, \dots, 2N - 1$. The filtered symbols at the receiver become

$$y_n = x_n * p_n * c_n * p_{-n} + w_n * p_{-n} \quad (3.34)$$

and can be shortly represented as

$$y_n = x_n * h_n + z_n. \quad (3.35)$$

MMSE equalizer coefficients ω_n can then be found by using

$$E[(x_n - \sum_{j=-\infty}^{\infty} \omega_j y_{n-j}) y_{n-l}^*] = 0, -\infty < l < \infty \quad (3.36)$$

which is equal to

$$E[x_n y_{n-l}^*] = \sum_{j=-\infty}^{\infty} \omega_j E[y_{n-l}^* y_{n-j}]. \quad (3.37)$$

Frequency domain representation of Eqn. (3.37) can be given as

$$F\{\omega_j\} = \frac{F\{E[x_n y_{n-l}^*]\}}{F\{E[y_{n-l}^* y_{n-j}]\}} \quad (3.38)$$

where $F\{\cdot\}$ denotes Fourier transform and Eqn. (3.38) can be written by considering i.i.d. transmitted symbols as

$$W(\Omega) = \frac{H^*(\Omega)}{|H(\Omega)|^2 + \sigma^2 |P(\Omega)|^2} \quad (3.39)$$

where $W(\Omega)$, $H(\Omega)$ and $P(\Omega)$ are DTFT of ω_n , h_n and p_n . Although Eqn. (3.39) is derived for infinite equalizer length, the same formula is obtained in case of finite equalizer length with the only exception that DTFT is replaced with DFT [38].

Equalizing the received signal results in

$$W(\Omega)Y(\Omega) = \frac{|H(\Omega)|^2}{|H(\Omega)|^2 + \sigma^2 |P(\Omega)|^2} X(\Omega) + W(\Omega)Z(\Omega) \quad (3.40)$$

where $X(\Omega)$, $Y(\Omega)$ and $Z(\Omega)$ are the DTFT of the input, output and noise respectively. This result is the counterpart of derivation in time domain analysis. Notice that MMSE matrix can be equivalently written in time domain as

$$\mathbf{W}_{mmse} = (\mathbf{H}_{ftsr}^H \mathbf{H}_{ftsr} + \mathbf{R}_z)^{-1} \mathbf{H}_{ftsr}^H \quad (3.41)$$

which results in

$$\mathbf{W}_{mmse} \mathbf{y}_{ftsr} = (\mathbf{H}_{ftsr}^H \mathbf{H}_{ftsr} + \mathbf{R}_z)^{-1} \mathbf{H}_{ftsr}^H \mathbf{H}_{ftsr} \mathbf{x} + \mathbf{W}_{mmse} \mathbf{z}_{ftsr}. \quad (3.42)$$

There are gaps in the spectrum before MMSE equalization due to using $p(-t)$ as a front-end filter and sampling the filtered signal with a period of $2/T$ as shown in Figure 3.5. However, Eqn. (3.39) is only applied to the bandwidth of interest, W . Moreover, these gaps do not constitute impediment, since they disappear at the output of MMSE equalization depending on the fact that decision is made with SR sampling. That is, the output samples of MMSE equalizer are T -spaced and have the following spectrum as in Figure 3.9 when ISI is perfectly eliminated.

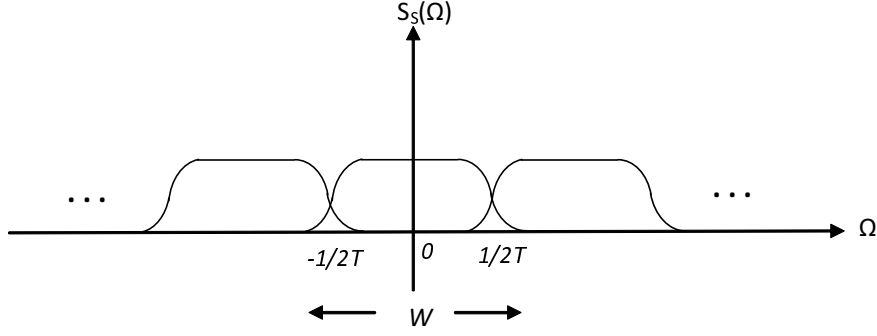


Figure 3.9: Spectrum of the MMSE equalized signal with sampling period of $T/2$

3.5 FTSR Sampled ZP Based MMSE Equalization: Equally Spaced Channel Taps

FTSR sampled ZP based MMSE equalization is firstly inspected when ISI channel taps are equally spaced with symbol period. The benefit of FTSR sampling is specified by finding the average SINR at the output of MMSE equalizer using Eqn. (3.32) for a sampling rate which is twice of SR and compare it with SR sampled MMSE equalization. In the comparisons, the same time interval is spanned by both equalizers, i.e., there are $2N$ equalizer taps with $T/2$ spacing for FTSR sampling and the number of T -spaced equalizer taps is N for SR sampling. It is assumed that there are 10 complex Gaussian channel taps which are equally spaced with symbol period T .

Although the time interval for transmission block length is NT , the observation interval at the receiver becomes $NT + GI$ where GI represents the guard interval for the maximum channel delay spread following transmission. We obtain the performance of MMSE equalization by disregarding the guard interval. The main rationale behind not using the guard interval stems from the fact that transmitted blocks interfere with each other due to FTSR sampling. The same problem occurs when channel taps are unequally spaced independent of sampling rate which is investigated in the subsequent section.

When the block length becomes 100, 500 and 1000 symbols in response to $\text{sinc}(t/T)$ pulse shape, the comparison of FTSR and SR sampled MMSE equalization is presented in Figure 3.10 where Signal to Noise Ratio (SNR) represents the channel SNR at the front of receiver and G represents FTSR to SR sampling ratio. It is impor-

tant to remind that $\text{sinc}(t/T)$ is a slowly decreasing function, and hence it can be completely represented for infinite block length, whereas finite block length leads to truncated $\text{sinc}(t/T)$ function. Therefore, the impact of $\text{sinc}(t/T)$ for MMSE equalization is evaluated when block length goes to infinity. It can be deduced from Figure 3.10 that FTSR sampled MMSE equalization coincides with the SR sampled one as block length goes to infinity and inferred that FTSR sampling is not advantageous for $\text{sinc}(t/T)$ as expected based on the Nyquist sampling theorem in which SR sampling satisfies the Nyquist sampling rate.

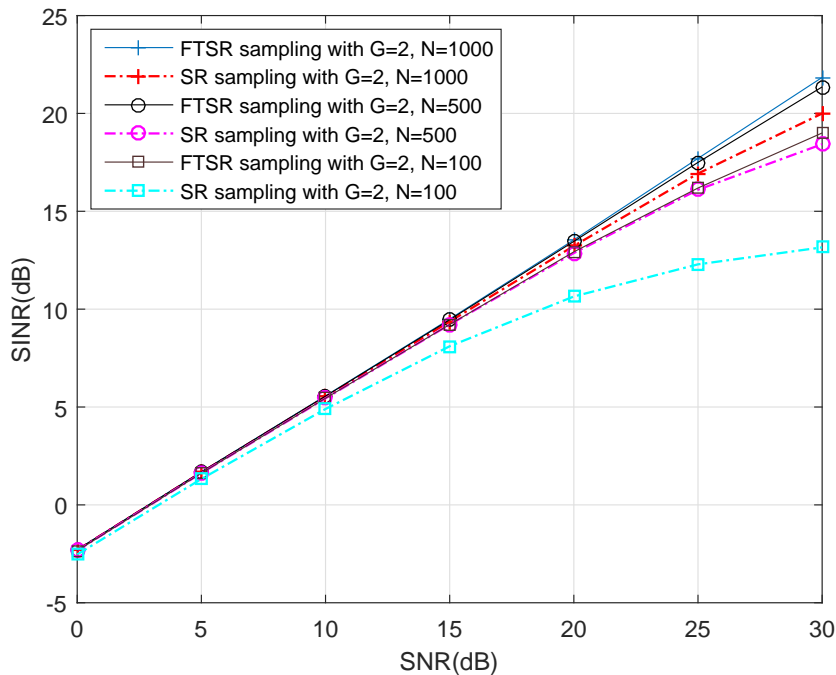


Figure 3.10: The comparison of FTSR and SR sampled MMSE equalization for a pulse shape without excess bandwidth

When 0.5 roll off factor raised cosine pulse shape is used instead of $\text{sinc}(t/T)$ function for a finite block length of 50, the superiority of the FTSR sampling for MMSE equalization is shown in Figure 3.11. This result suggests that the benefit of FTSR sampling continues even if perfect timing synchronization is available, which is rather different than the earlier results of FSE in which the MMSE equalizer performance is enhanced when timing errors are present.

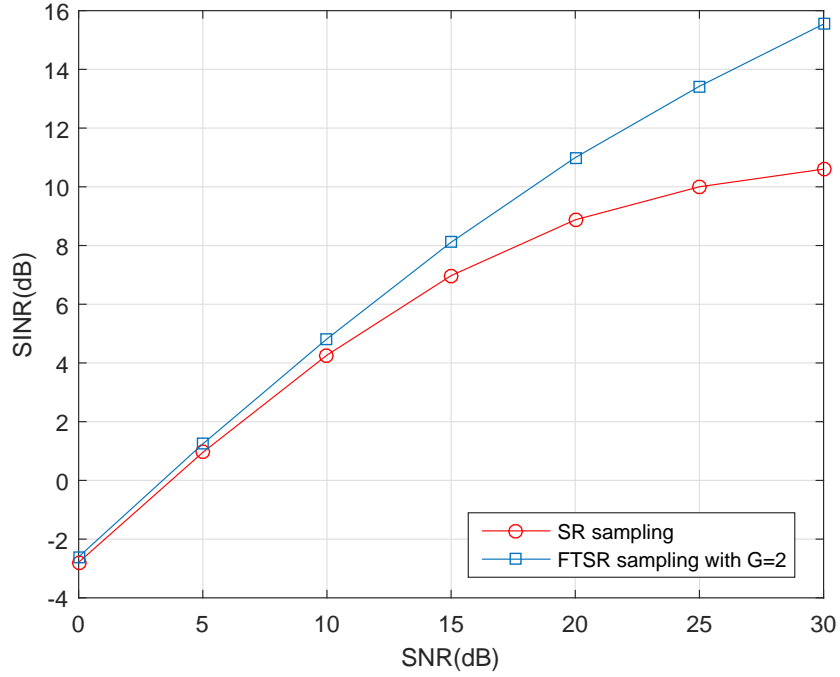


Figure 3.11: The impact of FTSR sampling for 10 equally spaced channel taps and a block length of 50

It is known that the smallest MSE value of an equalizer is obtained when block length goes to infinity. In particular, the smaller the block length is, the higher the MSE value is observed. In addition to smaller block length, further loss occurs when the guard interval is removed and not used for MMSE equalization. To illustrate, in a block transmission with $(L + 1)$ channel taps, all $(L + 1)$ echos of the symbols in the beginning of a block are observed in the length- N received sequence to be used in MMSE equalization. On the other hand, the number of echos used in MMSE equalization decreases more and more for the end of block and becomes 1 for the last symbol, because the guard interval is discarded. Since performance is averaged for all transmitted symbols in one block, this problem grows for smaller block lengths due to last symbols. FTSR sampling can be instrumental to compensate this loss. That is, in case of SR sampling, MMSE equalizer uses only one echo for the last symbol whose energy is

$$E_c = E_s |\alpha_0|^2 \quad (3.43)$$

where E_c is the symbol energy after passing through the channel and E_s is the symbol energy at transmitter. On the other hand, it uses all $(L + 1)$ echos of the last symbol though not with full energy due to FTSR sampling with sampling period $T/2$. The

energy due to extra samples is equal to

$$E_c = E_s \sum_{k=0}^L |\alpha_k \tilde{p}(kT + T/2)|^2. \quad (3.44)$$

As can be seen from Eqn. (3.44), the echos of the last symbol can be taken into account for MMSE equalization even if guard interval is discarded at the cost of some loss due to $\tilde{p}(\cdot)$ terms whose maximum value is attained for $\tilde{p}(0) = 1$. If all echos of a symbol are observed at $\tilde{p}(0)$, the energy will become

$$E_c = E_s \sum_{k=0}^L |\alpha_k|^2. \quad (3.45)$$

Although Eqn. (3.44) has degraded performance with respect to Eqn. (3.45), it has significant contribution considering Eqn. (3.43). In fact, FTSR sampling better accumulates the energy of a symbol such that total energy of the m^{th} symbol in one block for FTSR and SR sampling can be compared as

$$\sum_{k=0}^{N-1} |h(kT)|^2 < \sum_{k=0}^{2N-1} |h(kT/2)|^2. \quad (3.46)$$

These explanations are supported by an example such that the numerical result for a block length of 50 is repeated in case of a block length of 500. As can be shown in Figure 3.12, FTSR sampling brings less gain with respect to SR sampling for a block length of 50, though it has still a significant contribution to the MMSE equalization performance. As a result, the impact of removing the guard interval at the receiver and the advantage of FTSR sampling decrease with incremental block length.

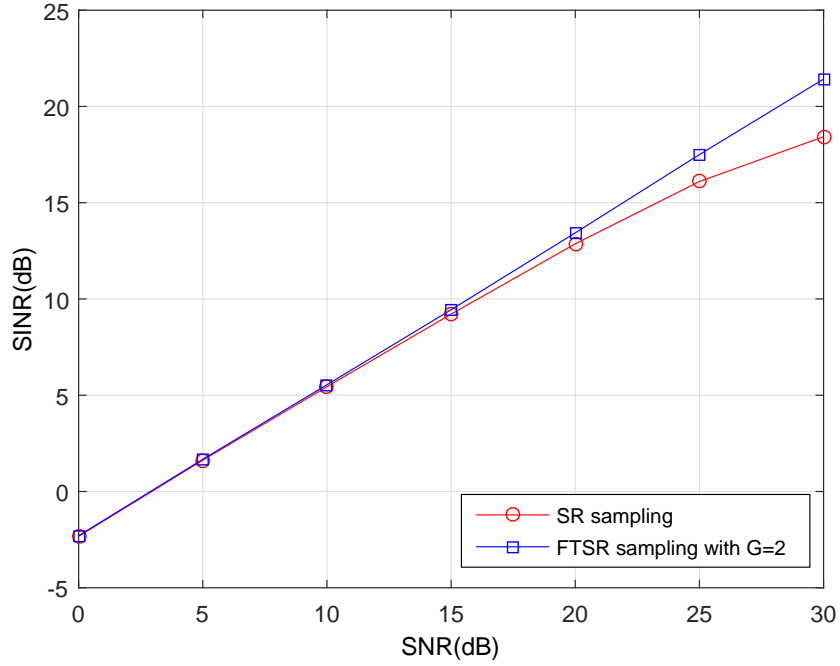


Figure 3.12: The impact of FTSR sampling for 10 equally spaced channel taps and a block length of 500

3.6 FTSR Sampled ZP Based MMSE Equalization: Unequally Spaced Channel Taps

Practical channels have unequally spaced channel taps whose propagation delays are randomly distributed in between 0 and a maximum channel delay spread. We investigate the impact of FTSR sampling for MMSE equalization when channel taps are unequally spaced in terms of pulse shape and block length. For this case, 2 different sampling rates are studied including a sampling rate of $2/T$ which exceeds the Nyquist sampling rate unless $r = 1$ and $(1 + r)/T$ sampling rate which equals the Nyquist sampling rate. It is assumed that there are 10 unequally spaced complex Gaussian taps whose propagation delays are uniformly distributed in $[0, 20T]$. Only the NT portion of $NT + GI$ observation interval is used for each block in MMSE equalization due to IBI stemming from unequally spaced channel taps.

Firstly, the effect of excess bandwidth on FTSR sampled MMSE equalization is studied for a block length of 500 and $G = 2$. Figure 3.13 presents the results for various roll off factors. As can be observed, the extent of roll off factor affects the FTSR sampled MMSE equalizer performance. In this manner, the potential of excess bandwidth

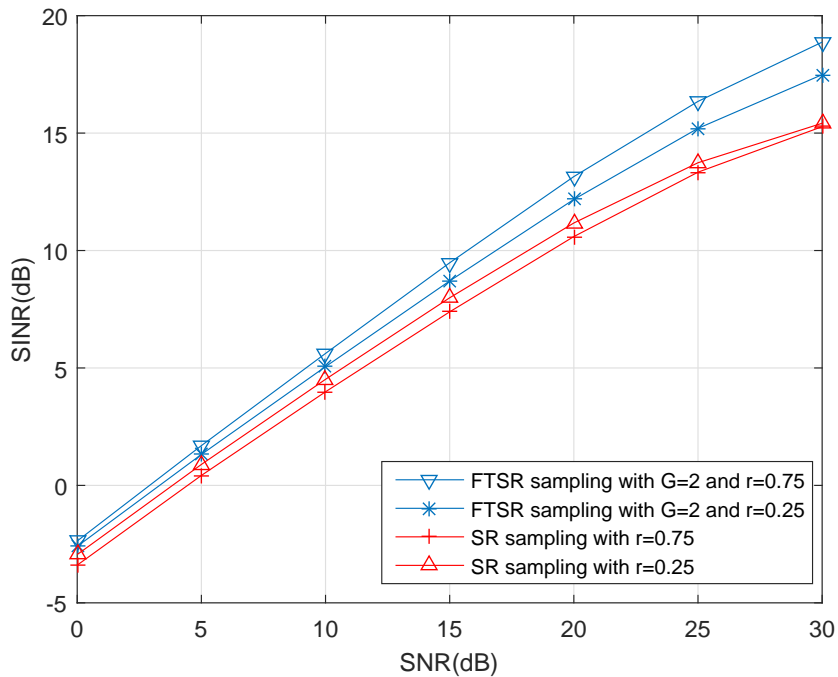


Figure 3.13: Excess bandwidth effect on FTSR sampled MMSE equalizer

is presented in Appendix A which shows that the capacity linearly increases with excess bandwidth when SNR goes to infinity. Furthermore, there is a little performance degradation with incremental excess bandwidth for SR sampling. The rationale behind that is to increase the level of aliasing in the signal due to excess bandwidth as stated in [15].

Secondly, it is analyzed how block length affects the benefit of FTSR sampling for MMSE equalization in response to unequally spaced channel taps. The effect of block length that is discussed for equally spaced channel taps is valid for unequally spaced channel taps as well. However, it is possible to use guard interval in case of equally spaced channel taps once sampling is performed at SR. On the other hand, there always exists interference at the guard interval irrespective of sampling rate for unequally spaced channel taps and this guard interval cannot be used. To observe the effect of block length for FTSR sampled MMSE equalization with $G = 2$, block length is firstly chosen 50 with 0.5 roll off factor raised cosine pulse shape. The SINR advantage of FTSR sampling is given in Figure 3.14. When the block length is increased from 50 to 500, the SINR advantage disappears to some extent as shown in Figure 3.15. Although larger block length enhances the MMSE equalizer performance and the curves in Figure 3.15 reveal higher SINR values than those of Figure

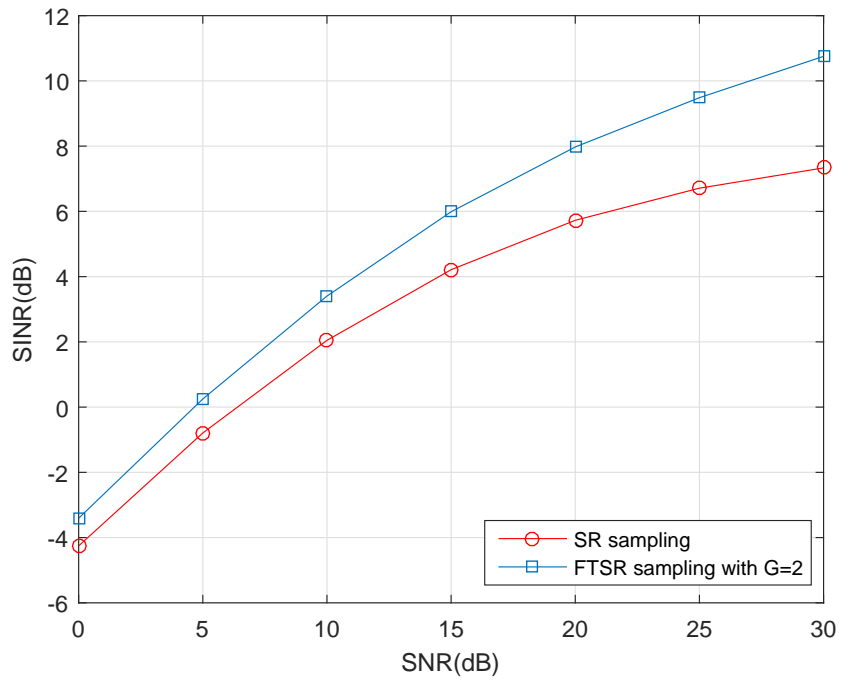


Figure 3.14: The effect of FTSR sampling for 10 unequally spaced channel taps and a block length of 50

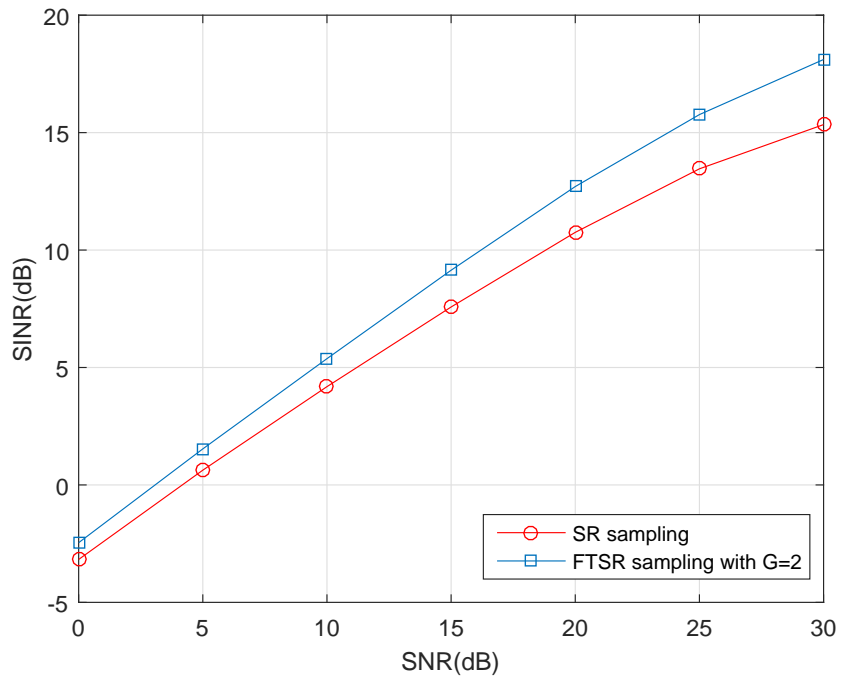


Figure 3.15: The effect of FTSR sampling for 10 unequally spaced channel taps and a block length of 500

3.14, the impact of FTSR sampling decreases for larger block length. The rationale behind that is the impact of losing the samples at guard interval diminishes with in-

cremental block length due to averaging. Note that the advantage of FTSR sampling becomes independent of block length if guard interval is further enlarged to avoid interference and used for MMSE equalization at the expense of spectral inefficiency. This situation resembles the case of using CP which will be investigated in the next chapter.

We consider 2 different faster sampling rates, a sampling rate of $2/T$ which exceeds the Nyquist sampling rate unless $r = 1$ and a sampling rate of $(1 + r)/T$ which equals the Nyquist sampling rate. Indeed, a sampling rate of $(1 + r)/T$ can grab all the information coming from the continuous time signal, because it satisfies the Nyquist sampling rate. The major difference of these sampling rates arises in the statistics of noise samples such that the sampling rate of $2/T$ results in correlated noise samples, whereas the sampling rate of $(1 + r)/T$ leads to uncorrelated noise samples. Figure 3.16 shows the comparison between these sampling rates for 0.5 roll off factor raised cosine pulse shape and a block length of 500. As can be seen, these sampling rates have nearly the same performance.

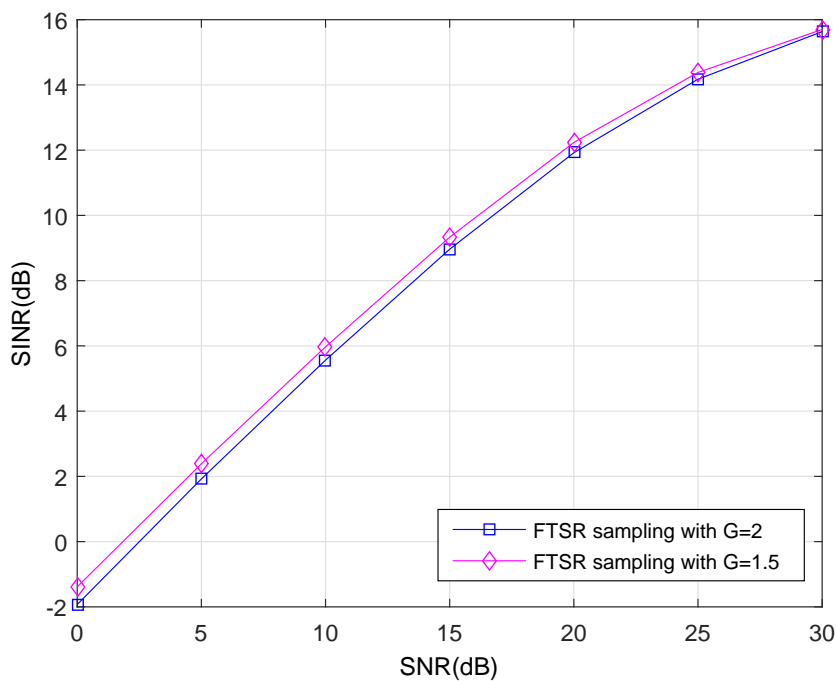


Figure 3.16: The comparison of faster sampling rates for 10 unequally spaced channel taps and a block length of 500

3.7 Conclusions

The technique of FTSR sampling is explained both in time and frequency domain. We prove that SR sampling constitutes sufficient statistics despite pulse matched filtering and excess bandwidth provided that channel taps are equally spaced, whereas it does not become sufficient statistics for unequally spaced channel taps. Following that, the technique of FTSR sampling is applied to MMSE equalization and shown that FTSR sampled MMSE equalization mitigates ISI more efficiently than the conventional SR sampled MMSE equalizer when the guard interval is removed, i.e., the degraded MMSE equalizer performance due to removing the guard interval is compensated by FTSR sampling. Therefore, FTSR sampling always outperforms SR sampling for finite MMSE equalizer lengths even if perfect timing information is available. The simulation results further illustrate that block length is the key parameter affecting the MMSE equalizer performance depending on the sampling rate such that the impact of FTSR sampling grows with smaller block lengths. This result is particularly important when low latency that goes along with small block lengths is becoming a necessity. Other parameters such as the properties of channel taps and excess bandwidth have influence on the performance of FTSR sampled MMSE equalization.

CHAPTER 4

FASTER THAN SYMBOL RATE SAMPLING IN SINGLE USER COMMUNICATION: CP BASED TRANSMISSION

Single user frequency selective wireless channels with multipath propagation lead to IBI for a block transmission in addition to ISI and CP based MMSE equalization with FTSR sampling is employed as a remedy to mitigate these interference sources in this chapter. Note that non-adaptive analog pulse matched filtering is used at the receiver instead of adaptive channel matched filtering prior to MMSE equalization in this chapter as the same with the previous chapter. The primary distinction of this chapter from the previous one is to utilize CP instead of ZP to prevent IBI and observe the effect of FTSR sampling for MMSE equalization once CP is appended for each transmission block. The ultimate aim is to exploit the excess bandwidth by FTSR sampling and improve the interference mitigation capability of CP based MMSE equalization. The complexity increase stemming from the matrix inversion within equalization due to FTSR sampling is avoided by proposing a lower complexity implementation of FTSR sampled CP based MMSE equalization. Moreover, FTSR sampling is studied to compensate the performance loss of MMSE equalization when there is insufficient CP or 1-bit quantization.

4.1 CP Based Transmission for FTSR sampled MMSE Equalization

Multipath channels in a frequency selective fading environment cause interference among consecutively transmitted blocks in addition to ISI. CP based MMSE equalization is a popular technique existing in many systems to prevent both IBI and ISI

in the channel. One of the critical point that affects the performance of CP based MMSE equalization is the sampling rate when pulse matched filtering is used instead of channel matched filtering before equalization relying on the fact that using a non-adaptive analog filter is highly preferable to an adaptive analog filter. However, the sufficient statistics condition in [1], [2] is not valid for CP based MMSE equalization when channel matched filtering is not utilized and SR sampling remains below the Nyquist sampling rate when excess bandwidth exists. Therefore, it is worth to evaluate the influence of faster sampling rates on CP based MMSE equalization with pulse matched filtering.

CP based transmission simplifies the implementation of MMSE equalization tremendously such that the channel can be equalized in frequency domain without matrix inversion operation which is the main advantage of CP for equalization and the basic motivation of MMSE SC-FDE [40], [41], [42]. However, FTSR sampling will require matrix inversion for CP based MMSE equalization. The reason behind this depends on disturbing the circulant channel matrix structure for CP based transmission and creating colored noise due to FTSR sampling. Notice that, due to the existence of other transmissions in adjacent channels, filtering that encompasses only the band of the desired signal is applied in communication systems which results in colored noise processes at the receiver with FTSR sampling. Beyond these, unequally spaced channel taps make channel matrix non-circulant and requires matrix inversion even if CP is used independent of sampling rate. Note that a matrix inversion brings a complexity of $O(N^3)$ for an $N \times N$ matrix. To compensate this complexity increase, more efficient FTSR sampled CP based MMSE equalization structures are required and we will propose one low complexity implementation for this by taking into account the practical channel conditions.

FTSR sampling can improve the performance of CP based MMSE equalization against practical problems. Reducing the CP length to enhance transmission efficiency and power consumption is one important problem in practice for CP based MMSE equalization. Although insufficient CP degrades the system performance significantly [43], FTSR sampling can be a remedy to compensate the performance loss of CP based MMSE equalization. Further desire in practical systems is to lower the precision of ADC in order to reduce power consumption which is an earlier idea whose extreme

case is 1-bit ADC [44], [45]. It is interesting to explicitly observe the performance of CP based MMSE equalization with 1-bit ADC and FTSR sampling.

FTSR sampling for CP based equalization has been studied in two different point of views in the literature. The first one is based on linear polyphase channel models such that SR and extra samples are equalized at different branches and their outputs are combined [10], [11], [12]. The second one is to jointly process all the samples without separating them into branches [9], [15], [16]. In this study, all of the samples are processed jointly. The primary difference of our work is to explicitly study the influence of FTSR sampling on CP based MMSE equalization regarding practical channel conditions and directly compare it with SR sampling under the constraint of colored noise, which is overlooked in [9], [15], [16]. Moreover, those previous works did not address the practical benefits of FTSR sampling in response to insufficient CP or 1-bit quantization. Although the capacity due to lower precision ADC is characterized and performance limits are obtained for SR and FTSR sampling in [46]-[55], those studies did not cover how equalization is affected by 1-bit ADC.

The contributions of this chapter are the following. We characterize the performance of CP based MMSE equalization with FTSR sampling by deriving average MSE expression. In practice, ISI channels due to frequency selective fading have unequally spaced taps and excess bandwidth. We study how efficiently CP based MMSE equalization uses the extra bandwidth under the condition of unequally spaced channel taps with faster sampling rates when pulse matched filtering is used as a front-end filter according to derived MSE expression. Moreover, a low complexity implementation of CP based MMSE equalization is proposed to avoid the complexity increase due to FTSR sampling. Following that, the faster sampling rates are studied to obtain more robust equalization against the shortcoming of CP. Lastly, the impact of 1-bit quantization on the error rate of CP based MMSE equalization is investigated.

In Section 4.2, system model is given and the impact of FTSR sampling on the CP based MMSE equalization is analyzed in Section 4.3. A novel CP based MMSE equalization based on FTSR sampling is stated in Section 4.4. The reduced CP length for FTSR sampled MMSE equalization is discussed in Section 4.5. The investigation of 1-bit quantization for CP based MMSE equalization is given in Section 4.6 and the

chapter ends with the concluding remarks in Section 4.7.

4.2 System Model for FTSR Sampled CP based MMSE Equalization

The effect of FTSR sampling for CP based MMSE equalization is studied when symbols are transmitted as blocks and CP is appended for each block whose length is N_{cp} . A detailed representation of our system model is given in Figure 4.1. Accordingly,

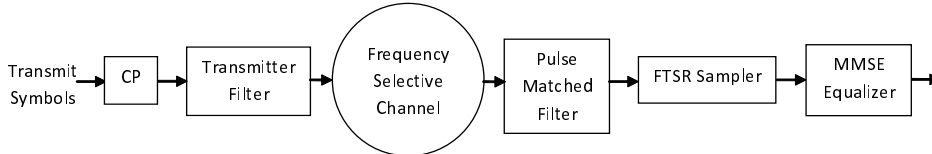


Figure 4.1: FTSR sampled CP based MMSE equalization with pulse matched filtering

i.i.d. transmitted symbols x_n 's feed a transmitter filter $p(t)$ and the transmitted signal in response to one block becomes

$$s(t) = \sum_{n=-N_{cp}}^{N-1} x_n p(t - nT) \quad (4.1)$$

where T is the symbol interval. Transmitted signal propagates through an ISI channel that has $(L + 1)$ multipath components as

$$c(t) = \sum_{k=0}^L \alpha_k \delta(t - \tau_k) \quad (4.2)$$

where α_k represents the complex Gaussian path coefficient and τ_k is the propagation delay. The received signal becomes

$$r(t) = \sum_{n=-N_{cp}}^{N-1} x_n p_c(t - nT) + w(t) \quad (4.3)$$

such that $p_c(t) = p(t) * c(t)$, $w(t)$ is the circularly symmetric complex white Gaussian noise process with zero mean and power spectral density N_0 . The received signal is filtered by a pulse matched filter $p(-t)$ and CP is removed that yields

$$y(t) = \sum_{n=0}^{N-1} x_n h(t - nT) + z(t). \quad (4.4)$$

Sampling the Eqn. (4.4) at time mT with FTSR sampling ratio G for $g = 0, \dots, G-1$ gives

$$y(mT+gT/G) = \sum_{n=0}^{N-1} x_n h(mT+gT/G-nT) + z(mT+gT/G), \quad m = 0, 1, \dots, N-1. \quad (4.5)$$

Defining $y(mT + gT/G) = y_m^g$, $h(mT + gT/G) = h_m^g$ and $z(mT + gT/G) = z_m^g$ yield the following matrix representation

$$\mathbf{y}_{ftsr} = \mathbf{H}_{ftsr} \mathbf{x} + \mathbf{z}_{ftsr} \quad (4.6)$$

where $\mathbf{y}_{ftsr} = [\mathbf{y}_0 \mathbf{y}_1 \dots \mathbf{y}_{N-1}]^T$ is a $GN \times 1$ output vector and $\mathbf{y}_m = [y_m^0 y_m^1 \dots y_m^{G-1}]$ and the $GN \times N$ channel matrix \mathbf{H}_{ftsr} is equal to

$$\mathbf{H}_{ftsr} = \begin{pmatrix} h_0^0 & h_{-1}^0 & \dots & h_{-N+N_{cp}}^0 + h_{N_{cp}}^0 & \dots & h_{-N+1}^0 + h_1^0 \\ \vdots & \vdots & \vdots & \vdots & \vdots & \vdots \\ h_0^{G-1} & h_{-1}^{G-1} & \dots & h_{-N+N_{cp}}^{G-1} + h_{N_{cp}}^{G-1} & \dots & h_{-N+1}^{G-1} + h_1^{G-1} \\ \vdots & \vdots & \vdots & \vdots & \vdots & \vdots \\ h_{N-1}^0 & h_{N-2}^0 & \dots & \dots & \dots & h_0^0 \\ \vdots & \vdots & \vdots & \vdots & \vdots & \vdots \\ h_{N-1}^{G-1} & h_{N-2}^{G-1} & \dots & \dots & \dots & h_0^{G-1} \end{pmatrix}.$$

Note that when $\tau_k = kT$, $h_q^0 = 0$ for $q < 0$ and $q > L$ and $N_{cp} = L$. The correlation among channel taps are

$$E[h_q^{g_1} h_r^{g_2}] = E \left[\sum_{s=0}^L \sum_{v=0}^L \alpha_s \alpha_v \tilde{p}(qT + g_1 T/G - \tau_s) \tilde{p}(rT + g_2 T/G - \tau_v) \right] \quad (4.7)$$

such that $\tilde{p}(t) = p(t) * p(-t)$. \mathbf{x} is an $N \times 1$ input vector with $\mathbf{x} = [x_0 x_1 \dots x_{N-1}]^T$ and $\mathbf{z}_{ftsr} = [\mathbf{z}_0 \mathbf{z}_1 \dots \mathbf{z}_{N-1}]^T$ is a colored $GN \times 1$ additive Gaussian noise vector with $\mathbf{z}_m = [z_m^0 z_m^1 \dots z_m^{G-1}]$. It is crucial to emphasize that FTSR sampling leads to correlation among noise samples such that

$$E[z_q^{g_1} z_r^{g_2}] = \sigma^2 \tilde{p}((r - q)T + (g_2 - g_1)T/G) \quad (4.8)$$

where σ^2 is the variance of noise samples. MMSE equalization is performed in time domain after FTSR sampling, because frequency domain implementation does not bring complexity reduction due to FTSR sampling unlike traditional MMSE SC-FDE [40], [41]. However, the performance remains the same if MMSE equalization is performed in frequency domain as given in Appendix B.

4.3 Analysis of FTSR Sampled CP Based MMSE Equalization

To reduce the ISI at the receiver prior to decision, the vector \mathbf{y}_{ftsr} is processed by an MMSE matrix which can be found by using the orthogonality principle between the observation and the error of optimum estimator such that

$$E[(\mathbf{W}_{mmse}\mathbf{y}_{ftsr} - \mathbf{x})\mathbf{y}_{ftsr}^H] = 0 \quad (4.9)$$

where \mathbf{W}_{mmse} is the MMSE matrix and equal to

$$\mathbf{W}_{mmse} = \mathbf{H}_{ftsr}^H (\mathbf{H}_{ftsr} \mathbf{H}_{ftsr}^H + \mathbf{R}_z)^{-1} \quad (4.10)$$

such that \mathbf{R}_z is the auto-correlation matrix of the noise whose entries are specified by Eqn. (4.8). The total MSE after MMSE filtering becomes [56]

$$MSE = tr\{E[(\mathbf{W}_{mmse}\mathbf{y}_{ftsr} - \mathbf{x})(\mathbf{W}_{mmse}\mathbf{y}_{ftsr} - \mathbf{x})^H]\} \quad (4.11)$$

which can be written as

$$\begin{aligned} MSE = & tr\{E[\mathbf{x}\mathbf{x}^H] - \mathbf{H}_{ftsr}^H \mathbf{W}_{mmse}^H - \mathbf{W}_{mmse} \mathbf{H}_{ftsr} \\ & + \mathbf{W}_{mmse} E[\mathbf{y}_{ftsr} \mathbf{y}_{ftsr}^H] \mathbf{W}_{mmse}^H\}. \end{aligned} \quad (4.12)$$

When \mathbf{W}_{mmse} is written in terms of Eqn. (4.10) and $E[\mathbf{y}_{ftsr} \mathbf{y}_{ftsr}^H]$ is expressed by using Eqn. (4.6),

$$\begin{aligned} MSE = & tr\{E[\mathbf{x}\mathbf{x}^H] - \mathbf{H}_{ftsr}^H (\mathbf{H}_{ftsr} \mathbf{H}_{ftsr}^H + \mathbf{R}_z)^{-1} \mathbf{H}_{ftsr} - \\ & \mathbf{H}_{ftsr}^H (\mathbf{H}_{ftsr} \mathbf{H}_{ftsr}^H + \mathbf{R}_z)^{-1} \mathbf{H}_{ftsr} + \\ & \mathbf{H}_{ftsr}^H (\mathbf{H}_{ftsr} \mathbf{H}_{ftsr}^H + \mathbf{R}_z)^{-1} \mathbf{H}_{ftsr}\}. \end{aligned} \quad (4.13)$$

Canceling common terms,

$$MSE = tr\{E[\mathbf{x}\mathbf{x}^H] - \mathbf{H}_{ftsr}^H (\mathbf{H}_{ftsr} \mathbf{H}_{ftsr}^H + \mathbf{R}_z)^{-1} \mathbf{H}_{ftsr}\}. \quad (4.14)$$

It is assumed that i.i.d. input symbols have unit variance, i.e., $tr\{E[\mathbf{x}\mathbf{x}^H]\} = N$ producing

$$MSE = N - tr\{\mathbf{H}_{ftsr}^H (\mathbf{H}_{ftsr} \mathbf{H}_{ftsr}^H + \mathbf{R}_z)^{-1} \mathbf{H}_{ftsr}\}. \quad (4.15)$$

Using Matrix Inversion Lemma, Eqn. (4.15) can be further expressed as

$$\begin{aligned} MSE = & N - tr\{\mathbf{H}_{ftsr}^H (\mathbf{R}_z^{-1} - \mathbf{R}_z^{-1} \mathbf{H}_{ftsr} \\ & (\mathbf{I}_N + \mathbf{H}_{ftsr}^H \mathbf{R}_z^{-1} \mathbf{H}_{ftsr})^{-1} \mathbf{H}_{ftsr}^H \mathbf{R}_z^{-1}) \mathbf{H}_{ftsr}\} \end{aligned} \quad (4.16)$$

and

$$MSE = N - \text{tr}\{\mathbf{H}_{f_tsr}^H \mathbf{R}_z^{-1} \mathbf{H}_{f_tsr} - \mathbf{H}_{f_tsr}^H \mathbf{R}_z^{-1} \mathbf{H}_{f_tsr} (\mathbf{I}_N + \mathbf{H}_{f_tsr}^H \mathbf{R}_z^{-1} \mathbf{H}_{f_tsr})^{-1} \mathbf{H}_{f_tsr}^H \mathbf{R}_z^{-1} \mathbf{H}_{f_tsr}\}. \quad (4.17)$$

Eqn. (4.17) can be expressed in terms of the eigenvalues of $\mathbf{H}_{f_tsr}^H \mathbf{R}_z^{-1} \mathbf{H}_{f_tsr}$ as

$$MSE = N - \sum_{i=0}^{N-1} \lambda_i + \sum_{i=0}^{N-1} \frac{\lambda_i^2}{1 + \lambda_i} \quad (4.18)$$

where λ_i 's are the eigenvalues of $\mathbf{H}_{f_tsr}^H \mathbf{R}_z^{-1} \mathbf{H}_{f_tsr}$. The final expression is

$$MSE = N - \sum_{i=0}^{N-1} \frac{\lambda_i}{1 + \lambda_i}. \quad (4.19)$$

Since $MSE_{av} = MSE/N$, it is easily derived that

$$MSE_{av} = \frac{1}{N} \sum_{i=0}^{N-1} \frac{1}{1 + \lambda_i}. \quad (4.20)$$

Lemma 4.3.1 *Pulse matched filtering with SR sampling at $\{0, T, \dots, (N + L - 1)T\}$ constitutes sufficient statistics for estimating $\{x_n\}$ when ISI channel taps are equally spaced, i.e., $\tau_k = kT$ and excess bandwidth exists in case of CP based block transmission.*

Proof 4.3.2 *The length of observation window for one block at the receiver becomes $(N + L - 1)T$ when there are $(L + 1)$ equally spaced channel taps. Then, the orthogonal set $\{p(t - nT)\}$ for $n = 0, 1, \dots, (N + L - 1)$ becomes complete basis and constitutes orthogonal expansion basis functions as proved in Lemma 3.2.1, i.e., any received signal can be totally spanned by $\{p(t - nT)\}$ for $n = 0, 1, \dots, (N + L - 1)$. Thus, pulse matched filtering with SR sampling is sufficient to completely capture all available information in the signal which completes the proof.*

Corollary 4.3.3 *FTSR sampling does not decrease the average MSE in Eqn. (4.20) when ISI channel taps are equally spaced even if excess bandwidth exists in which SR sampling remains below the Nyquist sampling rate and the usage of pulse matched filtering disturbs the sufficient statistics condition in [1], [2].*

Proof 4.3.4 *SR sampling covers all relevant information when ISI channel taps are equally spaced even if pulse matched filtering and excess bandwidth are employed as proved in Lemma 4.3.1, and hence FTSR sampling does not bring any further information to enhance MMSE equalization performance.*

The effect of equally spaced channel taps for FTSR sampling is numerically evaluated as well based on Eqn. (4.20). We use a Monte Carlo method with 10,000 runs. It is assumed that there is an ISI channel with 8 complex Gaussian taps, pulse shape filter is raised cosine filter with 30% excess bandwidth and block length is 64. It can be observed in Figure 4.2 that FTSR sampling with $G = 2$ has the same MSE_{av} with SR sampling for equally spaced channel taps with respect to SNR which supports the Corollary 4.3.3.

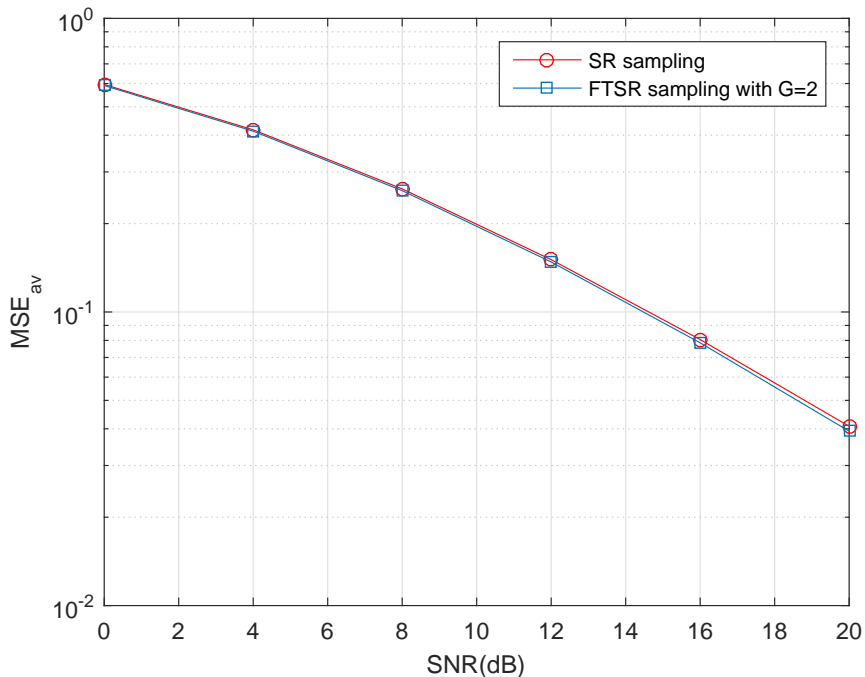


Figure 4.2: The performance of CP based MMSE equalization depending on sampling rate for 8 equally spaced channel taps and 30% excess bandwidth

Lemma 4.3.5 *Pulse matched filtering with SR sampling does not cover all the continuous time signal information when ISI channel taps are unequally spaced, i.e., $\tau_k \neq kT$ and excess bandwidth exists in case of CP based block transmission.*

Proof 4.3.6 *SR sampling remains below the Nyquist rate when excess bandwidth ex-*

ists. Moreover, the sufficient statistics condition for ISI channels stated in [1], [2] is no more valid, since we use pulse matched filter instead of channel matched filter. Then, the only remaining condition is to span the received signal by the orthogonal set $\{p(t - nT)\}$. However, it is clear that $\{p(t - nT)\}$ is not a complete orthogonal basis for a signal composed of $\{p(t - \tau_n)\}$ where $\tau_n = nT - t_n$ for $t_n \neq 0$. Thus, the orthogonal set $\{p(t - nT)\}$ does not span the received signal which implies that SR sampled pulse matched filter does not cover all the incoming information for CP based transmission when channel taps are unequally spaced.

Corollary 4.3.7 *FTSR sampling can decrease the average MSE in Eqn. (4.20) when ISI channel taps are unequally spaced and excess bandwidth exists in case of pulse matched filtering.*

Proof 4.3.8 *The received signal is not perfectly captured with SR sampled pulse matched filter when channel taps are unequally spaced and excess bandwidth exists as given in Lemma 4.3.5. Since the performance of MMSE equalization directly depends on the sample set at the output of pulse matched filter, any information loss in the channel immediately affects the equalizer, that is SR sampled pulse matched filter does not become sufficient statistics for estimating $\{x_n\}$ in the MMSE sense. Therefore, FTSR sampling can improve the equalization performance until the Nyquist sampling rate is obtained.*

Based on Corollary 4.3.7, one can expect that FTSR sampling decreases the average MSE expression in Eqn. (4.20) until the Nyquist sampling rate is reached. However, it is analytically intractable to obtain the eigenvalues of $\mathbf{H}_{ftsr}^H \mathbf{R}_z^{-1} \mathbf{H}_{ftsr}$ and quantify the improvement due to the complicated form of \mathbf{H}_{ftsr} and \mathbf{R}_z^{-1} . Yet, numerical computations can be instrumental in inspecting MSE_{av} . According to that, MSE_{av} in Eqn. (4.20) is calculated for FTSR and SR sampled CP based MMSE equalization by generating 10,000 random channel realizations with 8 complex Gaussian unequally spaced channel taps that are distributed uniformly between 0 and 8 symbol intervals for 30% excess bandwidth and a block length of 64. Figure 4.3 presents that FTSR sampling with $G = 2$ has a relatively good average MSE performance than SR sampling. The performance of $G = 3$ remains the same with $G = 2$, since $G = 2$ has

already satisfied the Nyquist sampling rate and there is no further incoming information for $G = 3$. Eventually, FTSR sampling leads to an improvement in average MSE

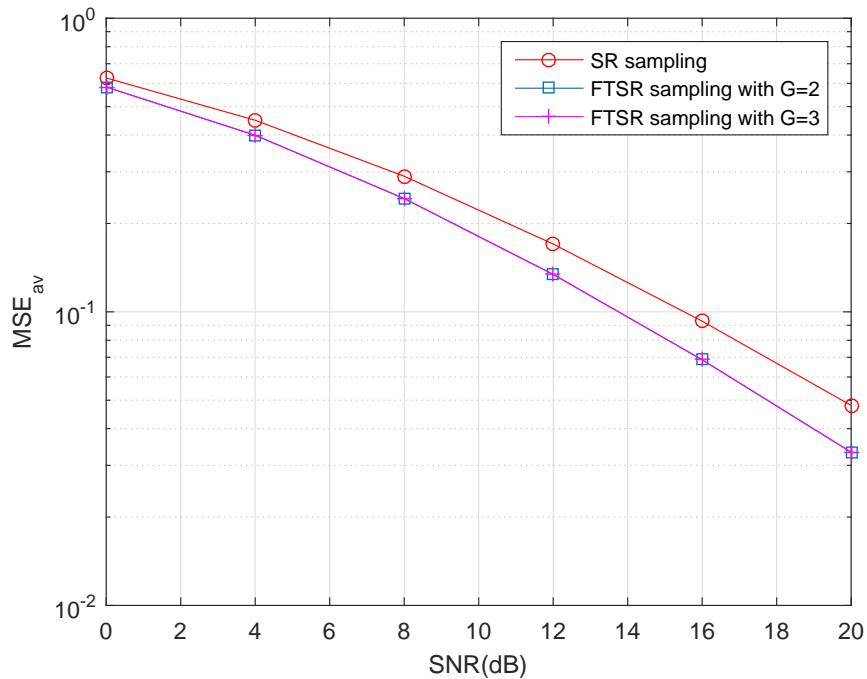


Figure 4.3: The performance of CP based MMSE equalization depending on sampling rate for 8 unequally spaced channel taps and 30% excess bandwidth

for CP based MMSE equalization.

Following that, FTSR sampling is studied for CP based MMSE equalization when there is no excess bandwidth in the pulse shape to emphasize the impact of excess bandwidth. Similarly, 8 complex Gaussian unequally spaced channel taps are uniformly distributed in $[0, 8T]$ for a block length of 64. As it can be seen from Figure 4.4, FTSR sampling does not bring any advantage even for unequally spaced channel taps. These results suggest that FTSR sampling improves the equalization performance only if there exists excess bandwidth which is also intuitive based on the fact that SR sampling has already satisfied the Nyquist sampling rate.

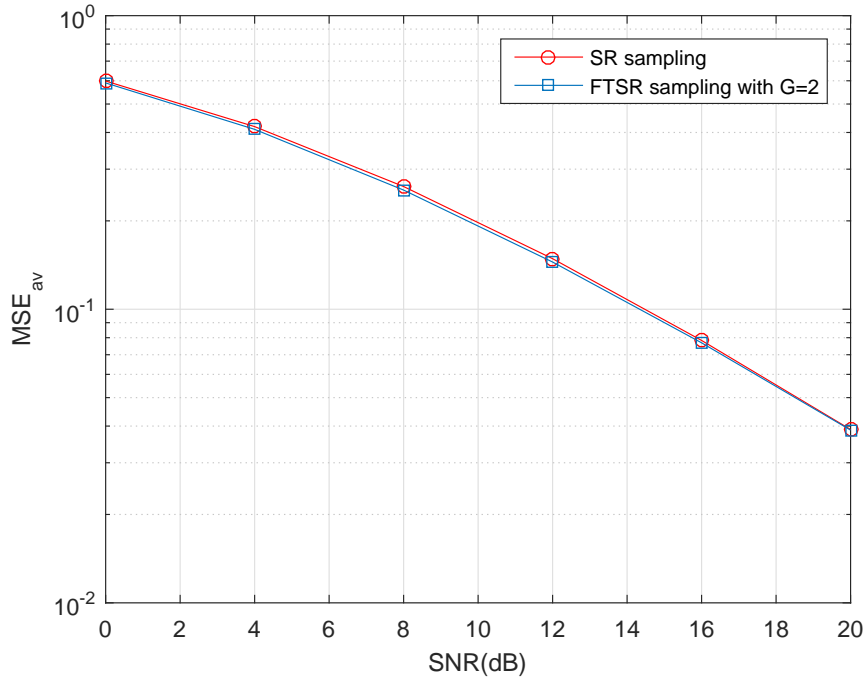


Figure 4.4: The performance of CP based MMSE equalization depending on sampling rate for 8 unequally spaced channel taps without excess bandwidth

It is presented that extra bandwidth disturbs the error performance of CP based MMSE equalization for SR sampling when unequally spaced channel taps exist such that the more excess bandwidth there is, the more performance degradation occurs [15]. We investigate FTSR sampling to avoid this adverse effect of excess bandwidth in case of unequally spaced ISI channels for CP based MMSE equalization in terms of Eqn. (4.20). Figure 4.5 shows that excess bandwidth improves the performance in case of FTSR sampling with $G = 2$ despite 8 complex Gaussian unequally spaced channel taps which are uniformly distributed in $[0, 8T]$ for a block length of 64. On the other hand, the performance of SR sampled MMSE equalization decreases with excess bandwidth when channel taps are unequally spaced. The level of aliasing increases due to larger excess bandwidth for SR sampling and the equalization performance degrades, whereas aliasing is avoided for FTSR sampling and performance improves depending on the increase in the bandwidth. Eventually, it is more critical to make use of FTSR sampling especially for larger excess bandwidth in case of unequally spaced channels.

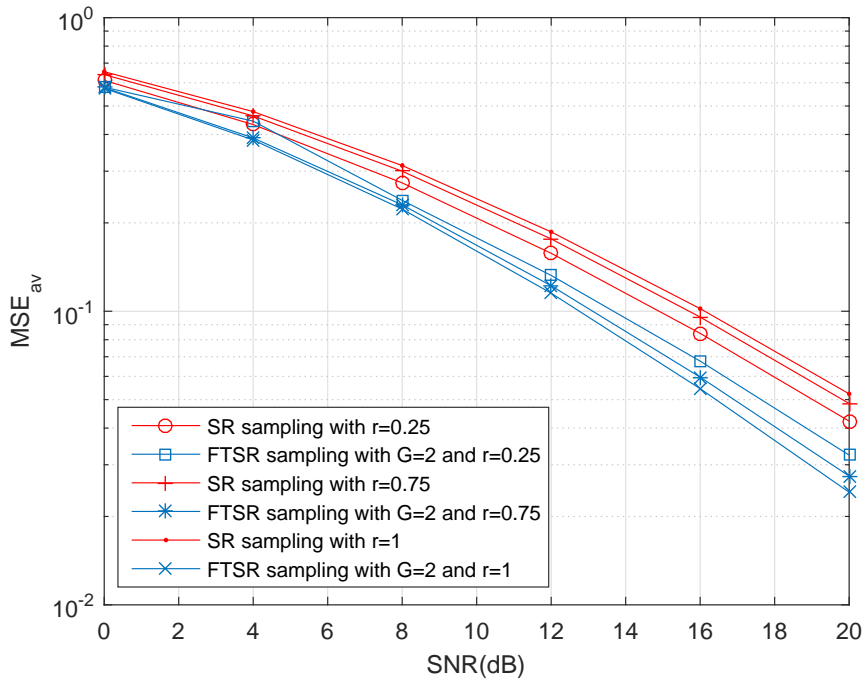


Figure 4.5: The impact of excess bandwidth for CP based MMSE equalization depending on sampling rate for 8 unequally spaced channel taps

Since this chapter addresses the performance of CP based MMSE equalization and block length is another question in mind while designing a system, we compare the performance of CP based MMSE equalizer for a block length of 64 and 128 in regard to average MSE in Eqn. (4.20). There are 8 ISI channel taps which are complex Gaussian and uniformly distributed in $[0, 8T]$ and 30% excess bandwidth exists. As can be seen from Figure 4.6, there is a slight change for both FTSR sampled with $G = 2$ and SR sampled MMSE equalizer for different block lengths.

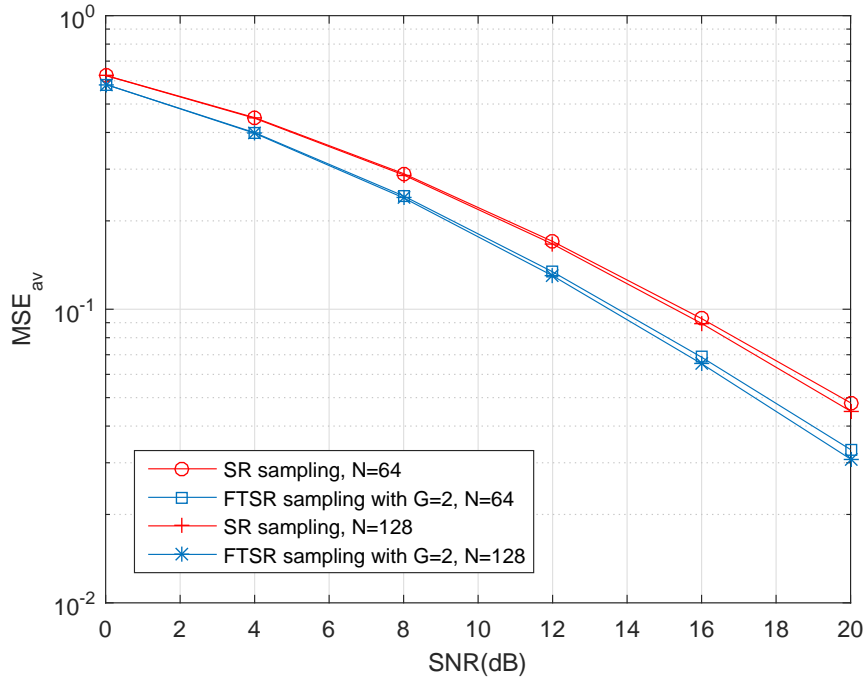


Figure 4.6: Block length effect for CP based MMSE equalization depending on sampling rate for 8 unequally spaced channel taps

Lastly, the effect of constellation size on the performance of FTSR sampled CP based MMSE equalization is investigated in terms of bit error rate (BER). The behavior of CP based MMSE equalizer for different modulation formats is discussed in [57], [58] without considering FTSR sampling and practical channel conditions. In this part, we generalize the influence of different modulation schemes for CP based MMSE equalization by taking into account the practical channel conditions and FTSR sampling. According to that, it is assumed that there is a multipath channel with 8 complex Gaussian taps whose propagation delays are uniformly distributed in $[0, 8T]$ for a block length of 64 and 30% excess bandwidth. The effect of modulation formats with these settings is given in Figure 4.7. The benefit of FTSR sampling increases when the constellation size grows.

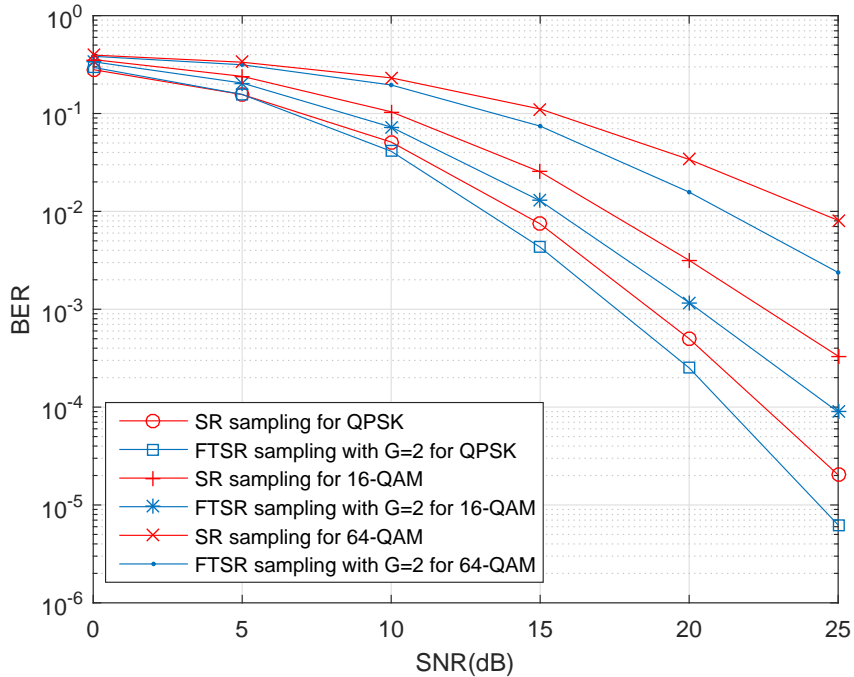


Figure 4.7: The performance of CP based MMSE equalization for different modulation formats depending on sampling rate for 8 unequally spaced channel taps

4.4 A Novel CP Based MMSE Equalization Implementation

MMSE equalization involves matrix inversion operation as given in Eqn. (4.10) and it is well-known that inverting an $N \times N$ matrix brings a complexity of $O(N^3)$. This high complexity can be avoided when the inverted matrix is circulant such that the equalizer is implemented in frequency domain and circulant matrix can be diagonalized by left and right multiplying the matrix with DFT and IDFT matrices respectively. Since CP based block transmission makes the inverted matrix circulant in case of SR sampling and equally spaced channel taps, traditional MMSE SC-FDE has a significant complexity reduction. However, unequally spaced channel taps, FTSR sampling and the resultant correlated noise auto-correlation matrix disturb the circulant matrix structure. This brings the complexity overhead of $O(N^3)$ due to the matrix inversion within MMSE equalization. Therefore, we propose a low complexity CP based MMSE equalizer implementation. Our method is based on the idea of inverting the block circulant matrix with the proposed method in [59] which has complexity $O(N)$ and implementing a mismatched MMSE equalizer. Notice that MMSE equalizer is denoted as mismatched MMSE equalizer when the true channel and noise

auto-correlation matrices are not used for equalization [60]. The proposed technique is:

1. Approximate $GN \times N$ channel matrix into a block circulant matrix by the following sequence of steps:
 - (a) Transform $GN \times N$ channel matrix to $GN \times GN$ matrix by appending zeros;
 - (b) Partition the $GN \times GN$ matrix into matrices of size $N \times N$;
 - (c) Transform each $N \times N$ matrix to a circulant channel matrix by eliminating some off-diagonal taps;
 - (d) Attain an $N \times N$ block circulant matrix with $G \times G$ blocks by elementary matrix operations.

We give an illustrative simple example corresponding to this step assuming that $G = 2$ for the sake of simplicity. Let us consider a $2N \times N$ channel matrix \mathbf{H}_{ftsr} as

$$\mathbf{H}_{ftsr} = \begin{pmatrix} a_{1,1} & a_{1,2} & \cdots & a_{1,N} \\ \vdots & \vdots & \vdots & \vdots \\ \vdots & \vdots & \vdots & \vdots \\ a_{N,1} & a_{N,2} & \cdots & a_{N,N} \\ b_{(N+1),1} & b_{(N+1),2} & \cdots & b_{(N+1),N} \\ \vdots & \vdots & \vdots & \vdots \\ \vdots & \vdots & \vdots & \vdots \\ b_{2N,1} & b_{2N,2} & \cdots & b_{2N,N} \end{pmatrix}. \quad (4.21)$$

After step 1a),

$$\mathbf{H}_{ftsr}^{1a} = \begin{pmatrix} a_{1,1} & a_{1,2} & \cdots & a_{1,N} & 0 & 0 & \cdots & 0 \\ \vdots & \vdots & \vdots & \vdots & \vdots & \vdots & \vdots & \vdots \\ \vdots & \vdots & \vdots & \vdots & \vdots & \vdots & \vdots & \vdots \\ a_{N,1} & a_{N,2} & \cdots & a_{N,N} & 0 & 0 & \cdots & 0 \\ b_{(N+1),1} & b_{(N+1),2} & \cdots & b_{(N+1),N} & 0 & 0 & \cdots & 0 \\ \vdots & \vdots & \vdots & \vdots & \vdots & \vdots & \vdots & \vdots \\ \vdots & \vdots & \vdots & \vdots & \vdots & \vdots & \vdots & \vdots \\ b_{2N,1} & b_{2N,2} & \cdots & b_{2N,N} & 0 & 0 & \cdots & 0 \end{pmatrix}. \quad (4.22)$$

Following step 1c),

$$\mathbf{H}_{ftsr}^{1c} = \begin{pmatrix} a_{1,1} & \cdots & a_{1,p} & 0 & 0 & 0 & \cdots & 0 \\ 0 & a_{1,1} & \cdots & \cdots & 0 & 0 & \cdots & 0 \\ \vdots & \vdots & \ddots & \vdots & \vdots & \vdots & \vdots & \vdots \\ \cdots & a_{1,p} & \cdots & a_{1,1} & 0 & 0 & \cdots & 0 \\ b_{1,1} & \cdots & b_{1,p} & 0 & 0 & 0 & \cdots & 0 \\ 0 & b_{1,1} & \cdots & \cdots & 0 & 0 & \cdots & 0 \\ \vdots & \vdots & \ddots & \vdots & \vdots & \vdots & \vdots & \vdots \\ \cdots & b_{1,p} & \cdots & b_{1,1} & 0 & 0 & \cdots & 0 \end{pmatrix} \quad (4.23)$$

where $p < N$. Finally, incorporating step 1d) results in

$$\mathbf{H}_{ftsr}^{1d} = \begin{pmatrix} a_{1,1} & 0 & a_{1,2} & 0 & \cdots & a_{1,p} & 0 & \cdots \\ b_{1,1} & 0 & b_{1,2} & 0 & \cdots & b_{1,p} & 0 & \cdots \\ 0 & 0 & a_{1,1} & 0 & a_{1,2} & \cdots & \cdots & 0 \\ 0 & 0 & b_{1,1} & 0 & b_{1,2} & \cdots & \cdots & 0 \\ \vdots & \vdots & \vdots & \vdots & \vdots & \vdots & \vdots & \vdots \\ \vdots & \vdots & \vdots & \vdots & \vdots & \vdots & \vdots & \vdots \\ a_{1,2} & 0 & \cdots & a_{1,p} & 0 & \cdots & a_{1,1} & 0 \\ b_{1,2} & 0 & \cdots & b_{1,p} & 0 & \cdots & b_{1,1} & 0 \end{pmatrix}. \quad (4.24)$$

2. Implement a mismatched MMSE equalizer as follows:

- (a) Utilize the resultant matrix after step 1 as the channel matrix instead of the true channel matrix;
- (b) Utilize an identity matrix as the noise auto-correlation matrix instead of the true noise auto-correlation matrix.

3. Perform the matrix inversion in MMSE equalizer with complexity of $O(N)$ as proposed in [59] for block circulant matrices.

The performance of the proposed method is compared with the classical FTSR sampled CP based MMSE equalization that requires matrix inversion in Figure 4.8 when Quadrature Phase Shift Keying (QPSK) modulation and 50% excess bandwidth are used with a block length of 64. In the simulation, there are 8 complex Gaussian

unequally spaced channel taps that are uniformly distributed in $[0, 8T]$. It can be observed that performance loss of the proposed method is small with an important complexity reduction and there is a still advantage of FTSR sampling with $G = 2$ even if QPSK modulation is employed which brings smaller enhancement with respect to higher constellation sizes due to FTSR sampling. The proposed equalization with complexity $O(N)$ will bring more SNR gain for higher constellation sizes. To illustrate, the benefit of proposed CP based MMSE equalization implementation with FTSR sampling is given for 16-Quadrature Amplitude Modulation (QAM) in Figure 4.9 and 64-QAM in Figure 4.10 for the same channel settings.

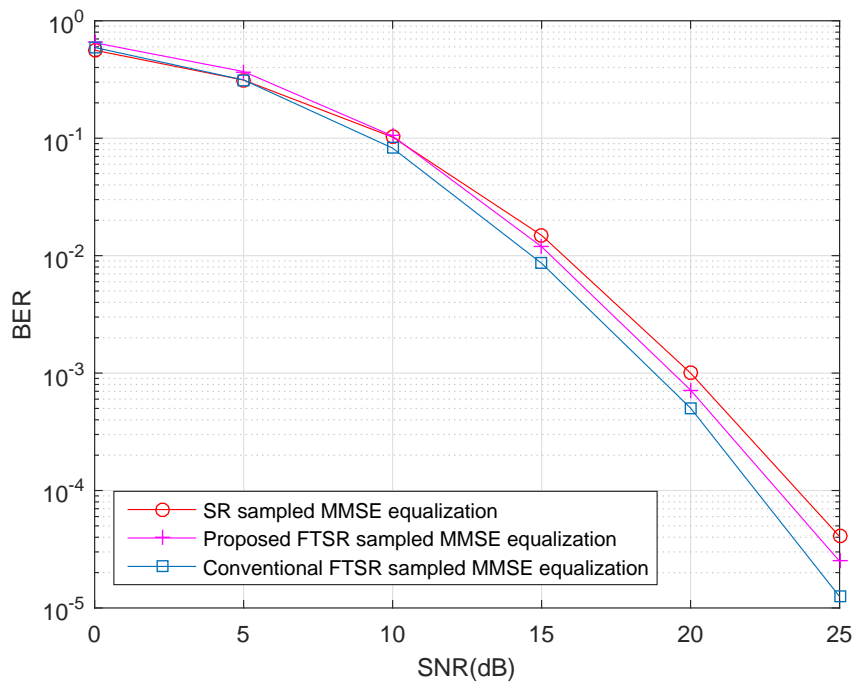


Figure 4.8: The error rate of the proposed FTSR sampled CP based MMSE equalization structure with complexity $O(N)$ for QPSK

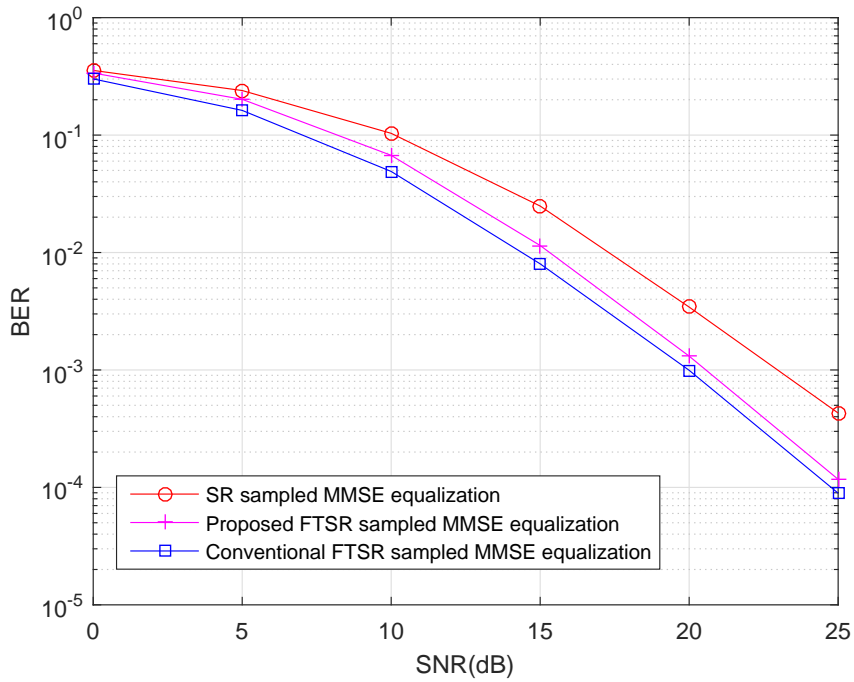


Figure 4.9: The error rate of the proposed FTSR sampled CP based MMSE equalization structure with complexity $O(N)$ for 16-QAM

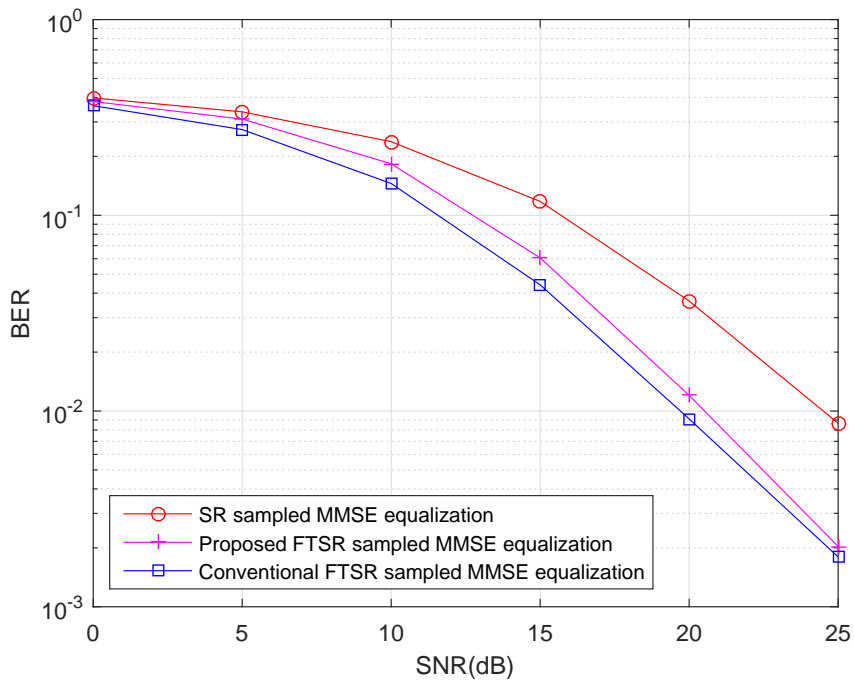


Figure 4.10: The error rate of the proposed FTSR sampled CP based MMSE equalization structure with complexity $O(N)$ for 64-QAM

4.5 CP Reduction

Although CP is widely utilized in block transmission for frequency selective channels, it lowers the power and transmission efficiency especially for smaller block lengths. Increasing the transmission block length can be one alternative to reduce the power and transmission inefficiency, however, CP length can become extremely long relying on maximum channel delay spread. Since channel coherence time limits the block length, this approach does not solve the problem properly. Reducing the CP length can be another method to enhance the power and transmission efficiency at the expense of performance degradation. There are some techniques to prevent the performance degradation due to insufficient CP such that [43], [61], [62] propose solutions to alleviate insufficient CP problem for OFDM systems. The same problem is studied for single carrier transmission as well in [63], [64] relying on iterative receivers which brings a complexity increase. [65] presents a technique without using an iterative receiver based on a specially designed frame structure at the transmitter and a special algorithm at the receiver making difficult to be adopted to the existing systems. We propose FTSR sampling to non-iterative linear receivers to compensate the performance loss in a practical manner, i.e., it can easily be adopted to current receivers without any modification at transmitters.

When full CP is used in a multipath propagation environment, vector-matrix representation of full CP based transmission for SR sampling under the condition of equally spaced channel taps becomes

$$\mathbf{y}_{sr} = \mathbf{H}_{sr} \mathbf{x} + \mathbf{z}_{sr} \quad (4.25)$$

where \mathbf{x} , \mathbf{y}_{sr} and \mathbf{z}_{sr} are $N \times 1$ input, output and noise vectors, and \mathbf{H}_{sr} is an $N \times N$

circulant matrix. Indeed, \mathbf{H}_{sr} can be expressed as

$$\mathbf{H}_{sr} = \begin{pmatrix} h_0 & 0 & 0 & \cdots & 0 & 0 & h_L & \cdots & h_2 & h_1 \\ h_1 & h_0 & 0 & \cdots & 0 & 0 & 0 & h_L & \cdots & h_2 \\ \vdots & \ddots & \ddots & \vdots & \vdots & \vdots & \vdots & \vdots & \ddots & \vdots \\ \vdots & \vdots & \ddots & \ddots & \vdots & \vdots & \vdots & \vdots & \ddots & h_L \\ h_L & \vdots & \vdots & \ddots & \ddots & \vdots & \vdots & \vdots & \ddots & \vdots \\ 0 & h_L & \cdots & \cdots & h_1 & h_0 & 0 & \vdots & \vdots & \vdots \\ 0 & 0 & h_L & \cdots & \cdots & h_1 & h_0 & 0 & \cdots & 0 \\ 0 & 0 & 0 & h_L & \cdots & \cdots & h_1 & h_0 & \cdots & 0 \\ \vdots & \vdots & \vdots & \vdots & \ddots & \vdots & \ddots & \ddots & \ddots & \vdots \\ 0 & 0 & 0 & 0 & \cdots & h_L & \cdots & \cdots & h_1 & h_0 \end{pmatrix}.$$

Then, the i^{th} component of \mathbf{y}_{sr} is equal to

$$y_{sr,i} = h_0 x_i + h_1 x_{|i-1|_N} + h_2 x_{|i-2|_N} + \cdots + h_L x_{|i-L|_N} + z_{sr,i} \quad (4.26)$$

where $|\cdot|_N$ represents the modulo N operation and $z_{sr,i}$ is the i^{th} component of \mathbf{z}_{sr} .

When CP is reduced by Δ number of samples, \mathbf{H}_{sr} is equal to

$$\mathbf{H}_{sr} = \begin{pmatrix} h_0 & 0 & 0 & \cdots & 0 & 0 & h_{L-\Delta} & \cdots & h_2 & h_1 \\ h_1 & h_0 & 0 & \cdots & 0 & 0 & h_{L-\Delta+1} & h_{L-\Delta} & \cdots & h_2 \\ \vdots & \ddots & \ddots & \vdots & \vdots & \vdots & \vdots & \vdots & \ddots & \vdots \\ \vdots & \vdots & \ddots & \ddots & \vdots & \vdots & \vdots & \vdots & \vdots & h_{L-\Delta} \\ h_L & \vdots & \vdots & \ddots & h_0 & \vdots & \vdots & \vdots & \vdots & \vdots \\ 0 & h_L & \cdots & \cdots & h_1 & \ddots & 0 & \vdots & \vdots & \vdots \\ 0 & 0 & h_L & \cdots & \cdots & \ddots & h_0 & 0 & \cdots & 0 \\ 0 & 0 & 0 & \ddots & \cdots & \cdots & h_1 & h_0 & \cdots & 0 \\ \vdots & \vdots & \vdots & \vdots & h_L & \vdots & \vdots & \ddots & \ddots & \vdots \\ 0 & 0 & 0 & 0 & 0 & \ddots & \cdots & \cdots & h_1 & h_0 \end{pmatrix}.$$

$y_{sr,i}$ is now expressed for $i = 0, \dots, (\Delta - 1)$

$$y_{sr,i} = h_0 x_i + h_1 x_{|i-1|_N} + h_2 x_{|i-2|_N} + \cdots + h_{i+L-\Delta} x_{|i-L+\Delta|_N} + z_{sr,i} \quad (4.27)$$

although it becomes as in Eqn. (4.26) for $i = \Delta, \dots, N$. It is known that a diversity order of $(L + 1)$ can be achieved for a multipath channel with $(L + 1)$ taps. However, it is straightforward to express that maximum diversity gain decreases from $(L + 1)$ to $(i + L - \Delta + 1)$ for $i = 0, \dots, (\Delta - 1)$ in Eqn. (4.27) due to reduced CP length which leads to significant loss.

FTSR sampling can compensate the missing terms in Eqn. (4.27) due to reduced CP similar to [66]. More specifically, in case of FTSR sampling, more than one samples are processed for each transmitted symbol. The extra samples $y_{e,i}$ caused by sampling at $\{mT + gT/G\}$ for $m = 0, 1, \dots, N - 1$ and $g \neq 0$ can take samples from the missing echos of first Δ symbols, since

$$\begin{aligned}
y_{e,i} = & c_0 h_0 x_i + c_1 h_1 x_i + \dots + c_L h_L x_i + & (4.28) \\
& c_{-1} h_0 x_{|i-1|_N} + c_0 h_1 x_{|i-1|_N} + \dots + c_{L-1} h_L x_{|i-1|_N} + \\
& \vdots \\
& c_{-N+1} h_0 x_{|i-N+1|_N} + c_{-N+2} h_1 x_{|i-N+1|_N} + \dots + c_{-N+L+1} h_L x_{|i-N+1|_N} + \\
& z_{ftsr,i}
\end{aligned}$$

where c_k 's are the coefficients coming from pulse shape and $z_{ftsr,i}$ is the noise for i^{th} sample.

Notice that taking the DFT of Eqn. (4.25) yields

$$\mathbf{Y}_{sr} = \mathbf{D}_{sr} \mathbf{X} + \mathbf{Z}_{sr} \quad (4.29)$$

where \mathbf{Y}_{sr} , \mathbf{X} and \mathbf{Z}_{sr} are the DFT representations of \mathbf{y}_{sr} , \mathbf{x} and \mathbf{z}_{sr} respectively. \mathbf{D}_{sr} is the $N \times N$ diagonal matrix. Eqn. (4.29) shows that the channel can be parallelized into N sub-channels and transmitted symbols do not affect each other once DFT is taken. Based on this model, MMSE equalization turns into single tap filtering. In particular, the MMSE filtering can be done for each symbol X_k as

$$\omega_k = \frac{D_k^*}{|D_k|^2 + \theta} \quad (4.30)$$

where ω_k is the MMSE filter coefficient for the k^{th} symbol, D_k is the k^{th} diagonal term of \mathbf{D}_{sr} and $\theta = E[|x_k|^2]/\sigma^2$ for any $k = 0, \dots, N - 1$. On the other hand, Eqn. (4.29) is no more valid in case of reduced CP length implying that symbols within one block interfere with each other and single tap filtering is not possible. Moreover,

FTSR sampling with G disturbs the circulant channel matrix structure independent of insufficient CP yielding non-circulant $GN \times N$ channel matrix even when full CP is appended. However, extra samples can only enhance the performance, because

$$I(\mathbf{x}; \mathbf{y}_{ftsr}) = I(\mathbf{x}; \mathbf{y}_{sr}) + I(\mathbf{x}; \mathbf{y}_e | \mathbf{y}_{sr}) \quad (4.31)$$

where $I(\cdot; \cdot)$ is the mutual information, \mathbf{y}_e and \mathbf{y}_{sr} are the extra and SR sampled samples implying that

$$I(\mathbf{x}; \mathbf{y}_{sr}) \leq I(\mathbf{x}; \mathbf{y}_{ftsr}). \quad (4.32)$$

Eqn. (4.32) proves that FTSR sampling does not undermine the performance of CP based MMSE equalization. However, Eqn. (4.30) cannot be used for the proposed FTSR sampled CP based MMSE equalization and MMSE filtering requires a matrix inversion with complexity $O(N^3)$. A quick remedy to decrease this excessive complexity increase is to employ the proposed lower complexity implementation in Section 4.4.

The main object of this part is to observe the performance of CP based MMSE equalization with insufficient CP depending on the sampling rate. The fundamental point is how much tolerance to the shortcoming of CP can be provided by different sampling rates. The effect of CP reduction is examined for a larger channel delay spread that requires longer CP, and hence it is more important to reduce the CP length. According to that, there are 8 channel taps that are randomly distributed in $[0, 20T]$ for a block length of 64. The pulse shaping filter has 50% excess bandwidth and 16-QAM is the modulation format. A Monte Carlo simulation with 10,000 runs is performed. The result presented in Figure 4.11 illustrates that FTSR sampling with $G = 2$ is much more tolerant to 20% reduced CP with respect to conventional SR sampled MMSE SC-FDE. This suggests that increasing the power and transmission efficiency is possible without any significant performance loss by reducing CP to some extent. On the other hand, Figure 4.12 presents that FTSR sampled MMSE equalizer has even degraded performance when the CP length is reduced by 40%.

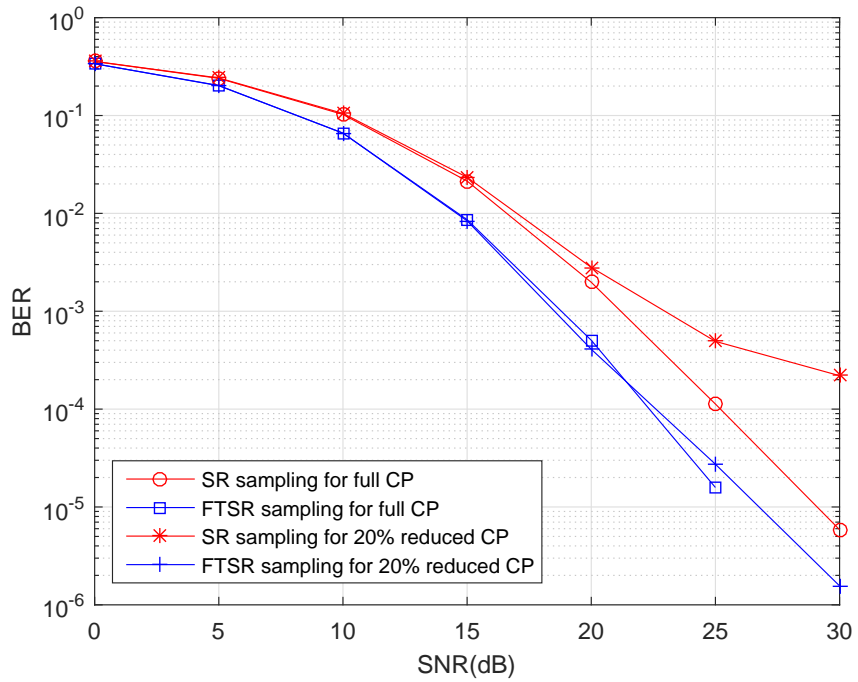


Figure 4.11: The effect of 20% reduced CP on the FTSR and SR sampled MMSE equalization

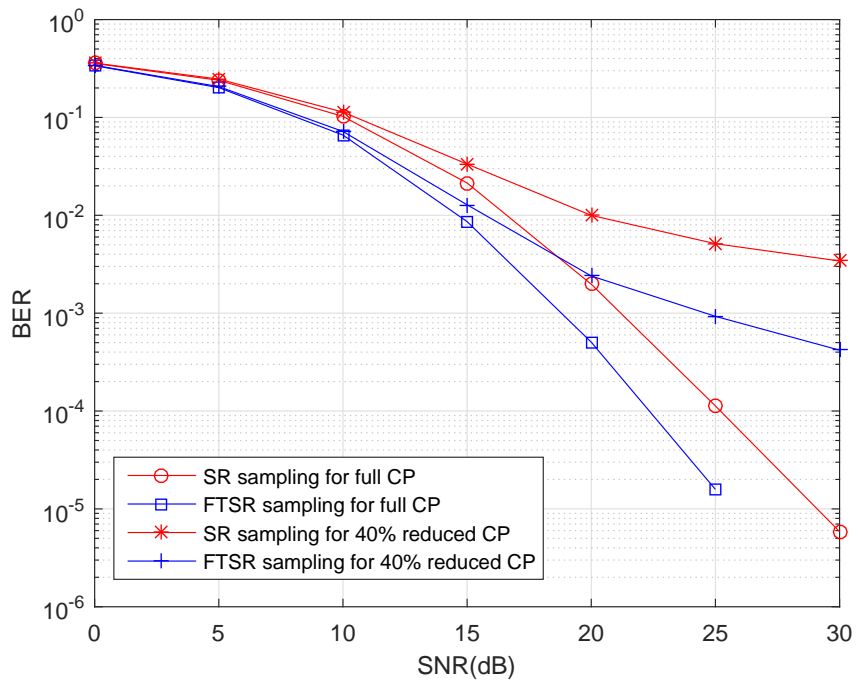


Figure 4.12: The effect of 40% reduced CP on the FTSR and SR sampled MMSE equalization

4.6 1-bit Quantization

One of the major source of cost and power dissipation in receivers is the ADC. Therefore, the idea of lowering the precision of ADC is highly appealing with an extreme case of 1-bit ADC. Although lowering the precision of ADC will affect the entire receiver structure including carrier synchronization, time synchronization, channel estimation, equalization, decoding, etc., its effect has mainly been studied from an information theoretic point of view for both SR and FTSR sampling in [46] - [55]. Our focus is the impact of 1-bit ADC on the equalization assuming that the channel is estimated with high precision ADC by training symbols and then the received samples are quantized with 1-bit ADC and equalized. In particular, this is an initial communication theoretical step of a complicated lower precision ADC problem.

The spectral efficiency of Binary Phase Shift Keying (BPSK) signaling scheme is 1 bit per channel use (bpcu) and information rate for 1-bit ADC at the receiver is 1 bpcu in case of SR sampling [50], [51]. It shows that there is not any data rate loss when BPSK is used even if 1-bit ADC is employed at the receiver. Moreover, 1-bit ADC achieves the Additive White Gaussian Noise (AWGN) channel capacity for BPSK signaling [46]. However, it is questionable how BPSK modulated signals can be equalized under the constraint of 1-bit quantization, since the amplitude and phase information of received signal are lost. The important point is to preserve the equalization performance as much as possible with 1-bit quantization and FTSR sampling is investigated to compensate the performance degradation due to 1-bit ADC.

The performance of CP based MMSE equalization in response to 1-bit ADC with BPSK signaling is not known. We concentrate on a scenario such that channel estimation is performed at the beginning of each block with high precision ADC by training symbols. Following that, other received samples are quantized by 1-bit ADC where the power saving comes from. It is assumed that channel is complex Gaussian with a random propagation delay and noise is circularly symmetric complex white Gaussian yielding a complex valued signal. The real and complex values of the received samples are quantized in separate 1-bit ADC and MMSE equalizer is performed with limited information due to 1-bit quantization as given in Figure 4.13. Accordingly, the equalizer can only reach the quantized version of the channel outputs, since the

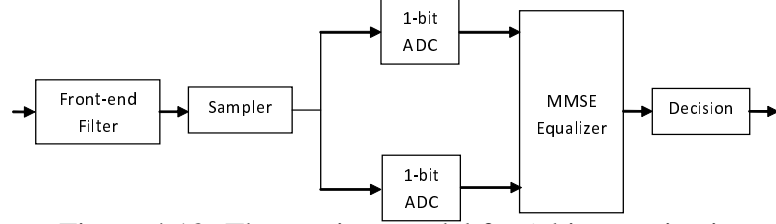


Figure 4.13: The receiver model for 1-bit quantization

sampled signals are quantized by 1-bit ADC with zero threshold comparator as

$$y_q(m, g) = \text{sign}(y_m^g) \quad (4.33)$$

which is equal to

$$y_q(m, g) = \begin{cases} -1 - 1j, & \Re\{y_m^g\} \leq 0, \Im\{y_m^g\} \leq 0 \\ -1 + 1j, & \Re\{y_m^g\} \leq 0, \Im\{y_m^g\} > 0 \\ 1 - 1j, & \Re\{y_m^g\} > 0, \Im\{y_m^g\} \leq 0 \\ 1 + 1j, & \Re\{y_m^g\} > 0, \Im\{y_m^g\} > 0 \end{cases} \quad (4.34)$$

where $\Re(\cdot)$, and $\Im(\cdot)$ denote the real and imaginary part of the sample respectively. Then, the mismatched MMSE filtering with identity noise auto-correlation matrix is performed as

$$\mathbf{W}_q = \mathbf{H}_{ftsr}^H (\mathbf{H}_{ftsr} \mathbf{H}_{ftsr}^H + \mathbf{I}_{GN})^{-1} \quad (4.35)$$

where \mathbf{I}_{GN} is a $GN \times GN$ identity matrix.

This model is numerically analyzed. According to that, there is a single tap Rayleigh fading channel whose propagation delay is uniformly distributed in $[0, T]$ for a modulation format BPSK in response to block length of 64 and 30% excess bandwidth. It is assumed that timing synchronization is not perfect and timing errors occur during timing synchronization creating ISI terms. The resultant impact of 1-bit ADC to the CP based MMSE equalization including FTSR sampling with $G = 2$ is given in Figure 4.14. Although 1-bit quantization with FTSR sampling achieves a closer equalization performance with respect to the unquantized one, SR sampling gradually deviates from the unquantized one with incremental SNR. Note that although this result presents the initial communication theoretical step regarding CP based equalization for the complex 1-bit quantization problem, the compensation of 1-bit quantization for equalization remains open when there are higher number of channel taps and constellation sizes.

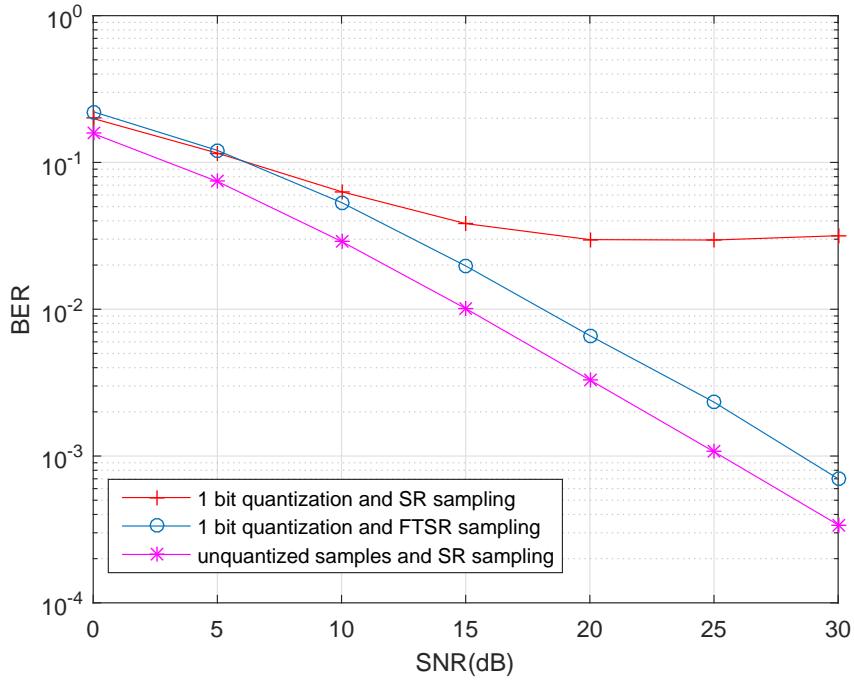


Figure 4.14: The performance of CP based MMSE equalization with 1-bit quantization for single tap Rayleigh fading channel

4.7 Conclusions

The impact of sampling rate on the performance of CP based MMSE equalization for frequency selective wireless channels is justified when pulse matched filtering is used. It is shown that FTSR sampling leads to an improvement in average MSE when there are unequally spaced ISI channel taps and excess bandwidth. Moreover, our BER results give that there is a significant gain due to FTSR sampling. The major drawback of the proposed FTSR sampling method is the high MMSE equalization complexity caused by matrix inversion despite CP. This complexity is compensated by proposing a novel approach with complexity $O(N)$ based on the property of inverting a block circulant matrix.

FTSR sampling is a remedy against two major problems in practice. The first one takes place in case of insufficient CP. By FTSR sampling 20% CP reduction can be tolerated, whereas the performance of SR sampled CP based MMSE equalization is heavily disturbed by 20% CP reduction. Another important application of FTSR sampling for CP based MMSE equalization arises in 1-bit quantization. In a special

scenario, we show that BPSK transmitted symbols can be satisfactorily equalized with the help of FTSR sampling.

CHAPTER 5

FASTER THAN SYMBOL RATE SAMPLING IN MULTIUSER COMMUNICATION

The major challenge of multiuser communication surfaces when multiple users transmit their symbols simultaneously. Principally, the maximum number of simultaneous transmissions is limited by DoF. Excess bandwidth creates additional DoF referring to increase in the number of simultaneous transmissions or users. However, excess bandwidth cannot be used efficiently by SR sampling and that's why Faster Than Nyquist (FTN) signaling is proposed. As an alternative to FTN signaling, FTSR sampling is studied for multiuser communication in this chapter. In particular, the results of FTSR sampling for single user communication in previous chapters are generalized to multiuser communication and how efficiently the potential of excess bandwidth has been used in a multiuser frequency selective wireless channel depending on sampling rate is investigated. At this point, FTSR sampling in a multiuser setting is analyzed regarding DoF and rank of channel matrix which are independent of noise statistics. Since FTSR sampling results in correlated noise, practical applications of FTSR sampling including MMSE multiuser detectors and canonical MMSE based iterative receivers are presented to observe the impact of correlated noise.

5.1 Interference Mitigation in Multiuser Communication by FTSR Sampling

Multiple users can transmit at the same time and frequency by using the same pulse shape or waveform. In this challenging multiuser settings, excess bandwidth becomes more critical, since it creates additional DoF and can increase the maximum number

of simultaneous transmissions [67]. However, it is crucial to emphasize that excess bandwidth disappears in case of SR sampling due to aliasing. Considering the fact that current resources are not enough to satisfy multiple users' demands on future wireless networks [68], it is further important to exploit all available bandwidth. FTN signaling is proposed to gain the benefit of excess bandwidth due to the fact that excess bandwidth disappears in SR sampling when symbols are orthogonally sent [69], [70], [71], [72]. Although it is shown that FTN signaling efficiently exploits the excess bandwidth, it leads to complicated receiver design [73]. Moreover, adopting the FTN signaling to the existing networks requires modification at transmitters as well as receivers. In this chapter, FTSR sampling is proposed as an alternative to FTN signaling in order to benefit from excess bandwidth with low complexity receiver operation and no modification at transmitters.

In FTSR sampling, the received signal is sampled at faster than transmission rate forming additional signal space dimension. Indeed, there is a similarity between FTSR sampling and multiple antenna systems when extra samples are regarded as virtual antennas. It is well-known that employing multiple antennas can reduce the MAI and enhance detection, because it creates additional DoF [74], [75]. Although one may expect that FTSR sampling can become advantageous because of the similarity with multiple antenna structure, FTSR sampling creates correlation among channel taps and correlated noise that may in the end counter-act the gain of additional signal space dimensions. Therefore, a detailed analysis of FTSR sampling is presented here to show its potential for multiuser communication.

There are various studies in which FTSR sampling is instrumental for interference suppression in multiuser communication [20], [21], [22], [23], [25]. However, those studies are short of fully characterizing FTSR sampling by considering the potential of excess bandwidth and drawback of correlated noise. Moreover, the concept of FTSR sampling was not investigated in detail, and it is unclear when and for which conditions FTSR sampling works better. Those studies did not consider FTSR sampling as an alternative to FTN signaling as well whose benefit can be exploited with simple receiver architectures.

A multiple access transmission is considered over frequency selective wireless chan-

nels with excess bandwidth leading to MAI, IBI and ISI. Our goal is to fully characterize the behavior of FTSR sampling for this environment with the ultimate aim of exploiting excess bandwidth, and hence mitigating interference sources more efficiently. Low complexity receiver is one of the primary concern while taking the advantage of excess bandwidth with FTSR sampling, that's why, simple receiver front-ends employing pulse matched filtering instead of channel matched filtering is preferred.

The contributions of this chapter are two-fold. The first contribution is to show that FTSR sampling can totally exploit DoF gain due to excess bandwidth in a multiple access frequency selective wireless channel. Further results illustrate that FTSR sampling introduces significant rank advantage provided that ISI channel taps due to frequency selective wireless channel are unequally spaced and excess bandwidth exists. The second contribution of this chapter is to observe the interference mitigation capability of FTSR sampling in practical applications including MMSE multiuser detectors and canonical MMSE based iterative receivers. It is illustrated that when two users transmit to a single receiver all with single antenna over a multiuser frequency selective wireless channel, MAI can be perfectly eliminated with FTSR sampling once ISI channel has unequally spaced taps and excess bandwidth exists. This result trivially refers to the fact that number of subscribers in a TDMA or FDMA network can be doubled.

The chapter is organized as follows. The efficiency of FTSR sampling in multiuser communication is analyzed in Section 5.2. The applications of FTSR sampling are presented in Section 5.3 and the chapter concludes with Section 5.4.

5.2 Analysis of FTSR Sampling in Multiuser Communication

A multiple access channel is considered throughout the chapter such that each user sends their symbols to a single receiver all equipped with single antenna over a frequency selective wireless channel. FTSR sampling is assessed for this scenario to improve the system performance by making use of excess bandwidth. More specifically, the aim is to obtain more efficient interference mitigation by sampling the received signal faster than transmission rate over superimposed ISI channel. Our analysis is

divided into 2 main parts including DoF analysis at infinite SNR for Gaussian distributed input symbols, and rank analysis for any SNR and input distribution. Since FTSR sampling is proposed as an alternative to FTN signaling, a comparison is made between these two methods as well.

5.2.1 DoF Analysis

We concentrate on a canonical multiple access channel such that there are many transmitters and a single receiver all with single antenna. Transmitters perform linear modulation for all M users

$$s^i(t) = \sum_n x_n^i p(t - nT) \quad (5.1)$$

such that $i = 1, 2, \dots, M$, x_n^i is the n^{th} transmitted symbol of i^{th} user, $p(t)$ is a real transmitter filter and T is the symbol period. It is assumed that total average transmission power is E_s and each user transmits with an average power of E_s/M . Users' channels are modeled as having $(L + 1)$ multipath components such that

$$c^i(t) = \sum_{k=0}^L \alpha_k^i \delta(t - \tau_k^i) \quad (5.2)$$

where α_k^i represents k^{th} path's complex channel coefficient and τ_k^i is its propagation delay which is uniformly distributed between 0 and the maximum channel delay spread. Channel coefficients are zero-mean complex Gaussian. It is assumed that channel state information of users are perfectly known at the receiver. Symbols are transmitted in blocks with block length N in which $(L + 1) < N$ and the channel is taken as static during each block and changes independently among blocks [35]. Moreover, zeros are padded among blocks at the transmitter to avoid IBI and then removed at the receiver.

The symbol block after passing through the channel can be represented as

$$\tilde{s}^i(t) = \sum_{n=0}^{N-1} x_n^i p_c^i(t - nT) \quad (5.3)$$

where $p_c^i(t) = p(t) * c^i(t)$. The received signal can then be written as

$$r(t) = \tilde{s}^i(t) + w(t) \quad (5.4)$$

where $w(t)$ is the additive circularly symmetric complex white Gaussian noise with zero mean and power spectral density N_0 . To analyze the DoF for this model, the capacity of single user continuous time ISI channel is firstly stated when excess bandwidth is r . Accordingly, the capacity can be expressed for Gaussian input distribution by omitting the superscript i as [76]

$$C(\Gamma) = \int_0^{\frac{1+r}{2T}} \log_2(1 + \Gamma|P_c(f)|^2)df \quad (5.5)$$

where $\Gamma = E_s/MN_0$ and

$$P_c(f) = P(f) \sum_{k=0}^L \alpha_k \exp(-j2\pi f\tau_k) \quad (5.6)$$

such that $p_c(t) = p(t) * (\sum_{k=0}^L \alpha_k \delta(t - \tau_k))$. When the sampling rate is $1/T$, $P_c(f)$ is subject to aliasing due to excess bandwidth and the capacity becomes

$$C^{sr}(\Gamma) = \int_0^{\frac{1}{2T}} \log_2(1 + \Gamma|P_c^{sr}(f)|^2)df \quad (5.7)$$

such that

$$P_c^{sr}(f) = \sum_{k=-\infty}^{\infty} P_c(f + k/T), -1/2T \leq f \leq 1/2T. \quad (5.8)$$

When $\Gamma \rightarrow \infty$,

$$\lim_{\Gamma \rightarrow \infty} C^{sr}(\Gamma) = \frac{1}{2T} \log \Gamma. \quad (5.9)$$

On the other hand, faster sampling rates can yield

$$C^{ftsr}(\Gamma) = \int_0^{\frac{1+r}{2T}} \log_2(1 + \Gamma|P_c^{ftsr}(f)|^2)df \quad (5.10)$$

where

$$P_c^{ftsr}(f) = \sum_{k=-\infty}^{\infty} P_c(f + k(1+r)/T), -(1+r)/2T \leq f \leq (1+r)/2T \quad (5.11)$$

and

$$\lim_{\Gamma \rightarrow \infty} C^{ftsr}(\Gamma) = \frac{1+r}{2T} \log \Gamma. \quad (5.12)$$

Multiplexing gain is defined as $\lim_{\Gamma \rightarrow \infty} \frac{C(\Gamma)}{\log(\Gamma)}$ [77]. The multiplexing gain ratio of $C^{ftsr}(\Gamma)$ to $C^{sr}(\Gamma)$ can then be found by using Eqn. (5.9) and Eqn. (5.12) as

$$\lim_{\Gamma \rightarrow \infty} \frac{C^{ftsr}(\Gamma)}{C^{sr}(\Gamma)} = 1 + r. \quad (5.13)$$

Generalizing this result from single user channel to the multiple access channel when $\Gamma \rightarrow \infty$ [67]

$$R_i < C^{ftsr}(\Gamma) = (1 + r)C^{sr}(\Gamma) \quad (5.14)$$

$$\vdots \quad (5.15)$$

$$\sum_{i=1}^M R_i < C^{ftsr}(M\Gamma) = (1 + r)C^{sr}(M\Gamma) \quad (5.16)$$

where R_i represents the i^{th} user's achievable rate. Eqn. (5.14), Eqn. (5.15) and Eqn. (5.16) state that there is a $(1 + r)$ -fold multiplexing gain improvement for FTSR sampling due to excess bandwidth. Since multiplexing gain refers to DoF [78], there is a DoF advantage for a multiple access channel in case of FTSR sampling once excess bandwidth is employed. To summarize, SR sampled channel cannot exploit the all available DoF in the channel, whereas FTSR sampled channel can make use of it.

5.2.2 Rank Analysis

A certain portion of bandwidth and time are assigned to a user for communication. The desire is to pack more than one user for the given bandwidth and time with FTSR sampling by exploiting excess bandwidth properly when users employ the same waveform. In fact, SR sampling cannot use excess bandwidth efficiently, whereas FTSR sampling can according to DoF analysis. We investigate the possible increase in the number of users for both orthogonal and non-orthogonal signaling. Here, orthogonal signaling refers to the case of equally spaced channel taps with symbol period and non-orthogonal transmission occurs when channel taps are unequally spaced. Our performance measure is the rank of the FTSR sampled channel matrix normalized with transmission block length.

DoF advantage indicates the maximum increase in normalized rank depending on FTSR sampling and excess bandwidth, and its importance comes from this fact. Hence, one can know that normalized rank can become maximum $(1 + r)$ for strictly bandlimited channel which has excess bandwidth r due to FTSR sampling. Therefore,

normalized rank for strictly bandlimited channel lies in the interval of

$$1 \leq \text{normalized}(\text{rank}) \leq (1 + r). \quad (5.17)$$

Indeed, rank means the used DoF in the channel [79] and how much the available DoF can be used by FTSR sampled channel is investigated through a rank analysis.

To evaluate the inequality in Eqn. (5.17) more explicitly, two transmitters are considered without any loss of generality which have identical waveforms and send their signals at the same time and bandwidth to a single receiver. Transmitted symbols, $\{x_n^1\}$'s and $\{x_n^2\}$'s are i.i.d., where $\{x_n^1\}$ represents the first user's transmitted symbol sequence and $\{x_n^2\}$ belongs to the second transmitter. Pulse matched filtering the signal component in Eqn. (5.4) gives

$$d(t) = \sum_{n=0}^{N-1} x_n^1 \tilde{g}^1(t - nT) + \sum_{n=0}^{N-1} x_n^2 \tilde{g}^2(t - nT) \quad (5.18)$$

where $\tilde{g}^i(t) = p_c^i(t) * p(-t)$ and the overall signal is

$$y(t) = d(t) + z(t) \quad (5.19)$$

such that

$$z(t) = w(t) * p(-t). \quad (5.20)$$

Eqn. (5.18) can be written based on Eqn. (5.2) and Eqn. (5.3) as

$$d(t) = \sum_{n=0}^{N-1} \sum_{k=0}^L x_n^1 \alpha_k^1 \tilde{p}(t - nT - \tau_k^1) + \sum_{n=0}^{N-1} \sum_{k=0}^L x_n^2 \alpha_k^2 \tilde{p}(t - nT - \tau_k^2) \quad (5.21)$$

where $\tilde{p}(t) = p(t) * p(-t)$. Sampling the signal for $l = 0, \dots, N - 1$ and $g = 0, 1, \dots, G - 1$ yields $\{d(lT - gT/G)\}$ where G is the oversampling ratio, which is 2 here for ease of explanation. In accordance with that, the samples at lT correspond to SR samples for $g = 0$

$$d_l^{\text{SR}} = d(lT) \quad (5.22)$$

and extra samples for $g = 1$

$$d_l^{\text{OS}} = d(lT - T/2). \quad (5.23)$$

For ease of presentation, the summations in Eqn. (5.21) will be written somewhat differently so that

$$d_l^{\text{srs}} = \sum_{m=l-N+1}^l \sum_{k=0}^L x_{l-m}^1 \alpha_k^1 \tilde{p}(mT - \tau_k^1) + \sum_{m=l-N+1}^l \sum_{k=0}^L x_{l-m}^2 \alpha_k^2 \tilde{p}(mT - \tau_k^2). \quad (5.24)$$

On the other hand, oversampling results in

$$d_l^{\text{os}} = \sum_{m=l-N+1}^l \sum_{k=0}^L x_{l-m}^1 \alpha_k^1 \tilde{p}(mT - T/2 - \tau_k^1) + \sum_{m=l-N+1}^l \sum_{k=0}^L x_{l-m}^2 \alpha_k^2 \tilde{p}(mT - T/2 - \tau_k^2). \quad (5.25)$$

In order to write Eqn. (5.24) and Eqn. (5.25) in matrix notation, we define

$$\gamma_m^i = \sum_{k=0}^L \alpha_k^i \tilde{p}(mT - \tau_k^i) \quad (5.26)$$

and

$$\beta_m^i = \sum_{k=0}^L \alpha_k^i \tilde{p}(mT - T/2 - \tau_k^i). \quad (5.27)$$

The overall vector-matrix representation is obtained as in Eqn. (5.28)

$$\begin{pmatrix} y_0^{\text{srs}} \\ y_1^{\text{srs}} \\ \vdots \\ y_{N-1}^{\text{srs}} \\ y_0^{\text{os}} \\ y_1^{\text{os}} \\ \vdots \\ y_{N-1}^{\text{os}} \end{pmatrix} = \begin{pmatrix} \gamma_0^1 & \gamma_{-1}^1 & \cdots & \gamma_{-N+1}^1 & \gamma_0^2 & \gamma_{-1}^2 & \cdots & \gamma_{-N+1}^2 \\ \gamma_1^1 & \gamma_0^1 & \cdots & \gamma_{-N+2}^1 & \gamma_1^2 & \gamma_0^2 & \cdots & \gamma_{-N+2}^2 \\ \vdots & \vdots & \vdots & \vdots & \vdots & \vdots & \vdots & \vdots \\ \gamma_{N-1}^1 & \gamma_{N-2}^1 & \cdots & \gamma_0^1 & \gamma_{N-1}^2 & \gamma_{N-2}^2 & \cdots & \gamma_0^2 \\ \beta_0^1 & \beta_{-1}^1 & \cdots & \beta_{-N+1}^1 & \beta_0^2 & \beta_{-1}^2 & \cdots & \beta_{-N+1}^2 \\ \beta_1^1 & \beta_0^1 & \cdots & \beta_{-N+2}^1 & \beta_1^2 & \beta_0^2 & \cdots & \beta_{-N+2}^2 \\ \vdots & \vdots & \vdots & \vdots & \vdots & \vdots & \vdots & \vdots \\ \beta_{N-1}^1 & \beta_{N-2}^1 & \cdots & \beta_0^1 & \beta_{N-1}^2 & \beta_{N-2}^2 & \cdots & \beta_0^2 \end{pmatrix} \begin{pmatrix} x_0^1 \\ x_1^1 \\ \vdots \\ x_{N-1}^1 \\ x_0^2 \\ x_1^2 \\ \vdots \\ x_{N-1}^2 \end{pmatrix} + \begin{pmatrix} z_0^{\text{srs}} \\ z_1^{\text{srs}} \\ \vdots \\ z_{N-1}^{\text{srs}} \\ z_0^{\text{os}} \\ z_1^{\text{os}} \\ \vdots \\ z_{N-1}^{\text{os}} \end{pmatrix} \quad (5.28)$$

where y_l^{srs} and z_l^{srs} represent the SR samples of the received signal and the noise respectively. Similarly, y_l^{os} and z_l^{os} denote the additional samples. Then, the discrete-time model can be expressed for a total transmission power E_s as

$$\mathbf{y} = \sqrt{\frac{E_s}{2}} \mathbf{H} \mathbf{x} + \mathbf{z} \quad (5.29)$$

where $\mathbf{y} = [y_0^{\text{srs}} \cdots y_{N-1}^{\text{srs}} y_0^{\text{os}} \cdots y_{N-1}^{\text{os}}]^T$, $\mathbf{x} = [x_0^1 \cdots x_{N-1}^1 x_0^2 \cdots x_{N-1}^2]^T$, and \mathbf{z} is the additive Gaussian noise such that $\mathbf{z} = [z_0^{\text{srs}} \cdots z_{N-1}^{\text{srs}} z_0^{\text{os}} \cdots z_{N-1}^{\text{os}}]^T$. The channel matrix \mathbf{H} is of size $2N \times 2N$ due to FTSR sampling, whereas it is a $N \times 2N$ matrix in case of SR sampling. The rank of \mathbf{H} will state whether one system can achieve the benefit of excess bandwidth by FTSR sampling or not. Although there is a DoF gain in the channel due to excess bandwidth exploited by FTSR sampling, it may not necessarily mean that all FTSR sampled channels employing excess bandwidth can achieve a rank enhancement. We evaluate this for orthogonal signaling when channel taps are equally spaced with $\tau_k = kT$ and non-orthogonal signaling in case of unequally spaced channel taps with $\tau_k \neq kT$.

Lemma 5.2.1 *Equally spaced channel taps, i.e., $\tau_k = kT$ for integer k , cannot create extra rank and normalized rank remains the same in bandlimited multiple access channels despite excess bandwidth and FTSR sampling.*

Proof 5.2.2 *Consider a channel matrix when $N = 4$ and $L = 2$*

$$\mathbf{H}_{syn} = \begin{pmatrix} \alpha_0^1 & \alpha_1^1 & \alpha_2^1 & 0 & \alpha_0^2 & \alpha_1^2 & \alpha_2^2 & 0 \\ 0 & \alpha_0^1 & \alpha_1^1 & \alpha_2^1 & 0 & \alpha_0^2 & \alpha_1^2 & \alpha_2^2 \\ 0 & 0 & \alpha_0^1 & \alpha_1^1 & 0 & 0 & \alpha_0^2 & \alpha_1^2 \\ 0 & 0 & 0 & \alpha_0^1 & 0 & 0 & 0 & \alpha_0^2 \\ \beta_0^1 & \beta_1^1 & \beta_2^1 & \beta_3^1 & \beta_0^2 & \beta_1^2 & \beta_2^2 & \beta_3^2 \\ \beta_{-1}^1 & \beta_0^1 & \beta_1^1 & \beta_2^1 & \beta_{-1}^2 & \beta_0^2 & \beta_1^2 & \beta_2^2 \\ \beta_{-2}^1 & \beta_{-1}^1 & \beta_0^1 & \beta_1^1 & \beta_{-2}^2 & \beta_{-1}^2 & \beta_0^2 & \beta_1^2 \\ \beta_{-3}^1 & \beta_{-2}^1 & \beta_{-1}^1 & \beta_0^1 & \beta_{-3}^2 & \beta_{-2}^2 & \beta_{-1}^2 & \beta_0^2 \end{pmatrix} \quad (5.30)$$

where

$$\begin{aligned} \beta_{-3}^i &= c_3\alpha_0^i + c_4\alpha_1^i + c_5\alpha_2^i \\ \beta_{-2}^i &= c_2\alpha_0^i + c_3\alpha_1^i + c_4\alpha_2^i \\ \beta_{-1}^i &= c_1\alpha_0^i + c_2\alpha_1^i + c_3\alpha_2^i \\ \beta_0^i &= c_0\alpha_0^i + c_1\alpha_1^i + c_2\alpha_2^i \\ \beta_1^i &= c_0\alpha_0^i + c_0\alpha_1^i + c_1\alpha_2^i \\ \beta_2^i &= c_1\alpha_0^i + c_0\alpha_1^i + c_0\alpha_2^i \\ \beta_3^i &= c_2\alpha_0^i + c_1\alpha_1^i + c_0\alpha_2^i \end{aligned} \quad (5.31)$$

such that $c_q = \tilde{p}(-qT - T/2)$ for $q = 0, 1, \dots, 5$ and recalling the symmetry in $\tilde{p}(t)$. The 5th row of \mathbf{H}_{syn} cannot be written in terms of a linear combination of the first 4 rows. That is, 5th row is linearly independent from the first 4 row. To illustrate, the first term of 5th row is composed of α_0^1 , α_1^1 and α_2^1 , whereas only α_0^1 is available in the first 4 row corresponding to the first term. The same discussion is valid for the 6th row such that it cannot be written by using the first 5 rows. This fact can be explained by considering the first term in the 6th row, which is composed of 3 terms, α_0^1 , α_1^1 and α_2^1 , however only 2 terms from the 1st and 5th row are available. On the other hand, once the first 6 rows are given, one can attain the remaining rows. This emphasizes that the rank of \mathbf{H}_{syn} is equal to $N + L$. Since this property is independent from the actual

values of N and L , it can be generalized for any N and L . Then, for a bandlimited channel, i.e., $N \rightarrow \infty$, the normalized rank becomes

$$\lim_{N \rightarrow \infty} \frac{N + L}{N} = 1 \quad (5.32)$$

showing that the equally spaced channel taps cannot benefit from excess bandwidth.

This result can be supported by a numerical example. When the channel has 10 equally spaced complex Gaussian channel taps, the empirical cumulative distribution function (cdf) of the channel matrix rank is attained by generating 10,000 random channel realizations for 0.3 excess bandwidth. The cdf of rank, $F(\text{rank})$, is plotted for different block lengths and rank is normalized with respect to the block length N such that a rank of 1 expresses that there is no rank advantage of FTSR sampling. As can be seen in Figure 5.1, normalized rank goes to 1 for bandlimited channels, i.e., $N \rightarrow \infty$.

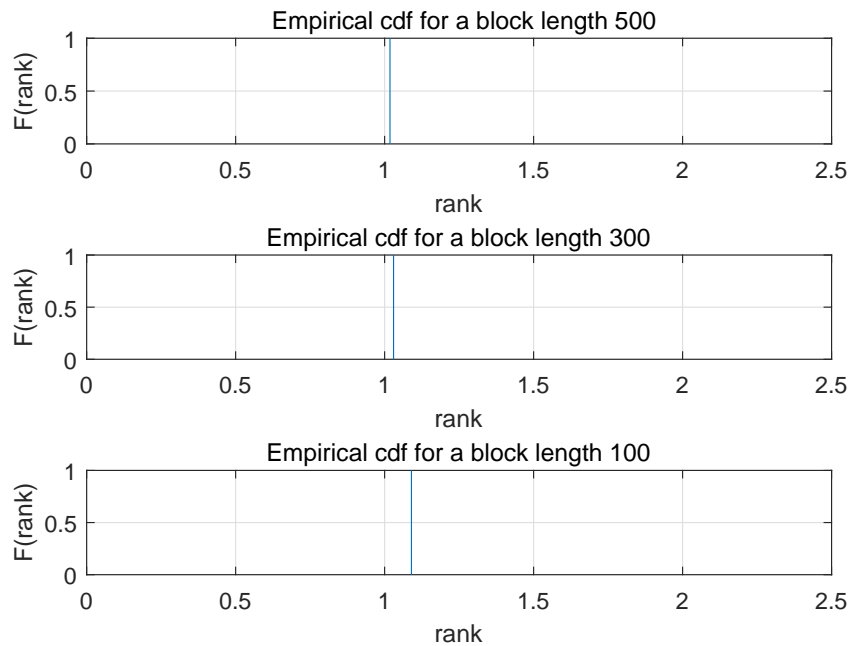


Figure 5.1: The cdf of FTSR sampled channel matrix rank for 10 equally spaced taps and 0.3 excess bandwidth for 2 users

Equally spaced channel taps with symbol period is a theoretical approach, since in practice channel taps are randomly distributed between 0 and a maximum delay spread implying that they are unequally spaced or asynchronous. Asynchronism creates linear independence among signals. In particular, it is straightforward to express that the rows and columns of FTSR sampled channel matrix becomes independent for small N when channel taps are unequally spaced unlike the channel matrix that forms in case of equally spaced channel taps in Eqn. (5.30). At this point, it is beneficial to give a simple example. Assume that $N = 4$ for both users and each user has a channel with 2 taps whose coefficients are equal but propagation delays are different as given in Table 5.1. Pulse shape is raised cosine with a roll off factor of 0.3.

1 th user channel	2 nd user channel
$\tau_0^1 = 0$	$\tau_0^2 = 0$
$\tau_1^1 = 3T/4$	$\tau_1^2 = 5T/4$
$\alpha_0^1 = 0.8$	$\alpha_0^2 = 0.8$
$\alpha_1^1 = 0.6$	$\alpha_1^2 = 0.6$

Table 5.1: Example channels of both users

Then, the resultant channel matrix becomes

$$\mathbf{H}_{asy} = \begin{pmatrix} 0.97 & 0.53 & -0.09 & 0.03 & 0.70 & 0.53 & 0.17 & -0.05 \\ 0.40 & 1.03 & 0.03 & 0 & 0.43 & 0.67 & 0.39 & -0.03 \\ -0.05 & 0.97 & 0.53 & -0.09 & 0.03 & 0.70 & 0.53 & 0.17 \\ -0.10 & 0.40 & 1.03 & 0.03 & -0.11 & 0.43 & 0.67 & 0.39 \\ 0.02 & -0.05 & 0.97 & 0.53 & -0.01 & 0.03 & 0.70 & 0.53 \\ 0.04 & -0.10 & 0.40 & 1.03 & 0.04 & -0.11 & 0.43 & 0.67 \\ 0 & 0.02 & -0.05 & 0.97 & 0 & -0.01 & 0.03 & 0.70 \\ -0.01 & 0.04 & -0.10 & 0.40 & -0.02 & 0.04 & -0.11 & 0.43 \end{pmatrix}. \quad (5.33)$$

Due to Eqn. (5.33), the rank becomes 8 even if channel coefficients are the same due to asynchronism among the matrix entries. Thus, normalized rank is equal to 2 referring that FTSR sampled channel matrix doubles the rank of SR sampling. However, it does not mean that FTSR sampling always doubles the normalized rank when channel taps are unequally spaced. In fact, the normalized rank gradually decreases

for finite N as will be explained in Lemma 5.2.3.

Lemma 5.2.3 *Normalized rank of the FTSR sampled channel matrix decreases with incremental and finite N when channel taps are unequally spaced.*

Proof 5.2.4 *The $2N \times 2N$ channel matrix \mathbf{H} in Eqn. (5.28) can be decomposed as*

$$\mathbf{H} = \begin{pmatrix} \mathbf{H}_{srs}^1 & \mathbf{H}_{srs}^2 \\ \mathbf{H}_{os}^1 & \mathbf{H}_{os}^2 \end{pmatrix} \quad (5.34)$$

where \mathbf{H}_{srs}^1 , \mathbf{H}_{srs}^2 , \mathbf{H}_{os}^1 , \mathbf{H}_{os}^2 can be taken as banded $N \times N$ non-Hermitian Toeplitz matrices and denote the matrix due to SR and FTSR sampling for the first and second user respectively. The band of these matrices increases for higher N and some eigenvalues exponentially go to zero implying rank degradation [80]. Note that \mathbf{H} can be viewed as a block Toeplitz matrix by elementary matrix operations with changing the order of rows and columns. Since the same property is still valid for block Toeplitz matrix, normalized rank decreases for higher block lengths [80].

Lemma 5.2.3 brings a boundary condition for the normalized rank advantage of FTSR sampling in case of finite N . Another limiting condition occurs for infinite N . It is known that rank cannot be greater than the available DoF as stated in Eqn. (5.17). Since DoF is equal to $2(1+r)WT$ for the excess bandwidth r , the normalized rank converges to $(1+r)$ when $N \rightarrow \infty$, i.e., in case of bandlimited channels. This gives the result of observing the extra normalized rank due to excess bandwidth implying that extra users can be packed for a given bandwidth.

Empirical cdf of the channel matrix rank can be obtained by generating 10,000 random channel realizations for 10 unequally spaced complex Gaussian channel taps that are distributed uniformly between 0 and 10 symbol intervals with a raised cosine pulse shape of 0.3 excess bandwidth. There is an asynchronism between users' channels as well as the channel taps. Rank is normalized with respect to the block length N and plotted for different block lengths as given in Figure 5.2. According to Figure 5.2, as the block length becomes larger, the rank converges to 1.3 as predicted by the expression in Eqn. (5.13). That is, the maximum simultaneous transmissions or total number of users in a multiple access ISI channel can be increased in direct proportion to excess bandwidth by FTSR sampling.

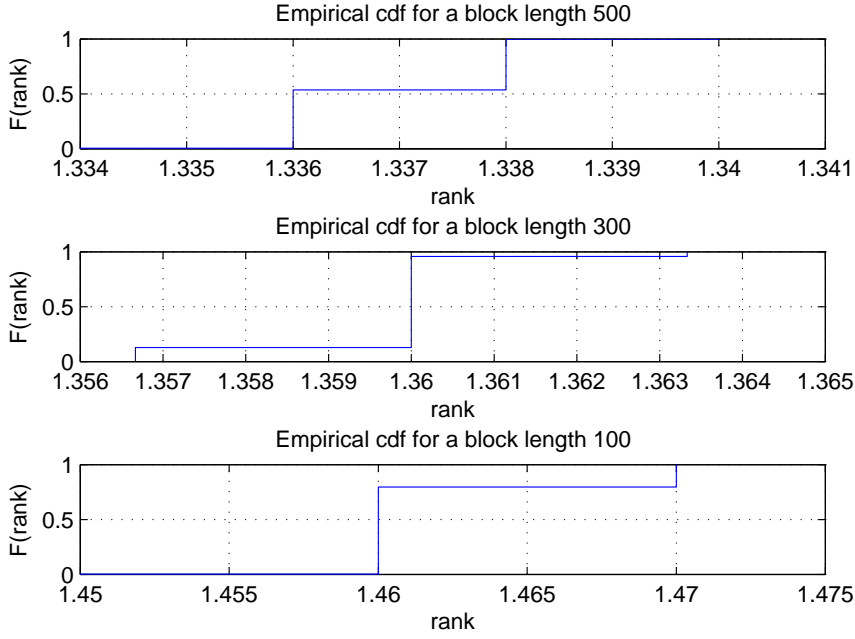


Figure 5.2: The cdf of FTSR sampled channel matrix rank for 10 unequally spaced taps and 0.3 excess bandwidth for 2 users

This result is generalized for 5 users which simultaneously transmit their symbols to a receiver. Similarly, there are 10 unequally spaced complex Gaussian channel taps that are distributed uniformly between 0 and 10 symbol intervals with a raised cosine pulse shape of 0.3 excess bandwidth and $G = 2$. The same result is observed with the previous case as presented in Figure 5.3. It shows that the increase in the normalized rank due to FTSR sampling is independent of the number of users provided that excess bandwidth exists and channel taps are unequally spaced. Note that increasing the sampling rate beyond 2 gives the same gain, since excess bandwidth has already been exploited and there is nothing to gain.

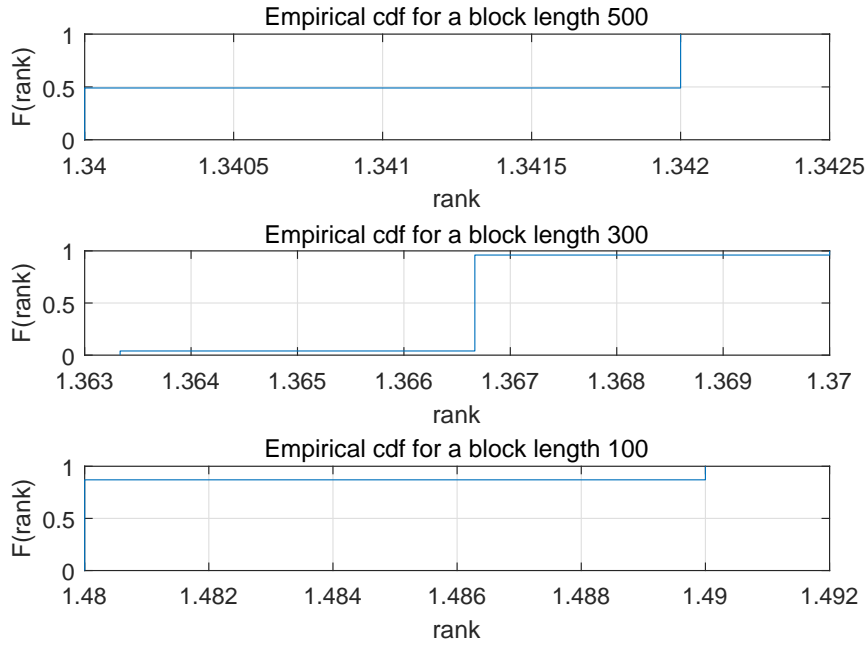


Figure 5.3: The cdf of FTSR sampled channel matrix rank for 10 unequally spaced taps and 0.3 excess bandwidth for 5 users

Users can experience similar multipath fading profiles in rural areas or urban areas when they are geographically close to each other. Even if the channel taps are unequally spaced, users may have nearly identical channels. This case is evaluated in Figure 5.4 showing that normalized rank becomes 1 despite FTSR sampling. Especially, it is not hard to predict this situation by observing the channel matrix in Eqn. (5.28). Therefore, it is important to have nonidentical channels among users as well as unequally spaced channel taps to exploit excess bandwidth advantage by FTSR sampling.

To summarize, additional DoF due to excess bandwidth cannot be exploited for synchronous transmission, whereas it is possible to attain this DoF for asynchronous multiuser transmission by FTSR sampling. Since the rank of \mathbf{H} does not depend on SNR [81], FTSR sampling can take advantage of the excess bandwidth at reasonable SNR for carefully designed systems. Moreover, our results are valid for any input distribution. Notice that the rank difference between the equally and unequally spaced taps can be explained as well based on a study that discusses the capacity of synchronous and asynchronous transmission which supports our results [79].

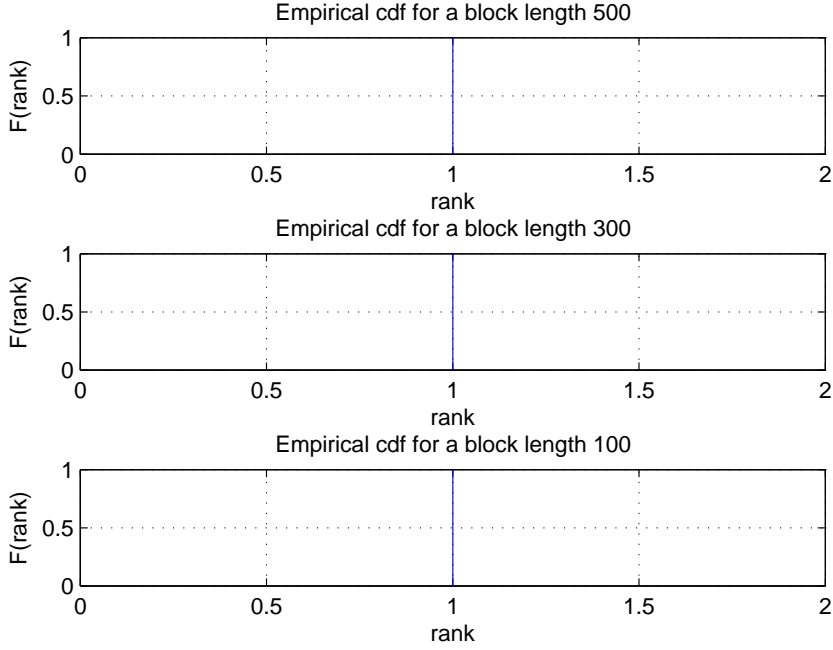


Figure 5.4: The cdf of FTSR sampled channel's matrix rank for 10 unequally spaced taps and 0.3 excess bandwidth when the user's channels are identical

5.2.3 Comparison with FTN Signaling

An alternative view of FTSR sampling is FTN signaling which is based on the idea of packing the orthogonal pulses closer than the Nyquist rate resulting in reduced symbol times without any loss in minimum Euclidean distance [82], [83]. However, it has recently been studied in a rather different concept such that conventional signaling does not exploit the available capacity due to excess bandwidth, whereas FTN signaling can achieve the potential capacity in the channel [69], [70], [71], [72]. Analogous to FTN signaling which aims to increase the number of bits for a given bandwidth, FTSR sampling can be used to increase the number of users. Although both methods can fully exploit the available DoF in the channel due to excess bandwidth, FTSR sampling is a more practical technique than FTN signaling. FTSR sampling requires modification only at the receiver side, while FTN needs modification at the transmitter side as well. Hence, FTSR sampling can be easily adopted in existing networks. Moreover, FTN complicates the receiver design that necessitates alternative methods [73]. The major impediment in FTSR sampling occurs when channel taps are equally spaced in which transmission become orthogonal. In this case, FTSR sampling cannot

exploit the advantage of excess bandwidth, however, this is a hypothetical situation not present in actual physical channels and practically unimportant.

5.3 Applications of FTSR Sampling

FTSR sampling has certain rank advantage in multiuser communication provided that excess bandwidth exists and channel taps are unequally spaced, which are inherent in today's communication systems. However, rank is independent of noise statistics. The basic goal of this part is to determine the benefits of FTSR sampling by considering the effect of correlated noise stemming from pulse matched filtering and FTSR sampling. Pulse matched filtering is preferred regarding practical concerns due to the fact that it is implemented with non-adaptive analog filter rather than channel matched filtering requiring adaptive analog filter. Moreover, it is important to show that the advantage of FTSR sampling can be exploited by practical receiver structures. Within this scope, a multiuser detector is firstly investigated, which is designed as the cascade of an FTSR sampled pulse matched filter and an MMSE filter. Although this detector has a well known structure, it is not analyzed in detail under different superimposed ISI channel conditions for practical system designs. The benefits of FTSR sampling are investigated for this detector by varying the pulse shaping filter, channel characteristics and sampling rate. To better explain the sampling rate effect, a virtual multiple input multiple output (MIMO) model is set up by FTSR sampling and analyzed for multiple access ISI channels with this equivalent MIMO structure in mind. Secondly, this FTSR sampled MMSE detector will be adapted to a canonical iterative receiver to increase the number of users in a multiple access network. What we propose is to add a new transmitter corresponding to each user that utilizes the same resources with this user, i.e., they transmit at the same time and frequency and use the same pulse shape for transmitter filter. If each pair of these two users' symbols are separated at the receiver, this will obviously double the number of users in a given TDMA or FDMA network. Therefore, throughout the chapter we focus on a scenario such that there are two transmitters and a single receiver all with single antenna and our aim is to separate these two users' symbols at the receiver with these settings.

5.3.1 FTSR Sampled MMSE Multiuser Detector

Multiuser detection is a highly utilized technique to suppress interference. The optimum multiuser detector has extreme complexity leading to growth in the popularity of sub-optimum multiuser detectors [33]. The sub-optimum detectors based on MMSE criterion have reasonable complexity with acceptable performance [33], [84], [85], [86], [87], [88]. A generic MMSE multiuser detector for 2 users is given in Figure 5.5 such that there are 2 channel matched filters each of which is matched to one user. It is important to emphasize that channel matched filters have to become adaptive and

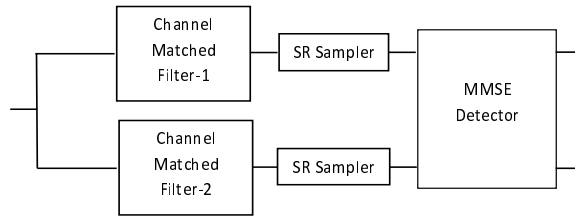


Figure 5.5: Conventional MMSE multiuser detector

change in each block because of varying channel conditions which results in high computational complexity. Therefore, we will study a lower complexity multiuser detector consisting of a pulse matched filter whose output is sampled at FTSR and processed by an MMSE detector given in Figure 5.6.

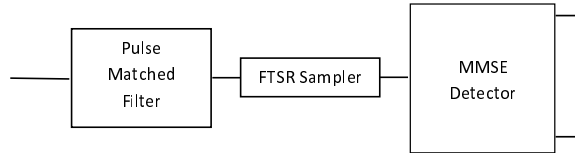


Figure 5.6: Low complexity MMSE multiuser detector

The noise becomes colored for the model in Figure 5.6 due to pulse matched filtering and FTSR sampling. Its auto-correlation function can be specified by using the Eqn. (5.20) such that

$$E[z(t)z^*(t + \tau)] = \sigma^2 \tilde{p}(\tau) \quad (5.35)$$

where σ^2 is the variance of $z(t)$. The noise auto-correlation matrix, $\mathbf{R}_z = E[\mathbf{z}\mathbf{z}^H]$ can be specified depending on Eqn. (5.35) in which the (q, r) element of \mathbf{R}_z becomes

$$[\mathbf{R}_z]_{q,r} = \sigma^2 \tilde{p}((q - r)T/2). \quad (5.36)$$

Since transmitted symbols are i.i.d., $E[\mathbf{x}\mathbf{x}^H] = \mathbf{I}_{2N}$, in which \mathbf{I}_{2N} is the $2N \times 2N$

identity matrix. Using orthogonality principle, the MMSE filter can be found as [56]

$$\mathbf{W}_{\text{mmse}} = \sqrt{\frac{E_s}{2}} \mathbf{H}^H \left(\frac{E_s}{2} \mathbf{H} \mathbf{H}^H + \mathbf{R}_z \right)^{-1} \quad (5.37)$$

where \mathbf{W}_{mmse} is the MMSE filter. The MMSE matrix, \mathbf{M} , which is equal to $E[(\mathbf{W}_{\text{mmse}} \mathbf{y} - \mathbf{x})(\mathbf{W}_{\text{mmse}} \mathbf{y} - \mathbf{x})^H]$, can then be written as

$$\begin{aligned} \mathbf{M} = & \mathbf{I}_{2N} - \sqrt{\frac{E_s}{2}} \mathbf{W}_{\text{mmse}} \mathbf{H} - \sqrt{\frac{E_s}{2}} \mathbf{H}^H \mathbf{W}_{\text{mmse}}^H + \\ & \mathbf{W}_{\text{mmse}} \left(\frac{E_s}{2} \mathbf{H} \mathbf{H}^H + \mathbf{R}_z \right) \mathbf{W}_{\text{mmse}}^H. \end{aligned} \quad (5.38)$$

The MSE of the m^{th} transmitted symbol is equal to

$$MSE_m = \mathbf{M}_{m,m} \quad (5.39)$$

for $m = 1, 2, \dots, 2N$, and $\mathbf{M}_{m,m}$ represents the m^{th} diagonal term of the matrix \mathbf{M} . In order to determine the SINR, a well known relation between the SINR and MSE is used [20], which is

$$SINR_m = \frac{1}{MSE_m} - 1. \quad (5.40)$$

The performance of detector presented in Figure 5.6 is determined in terms of Eqn. (5.40) when two single antenna transmitters send their symbols to a receiver which has also single antenna. Assume that there are 10 complex Gaussian channel taps and the propagation delay of each tap is uniformly distributed in $[0, 10T]$. The block length is 100 and G is equal to 2. The influence of excess bandwidth due to raised cosine pulse shape is observed in Figure 5.7. Excess bandwidth has a major effect on the SINR increase for FTSR sampling which is supported by the expression in Eqn. (5.13).

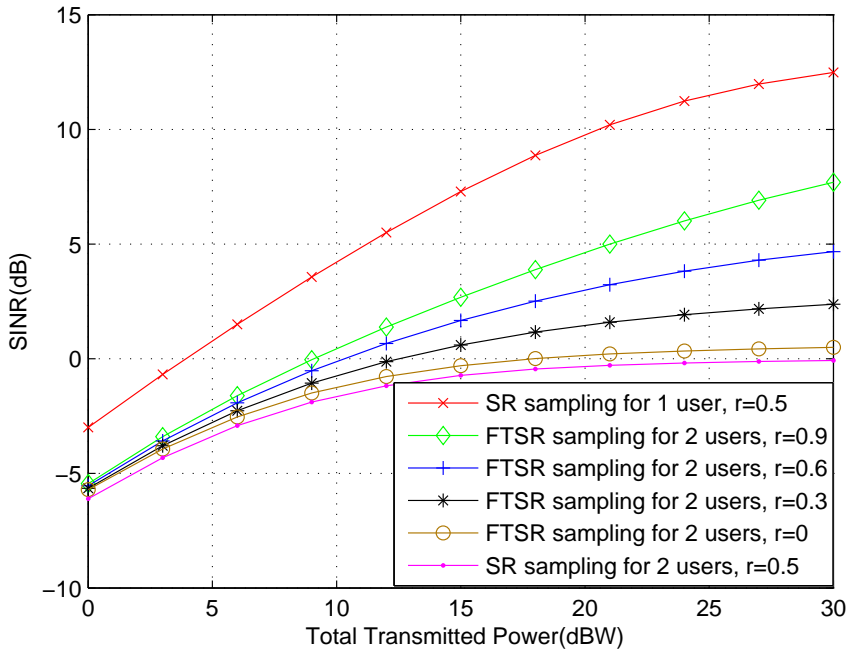


Figure 5.7: Excess bandwidth effect on the FTSR sampled MMSE detector for 10 unequally spaced complex Gaussian channel taps

The impact of FTSR sampling with $G = 2$ for equally T -spaced channel taps is studied in Figure 5.8. Similarly, there are 10 complex Gaussian channel taps, the block length is 100 and the pulse shaping filter is raised cosine with a roll off factor of 0.6. It is observed that FTSR sampling does not lead to any significant advantage for equally spaced channel taps even for a large excess bandwidth. The result is in parallel with Figure 5.1, which emphasizes the disappearance of the rank advantage for equally spaced channel taps.

To analyze the performance enhancement depending on the increase in sampling rate in a more rigorous manner, single antenna transmitters are regarded as a single transmitter with multiple antennas and extra samples in time domain are modeled as virtual antennas in spatial domain. This approach converts the multiple access channel into a virtual MIMO channel. The virtual MIMO has correlated channel taps and correlated noise due to FTSR sampling. Furthermore, separate coding has to be performed in virtual MIMO instead of joint coding due to independence of transmitted symbols from each other. Power is shared equally among users since channel state information at the transmitter is not available.

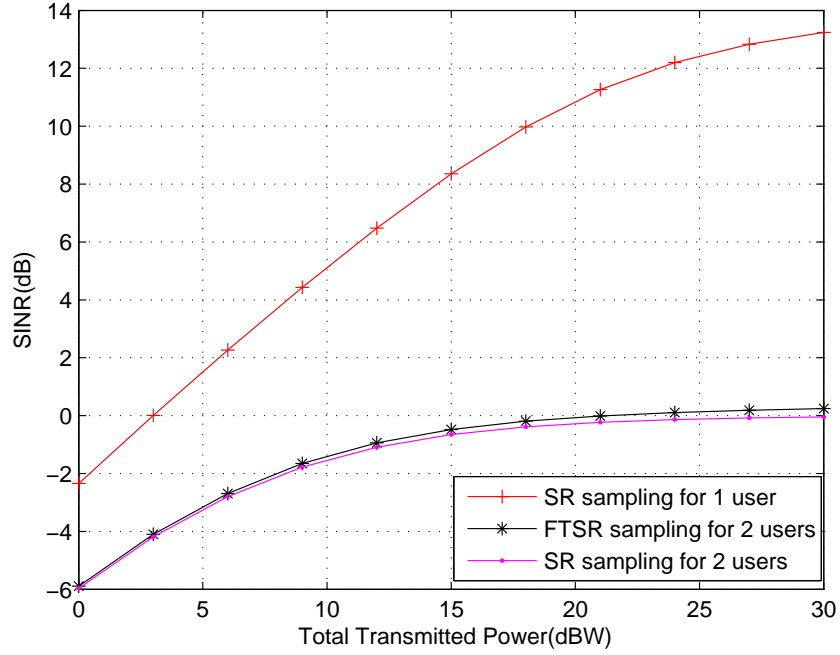


Figure 5.8: The effect of 10 equally spaced complex Gaussian channel taps on the FTSR sampled MMSE detector when roll off factor is 0.6

It is well known from MIMO systems that correlation among antennas leads to diminishing performance [81], [89]. In particular, when channel taps are fully correlated, the advantage of multiple antennas at receiver disappears [81], [89]. Since additional samples are considered as virtual antennas, there will be no gain after FTSR sampling if d_l^{os} in Eqn. (5.23) is fully correlated with d_l^{srs} in Eqn. (5.22) analogous to MIMO. On the other hand, there is a gain provided that d_l^{os} is not fully correlated with d_l^{srs} . The correlation between d_l^{os} and d_l^{srs} depends on the correlation among channel taps which can be found as

$$E[\gamma_m^i \beta_n^{j*}] = \sum_{k=0}^L E[|\alpha_k^i|^2] \tilde{p}_m \tilde{p}_n \delta[i - j] \quad (5.41)$$

where $\tilde{p}_m = \tilde{p}(mT - \tau_k^i)$ and $\tilde{p}_n = \tilde{p}(nT - T/2 - \tau_k^i)$. In case of normalized channel taps, Eqn. (5.41) becomes

$$E[\gamma_m^i \beta_n^{j*}] = \begin{cases} \langle \tilde{\mathbf{p}}_1, \tilde{\mathbf{p}}_2 \rangle & \text{if } i = j \\ 0 & \text{if } i \neq j \end{cases} \quad (5.42)$$

where $\tilde{\mathbf{p}}_1$ and $\tilde{\mathbf{p}}_2$ are $1 \times (L+1)$ vectors consisting of $(L+1)$ points on pulse shape $\tilde{p}(t)$. When $L \rightarrow \infty$, the correlation between consecutive channel taps can be represented

as

$$E[\gamma_m^i \beta_n^{i*}] = \int_{-\infty}^{\infty} \tilde{p}(t) \tilde{p}(t - T/2) dt. \quad (5.43)$$

When the offset between functions is T , they become orthogonal resulting in uncorrelated samples. On the other hand, they become fully correlated if there is no offset. The smaller the offset between functions, the higher the correlation among channel taps are. Since the offset is equal to gT/G , the biggest improvement of integer FTSR sampling occurs when $G = 2$ and the impact of FTSR sampling decreases by increasing G .

To observe this case numerically, assume that there are 10 complex Gaussian channel taps which have uniformly distributed propagation delays in $[0, 10T]$. The block length is 100 and pulse shape is raised cosine with 0.3 roll off factor. The highest change due to FTSR sampling is attained for $G = 2$ as shown in Figure 5.9. Further increases in the sampling rate has diminishing returns. In particular, there is no difference between $G = 3$ and $G = 5$.

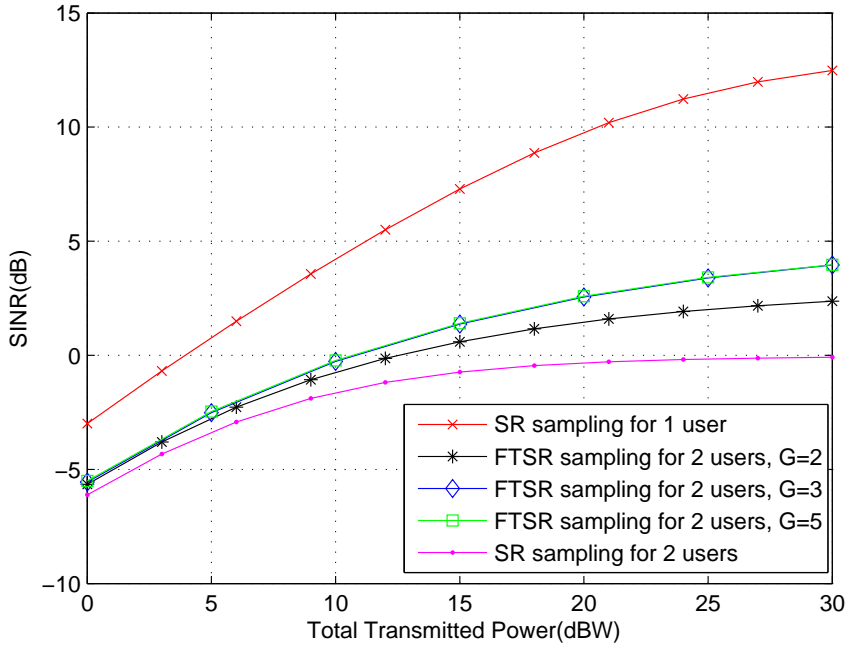


Figure 5.9: The effect of sampling rate for 10 unequally spaced complex Gaussian channel taps with a roll off factor 0.3 on the FTSR sampled MMSE detector

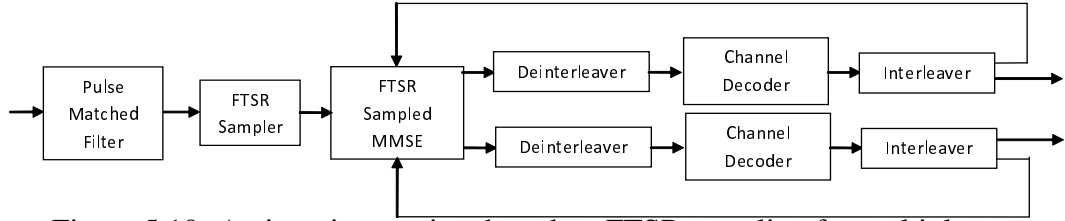


Figure 5.10: An iterative receiver based on FTSR sampling for multiple users

5.3.2 An Iterative Receiver Based on FTSR Sampling

It is appealing to share resources among users to increase the total number of users. Within this scope, two users transmit their symbols at the same time and frequency to a single receiver all with single antenna. They have the same pulse shape but different channels. The rationale behind the selection of two users stems from the fact that normalized rank doubles at most in case of $r = 1$ and takes more smaller values for $r < 1$ as found in the rank analysis section. Hence, the maximum benefit of FTSR sampling is observed for two users with $G = 2$, i.e., using more than two users with $G > 2$ gives less performance.

Although it is a difficult task to distinguish the symbols of multiple users, the problem may be solved using both FTSR sampling and iterative receiver. We study a receiver for FTSR sampling in case of two users based on the canonical iterative receiver [90] which is given in Figure 5.10. It comprises of an FTSR sampled MMSE detector and channel decoders working on the maximum a posteriori probability criterion. According to the output of the channel decoder soft estimation and interference cancellation is performed at the detector. Since pulse matched filter is used instead of channel matched filter, the receiver is more practical. Iterative receivers with FTSR sampled front-ends are mentioned in the literature [91], [92], however, they did not consider MAI, and performance comparisons between FTSR and SR sampled iterative receivers are not available.

Information sequence belonging to the first user, $\{I_n^1\}$ and second user, $\{I_n^2\}$ are convolutionally encoded, interleaved with distinct interleavers and then BPSK modulated. The resultant $N \times 1$ symbol vectors are represented as $\mathbf{a}^1 = [a_1 \ a_3 \ \cdots \ a_{2N-1}]$ and $\mathbf{a}^2 = [a_0 \ a_2 \ \cdots \ a_{2N-2}]$ for the first and second users that are transmitted in blocks with block length N . After passing through the ISI channels that are speci-

fied in Eqn. (5.2), the received signal is low pass filtered with pulse matched filter $p(-t)$ and FTSR sampled with period T' such that $T' < T$. Since there are two users, $T' = T/2$ is a sufficiently good choice. The system model becomes as Eqn. (5.29), where $\mathbf{x} = [\mathbf{a}^1 \ \mathbf{a}^2]$ with the only difference that the transmitted symbols are now convolutionally coded.

Throughout the process, extrinsic information between the detector and decoder is exchanged in an iterative manner [93]. The a posteriori log likelihood ratio of the FTSR sampled MMSE detector can be expressed as

$$\Lambda_1[a_n] = \log \frac{P(a_n = +1|\mathbf{y})}{P(a_n = -1|\mathbf{y})} \quad (5.44)$$

for $n = 0, \dots, 2N - 1$. Eqn. (5.44) is equal to

$$\Lambda_1[a_n] = \log \frac{P(\mathbf{y}|a_n = +1)}{P(\mathbf{y}|a_n = -1)} + \log \frac{P(a_n = +1)}{P(a_n = -1)}. \quad (5.45)$$

As stated in [90],

$$\lambda_1[a_n] = \log \frac{P(\mathbf{y}|a_n = +1)}{P(\mathbf{y}|a_n = -1)} \quad (5.46)$$

is the extrinsic information of the FTSR sampled MMSE detector that is sent to the channel decoder and the second term in the right hand side of Eqn. (5.45) is the a priori probability that comes from the channel decoder belonging to the previous iteration.

MMSE filtering is applied to the received signal in Eqn. (5.29) such that

$$\mathbf{v} = \mathbf{W}_{mmse}\mathbf{y} \quad (5.47)$$

where \mathbf{v} is a $1 \times 2N$ vector such that the odd terms of \mathbf{v} are utilized to decode the first user symbols, which are

$$\mathbf{v}^1 = [v_1 \ v_3 \ \dots \ v_{2N-1}]^T \quad (5.48)$$

and the even terms of \mathbf{v} are for the second user as

$$\mathbf{v}^2 = [v_0 \ v_2 \ \dots \ v_{2N-2}]^T. \quad (5.49)$$

The remaining interference and noise after MMSE filtering is approximated by Gaussian distribution [84]. Then, v_n can be expressed as [90]

$$v_n = \mu_n a_n + \eta_n \quad (5.50)$$

where μ_n is equal to

$$\mu_n = E[v_n a_n] \quad (5.51)$$

and η_n is a Gaussian noise. The extrinsic information generated by the FTSR sampled MMSE detector becomes [90]

$$\lambda_1[a_n] = \frac{4\Re(v_n)}{1 - \mu_n}. \quad (5.52)$$

The a posteriori log likelihood ratio of the channel decoder is [90]

$$\Lambda_2[a_n] = \log \frac{P(a_n = +1 | \{\lambda_1[a_n]\}_{n=0}^{2N-1})}{P(a_n = -1 | \{\lambda_1[a_n]\}_{n=0}^{2N-1})} \quad (5.53)$$

which is equal to

$$\Lambda_2[a_n] = \lambda_2[a_n] + \lambda_1[a_n] \quad (5.54)$$

where $\lambda_2[a_n]$ is the extrinsic information generated by the channel decoder and $\lambda_1[a_n]$ is the a priori information coming from the FTSR sampled MMSE detector.

$\lambda_2[a_n]$ can be found based on the modified BCJR algorithm as proposed in [90] such that

$$\lambda_2[a_n(t)] = \log \frac{\sum_{S^+} \hat{\alpha}_{t-1}(s') \hat{\beta}_t(s) \prod_{j \neq n} P(a_j(s', s))}{\sum_{S^-} \hat{\alpha}_{t-1}(s') \hat{\beta}_t(s) \prod_{j \neq n} P(a_j(s', s))} \quad (5.55)$$

where $a_n(t)$ is the n^{th} coded symbol at time t . S^+ and S^- correspond to the set of state pairs which result in $+1$ and -1 for the coded bits. $\hat{\alpha}_t(s)$ and $\hat{\beta}_t(s)$ are the forward and backward recursions coming from [94]. Moreover, $P(a_n(s', s))$ is equal to

$$P(a_n(s', s)) = \frac{1}{2} [1 + a_n(s', s) \tanh(0.5\lambda_1[a_n])]. \quad (5.56)$$

In the last iteration, information bit log likelihood ratio or $\Lambda_2[I_n^i]$ is determined and the decision is made according to the

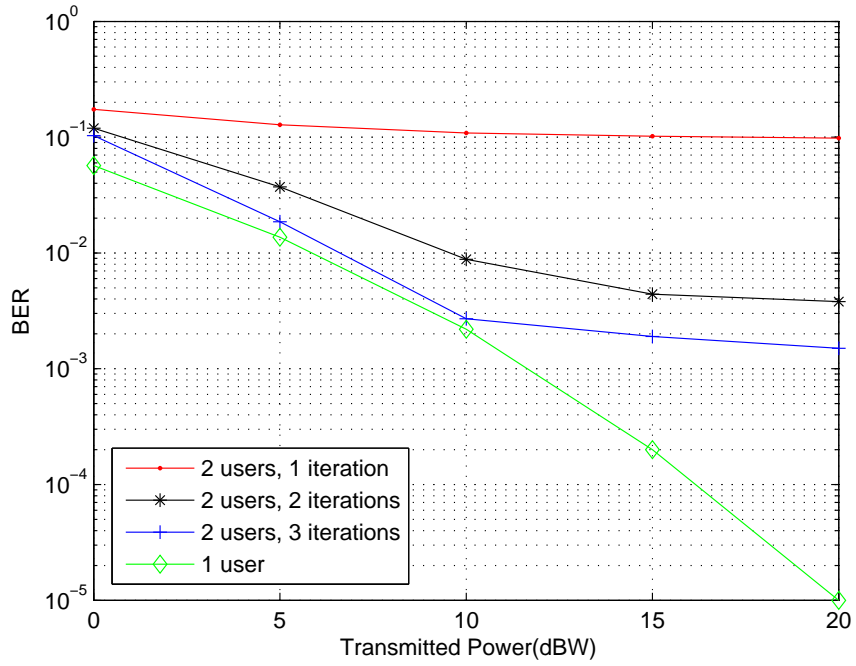
$$\hat{I}_n^i = \text{sign}(\Lambda_2[I_n^i]) \quad (5.57)$$

where \hat{I}_n^i is the estimated symbol for $i = 1, 2$.

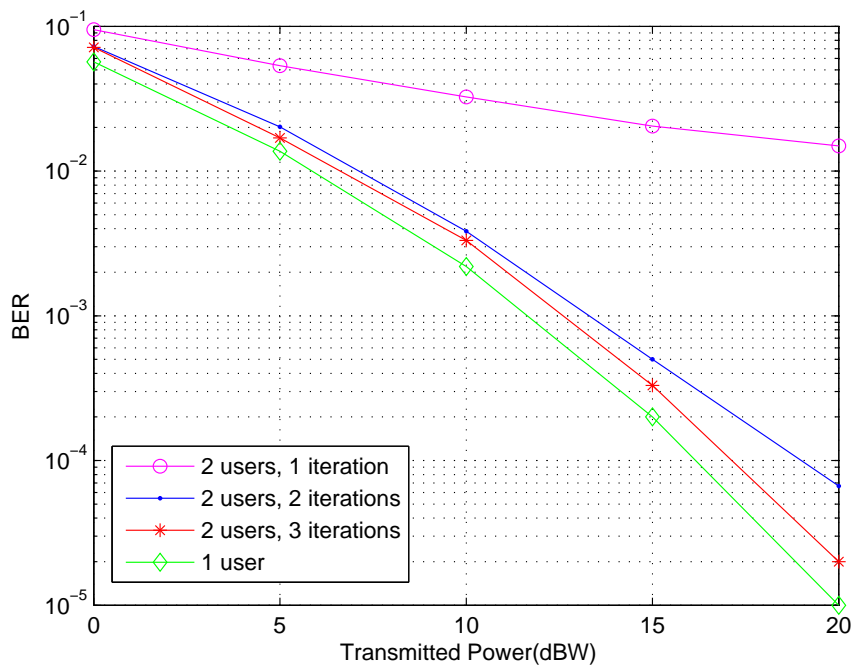
The FTSR sampled iterative receiver's performance is evaluated for a raised cosine pulse shape of roll off factor 0.3 when there are two transmitters and a single receiver. Convolutional coding is employed at the transmitters with coding rate $1/2$, constraint length 5, and generators are (23, 35) in terms of octal notation. The modulation

format is BPSK. The symbols are transmitted in blocks with block length 100, and the channel becomes constant within one block, and changes from block to block. Our aim is to observe how efficiently FTSR sampled iterative receiver eliminates the multiuser interference, therefore, single user system that has no multiuser interference is selected for comparison. A genie-aided interference cancellation scheme would perform the same as the single user receiver.

It is firstly assumed that both users have 2 complex Gaussian taps whose propagation delays are uniformly distributed in $[0, 5T]$. Accordingly, SR sampled iterative receiver's BER for two users is presented in Figure 5.11(a). It includes the single user non-iterative receiver performance as well to clarify the multiuser interference cancellation capability of the receiver. As can be observed, the SR sampled iterative structure does not reach the single user receiver performance. Hence, we can conclude that even an iterative receiver could not perform very well with SR sampling. On the other hand, FTSR sampled iterative receiver with $G = 2$ can greatly reduce the interference between users as can observed in Figure 5.11(b). The error rate difference between the single user receiver and the 3th iteration of the FTSR sampled iterative receiver is very small. One critical point about the iterative receivers is the initial BER. In the context of iterative receivers, it is shown that iterative structures with enhanced initial BER yield better results [95]. The increasing performance difference with iterations between the SR and FTSR sampled iterative receiver is compatible with this interpretation.



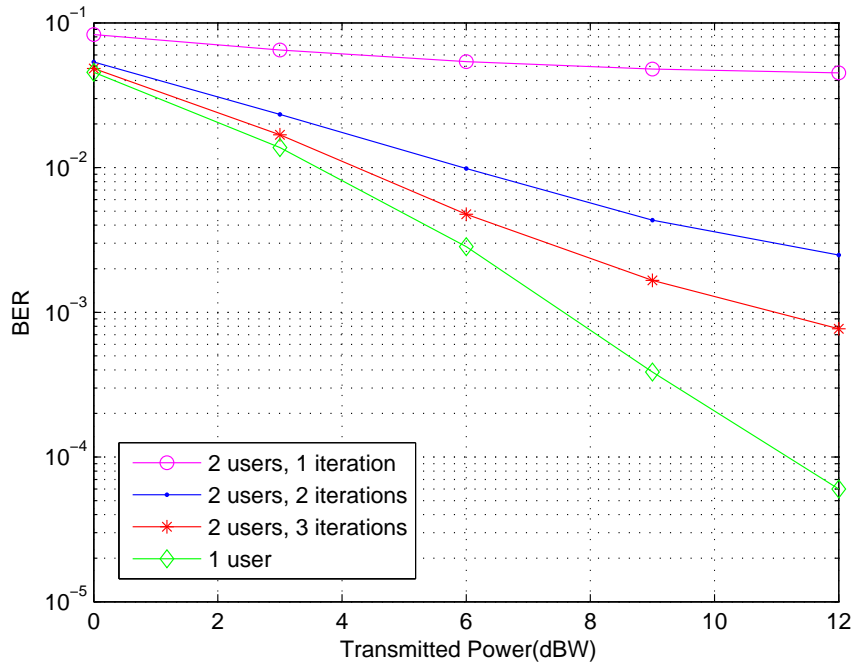
(a)



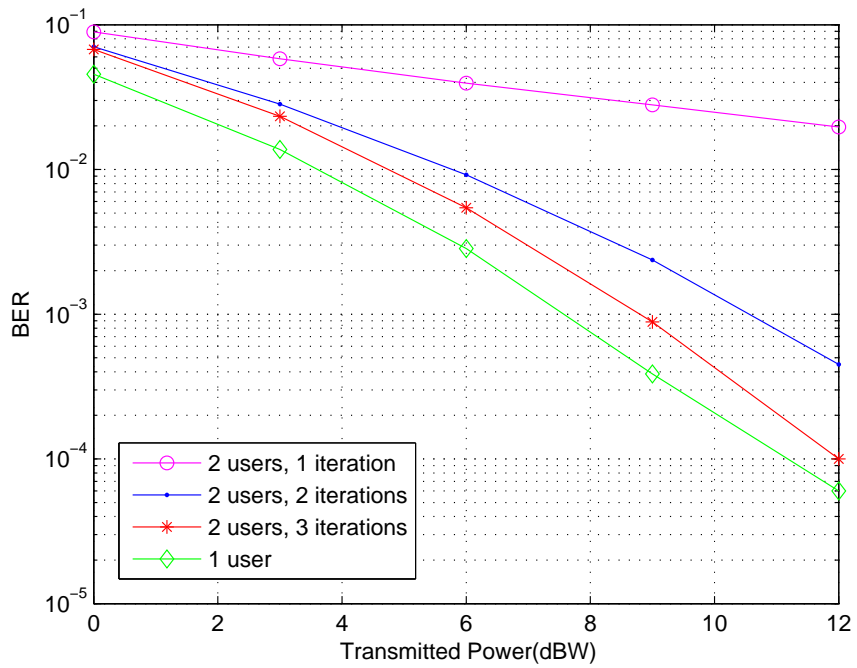
(b)

Figure 5.11: There are 2 transmitters and channel has 2 taps (a) Performance of the SR sampled iterative receiver (b) Performance of the FTSR sampled iterative receiver with $G = 2$.

The channel may have more than 2 taps, therefore, the simulation results are generalized to 5 taps. According to that, both users have 5 complex Gaussian taps whose propagation delays are uniformly distributed in $[0, 5T]$. SR and FTSR sampled iterative receiver performance for two users are presented in Figure 5.12(a) and Figure 5.12(b) respectively. Similar to the previous case, FTSR sampled iterative receiver gives reasonable results, while SR sampling cannot.



(a)



(b)

Figure 5.12: There are 2 transmitters and channel has 5 taps (a) Performance of the SR sampled iterative receiver (b) Performance of the FTSR sampled iterative receiver with $G = 2$.

The FTSR sampled iterative receiver is generalized for three transmitters and a single receiver when there are 2 channel taps whose propagation delays are uniformly distributed in $[0, 5T]$ and $G = 3$. The average error performance of the users for FTSR sampled iterative receiver with $G = 3$ is depicted in Figure 5.13. Although there is a degradation with respect to the two users with $G = 2$, it has satisfactory performance in the 3th iteration. Eventually, it can be inferred that increasing the number of users in parallel with the FTSR sampling ratio leads to a performance loss.

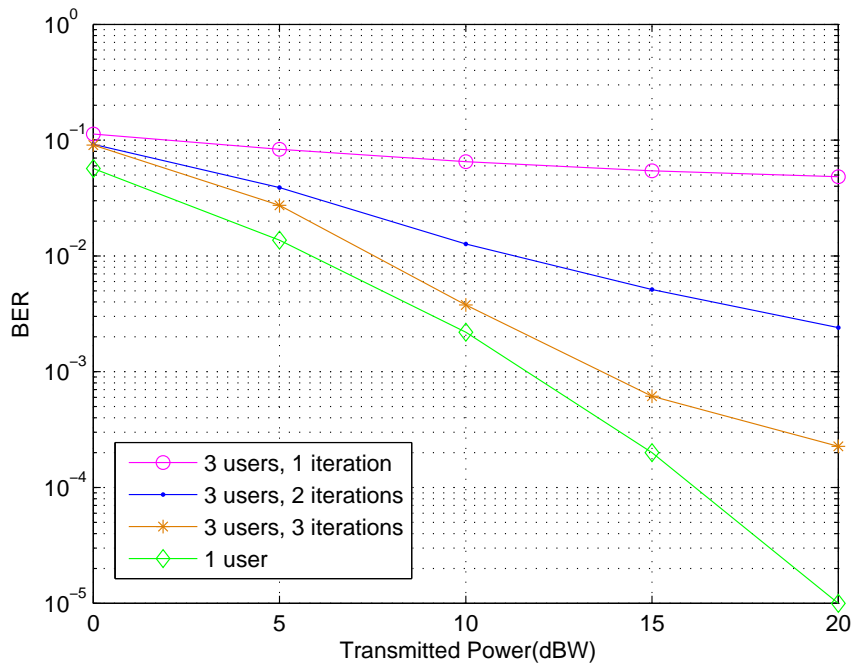


Figure 5.13: The performance of the FTSR sampled iterative receiver with $G = 3$ for 3 transmitters and a single receiver for 2 channel taps

5.4 Conclusions

FTSR sampling is studied in multiuser communication within the purpose of better interference mitigation to increase the number of users. DoF and rank analysis show that FTSR sampling can better exploit the excess bandwidth depending on unequally spaced channel taps and asynchronism among users for a multiple access channel. The level of improvement due to unequally spaced channel taps and excess bandwidth is quantified with an FTSR sampled MMSE detector. The results show that there is an advantage provided that excess bandwidth exists and channel taps are un-

equally spaced. These results are instrumental in designing an iterative receiver based on FTSR sampling. Simulation results illustrate that FTSR sampled iterative receiver better mitigates the interference among multiple users, and it makes possible to increase the number of users in a given network.

CHAPTER 6

FREQUENCY DOMAIN OVERSAMPLING

FDO method is a counterpart of FTSR sampling such that the latter one is based on taking more samples in time domain and the former one corresponds to taking more samples in frequency domain. The main idea of FDO is ZP at the receiver and studied for better channel equalization in response to frequency selective wireless channels in this chapter. More specifically, FDO method is investigated to further enhance the performance of MMSE SC-FDE which mitigates the interference efficiently with a reasonable complexity. In this chapter, CP is avoided at the transmitter that is conventionally utilized for SC-FDE. In particular, we propose to implement SC-FDE by ZP at the transmitter and receiver instead of CP. This approach reduces the power consumption due to CP. The efficiency of the proposed method is evaluated in regard to transmission block length to channel memory length ratio and modulation order.

6.1 Frequency Domain Oversampled MMSE SC-FDE

SC-FDE has become a significant alternative to the OFDM in recent years [40], [41], and has been utilized in standards such as in the uplink part of 3GPP Long Term Evaluation (LTE). It is appealing to replace CP with ZP while implementing SC-FDE [96], [97], since implementation of SC-FDE by ZP eliminates the power consumption due to redundant CP symbols. Moreover, increasing the number of zeros at the end of each transmission block can enhance the performance of linear equalizers [98]. However, the number of zeros are limited in accordance with the maximum channel delay spread, since ZP at the transmitter will decrease the bandwidth efficiency. One

more point is that ZP at the transmitter leads to higher block length that requires very high SNR to enhance the error performance [99]. On the other hand, ZP at the receiver makes possible to add a large number of zeros and satisfies the bandwidth efficiency at the same time. That's why, it is worth to investigate the method of ZP at the receiver before DFT or FDO in order to enhance the MMSE SC-FDE performance. Since block length, channel memory length and modulation order determine the MMSE SC-FDE performance [58], the impact of FDO is investigated based on these parameters.

It is important to remind that there is a performance loss in linear detectors compared with ML detectors. That is, the channel is not exploited as much efficient as ML detectors with linear detectors. For instance, the diversity gain introduced by multipath channels can be fully exploited by ML detectors. On the other hand, linear detectors have rather different diversity gain characteristics. Zero Forcing (ZF) detectors have always unity diversity gain, whereas MMSE detectors have a changing diversity order with the cardinality of the alphabet size such that its diversity gain degrades with incremental alphabet size [57], [58], [100]. It seems attractive to compensate this performance loss of MMSE detection with FDO. Although ZP does not carry information, it can prevent the potential information loss.

It is advocated that diversity gain inherent in the channel can be better exploited by FDO in OFDM [27]. Enhanced error rates of OFDM due to FDO is presented for underwater acoustic channels as well [28] analogous to the time domain oversampling method that improves the performance of OFDM in doubly selective underwater acoustic channels [101]. In case of single carrier transmission, FDO is proposed to implement SC-FDE [30]. However, [30] does not investigate the effect of FDO in combination with transmission block length, channel memory length and modulation order. Moreover, the effect of ZP at the transmitter and receiver is not separated in [30].

The contributions of this chapter are the following. An MMSE SC-FDE implementation based on FDO is proposed as a low complexity approximation of ZP transmission. ZP at the transmitter with FDO is compared with the conventional CP based transmission by finding the lower bounds for the outage probability of MMSE SC-FDE. Then, a direct outage probability comparison is performed, which shows that

ZP SC-FDE with FDO can achieve better outage probability compared with CP SC-FDE. Beside this, the effect of FDO on the MMSE SC-FDE performance is quantified in regard to transmission block length to channel memory length ratio and modulation order. The simulation results will clarify the effect of ZP at the transmitter and the receiver separately as well.

The system model is given in Section 6.2. An outage analysis is performed in Section 6.3. The simulation results are presented in Section 6.4 and the chapter ends with the concluding remarks in Section 6.5.

6.2 System Model

It is necessary to use either CP or ZP at the transmitter in a block transmission to avoid IBI for frequency selective channels. We prefer ZP in this study for SC-FDE which is used to mitigate ISI. Accordingly, the proposed model for the implementation of SC-FDE is given in Figure 6.1 such that a limited number of zeros, which is equal to the channel length, are appended at the transmitter to avoid IBI. Further to that, a large number of zeros are padded before DFT operation at the receiver. Following DFT, the samples are equalized in the MMSE sense and IDFT is taken prior to decision.

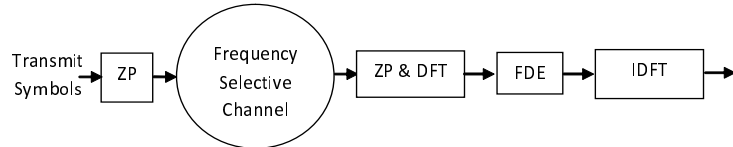


Figure 6.1: The implementation of MMSE SC-FDE with ZP

When L and $(M - N - L)$ zeros are padded to the transmitted symbol block with length N at the transmitter and receiver respectively, the matrix representation of the model becomes

$$\mathbf{y}_{zp} = \mathbf{H}_{zp}\mathbf{x}_{zp} + \mathbf{z}_{zp} \quad (6.1)$$

where \mathbf{y}_{zp} , \mathbf{x}_{zp} and \mathbf{z}_{zp} are $M \times 1$ vectors, and \mathbf{H}_{zp} is an $M \times M$ matrix. Since the entries belonging to last $(M - N)$ columns of \mathbf{H}_{zp} are multiplied by ZP terms in \mathbf{x}_{zp} , any value can be written to these entries. Therefore, \mathbf{H}_{zp} can be interpreted as a circulant channel matrix as explained in Appendix C. The MMSE filter is implemented by considering \mathbf{H}_{zp} as a circulant matrix to avoid large complexity due to ZP [96]. Thus,

ZP transmission causes a little complexity increase stemming from larger DFT block size, which can be easily tolerated.

6.3 Outage Analysis

Noise becomes correlated due to ZP at the receiver that makes analysis difficult. Therefore, it is assumed that zero mean unit variance i.i.d. Gaussian random variables are padded instead of zeros at the receiver in the rest of analysis for the sake of analytical simplicity. This assumption is validated for an ISI channel with $L = 2$, in which channel taps are symbol period spaced with a block length of 10. According to that, 2 zeros are inserted at the transmitter to avoid IBI, and padding 8 i.i.d. Gaussian random variables are compared with padding 8 zeros at the receiver in Figure 6.2. As can be observed, such an assumption has a negligible effect regarding the symbol error rate (SER) of QPSK symbols for MMSE SC-FDE at different SNR. Relying on

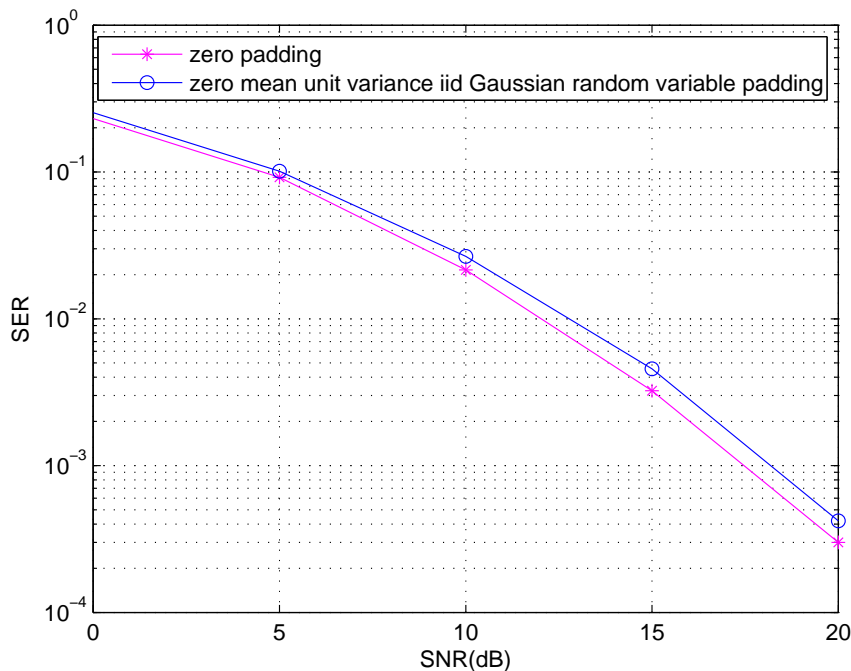


Figure 6.2: The performance specification of padding zero mean unit variance i.i.d. Gaussian random variables instead of zeros for the implementation of SC-FDE

this result, an MMSE SC-FDE implementation is proposed that can be seen as the low complexity approximation of ZP transmission. According to that method,

1. Insert zeros at the transmitter to avoid IBI.
2. Insert i.i.d. Gaussian random variables at the receiver to attain uncorrelated noise auto-correlation matrix.
3. Constitute the channel as a circulant matrix.
4. Take Fourier transform and apply MMSE filter.

The outage probability analysis of this model is performed by finding lower bounds as well as a direct computation.

6.3.1 Outage Probability Analysis with Lower Bounds

Any circulant matrix can be expressed as

$$\mathbf{H}_{zp} = \mathbf{Q}^H \mathbf{D}_{zp} \mathbf{Q} \quad (6.2)$$

where \mathbf{Q} is the M -point DFT matrix and \mathbf{D}_{zp} is the diagonal matrix. Therefore, taking the DFT of Eqn. (6.1) yields

$$\mathbf{Y}_{zp} = \mathbf{D}_{zp} \mathbf{X}_{zp} + \mathbf{Z}_{zp} \quad (6.3)$$

where \mathbf{Y}_{zp} , \mathbf{X}_{zp} , \mathbf{Z}_{zp} are the DFT of \mathbf{y}_{zp} , \mathbf{x}_{zp} , \mathbf{z}_{zp} such that $\mathbf{Y}_{zp} = \mathbf{Q} \mathbf{y}_{zp}$, $\mathbf{X}_{zp} = \mathbf{Q} \mathbf{x}_{zp}$ and $\mathbf{Z}_{zp} = \mathbf{Q} \mathbf{z}_{zp}$. Outage occurs when total mutual information between the input and output, $I(\mathbf{X}_{zp}; \mathbf{Y}_{zp})$ falls below the total target rate R_t such that

$$P_{out} = P(I(\mathbf{X}_{zp}; \mathbf{Y}_{zp}) < R_t). \quad (6.4)$$

The mutual information can be expressed as

$$I(\mathbf{X}_{zp}; \mathbf{Y}_{zp}) = H(\mathbf{Y}_{zp}) - H(\mathbf{Y}_{zp} | \mathbf{X}_{zp}) \quad (6.5)$$

where $H(\cdot)$ represents entropy function. Since the samples of \mathbf{Y}_{zp} are correlated, it can be written as

$$H(\mathbf{Y}_{zp}) \leq \sum_{k=1}^M H(Y_{zp}^k) \quad (6.6)$$

where Y_{zp}^k is the k^{th} term of the vector \mathbf{Y}_{zp} . On the other hand, the noise samples are uncorrelated due to our assumption that leads to

$$H(\mathbf{Y}_{zp}|\mathbf{X}_{zp}) = H(\mathbf{Z}_{zp}) = \sum_{k=1}^M H(Z_{zp}^k). \quad (6.7)$$

Similarly, Z_{zp}^k is the k^{th} component of \mathbf{Z}_{zp} and

$$I(\mathbf{X}_{zp}; \mathbf{Y}_{zp}) \leq \sum_{k=1}^M I(X_{zp}^k; Y_{zp}^k) \quad (6.8)$$

in which X_{zp}^k is the k^{th} term of \mathbf{X}_{zp} and $I(X_{zp}^k; Y_{zp}^k)$ represents the mutual information between input X_{zp}^k and output Y_{zp}^k that can be written in terms of MSE [102]

$$I(X_{zp}^k; Y_{zp}^k) = \frac{1}{2} \int_0^{s\tilde{n}r_k} MSE(\gamma) d\gamma \quad (6.9)$$

where $s\tilde{n}r_k$ represents the energy of symbol X_{zp}^k .

Eventually, implementing the SC-FDE by ZP yields the following outage probability

$$P_{out}^{zp} \geq P \left(\frac{1}{2} \sum_{k=1}^M \int_0^{s\tilde{n}r_k} MSE(\gamma) d\gamma < R_t \right). \quad (6.10)$$

On the other hand, the outage probability of conventional SC-FDE with CP becomes

$$P_{out}^{cp} \geq P \left(\frac{1}{2} \sum_{k=1}^N \int_0^{snr_k} MSE(\gamma) d\gamma < R_t \right) \quad (6.11)$$

where snr_k is the energy of k^{th} transmitted symbol in frequency domain. Since transmission power is constant and norm is preserved under unitary transformation,

$$\sum_{k=1}^M s\tilde{n}r_k = \sum_{k=1}^N snr_k. \quad (6.12)$$

Lemma 6.3.1 When $\underline{snr} = \frac{1}{N} \sum_{k=1}^N snr_k$,

$$N \int_0^{\underline{snr}} MSE(\gamma) d\gamma \geq \sum_{k=1}^N \int_0^{snr_k} MSE(\gamma) d\gamma. \quad (6.13)$$

Proof 6.3.2 Define

$$f(snr_k) = \int_0^{snr_k} MSE(\gamma) d\gamma \quad (6.14)$$

such that $f(\text{snr}_k)$ is a log-concave function through Eqn. (6.9). Due to Jensen's inequality

$$f(\underline{\text{snr}}) \geq \frac{1}{N} \sum_{k=1}^N f(\text{snr}_k) \quad (6.15)$$

which completes the proof.

Following Lemma 6.3.1, the outage probabilities are lower bounded by

$$P_{out}^{zp} \geq P \left(\frac{1}{2} M \int_0^{\underline{\text{s}\tilde{\text{n}}r}} \text{MSE}(\gamma) d\gamma < R_t \right) \quad (6.16)$$

where $\underline{\text{s}\tilde{\text{n}}r} = \frac{1}{M} \sum_{k=1}^M \text{s}\tilde{\text{n}}r_k$ and

$$P_{out}^{cp} \geq P \left(\frac{1}{2} N \int_0^{\underline{\text{snr}}} \text{MSE}(\gamma) d\gamma < R_t \right). \quad (6.17)$$

Lemma 6.3.3 Define $M = lN$ such that $l = 1, 2, \dots$. Then,

$$M \int_0^{\underline{\text{s}\tilde{\text{n}}r}} \text{MSE}(\gamma) d\gamma \geq N \int_0^{\underline{\text{snr}}} \text{MSE}(\gamma) d\gamma. \quad (6.18)$$

Proof 6.3.4 Due to Eqn. (6.12), it is obtained that

$$\underline{\text{snr}} = l \underline{\text{s}\tilde{\text{n}}r}. \quad (6.19)$$

Since $\text{MSE}(\gamma)$ is a monotonically decreasing function [103],

$$l \int_0^{\underline{\text{s}\tilde{\text{n}}r}} \text{MSE}(\gamma) d\gamma \geq \int_0^{l \underline{\text{s}\tilde{\text{n}}r}} \text{MSE}(\gamma) d\gamma \quad (6.20)$$

with equality if and only if $\text{MSE}(\gamma)$ is flat and

$$lN \int_0^{\underline{\text{s}\tilde{\text{n}}r}} \text{MSE}(\gamma) d\gamma \geq N \int_0^{l \underline{\text{s}\tilde{\text{n}}r}} \text{MSE}(\gamma) d\gamma. \quad (6.21)$$

Due to Lemma 6.3.1 and Lemma 6.3.3, the lower bound of P_{out}^{zp} is less than or equal to the lower bound of P_{out}^{cp} .

6.3.2 Direct Outage Probability Analysis

The outage probability of the proposed model can be specified as

$$P_{out}^{zp} = P \left(I(\mathbf{x}_{zp}; \mathbf{y}_{zp}) < R_t \right) \quad (6.22)$$

in which $\mathbf{x}_{zp} = [\mathbf{x}^H \mathbf{0}_{1 \times (M-N)}]^H$ with \mathbf{x} is the $N \times 1$ data vector, $\mathbf{y}_{zp} = [\mathbf{y}^H \tilde{\mathbf{y}}^H]^H$ where \mathbf{y} is the $(N+L) \times 1$ observation vector and $\tilde{\mathbf{y}}$ is an $(M-N-L) \times 1$ i.i.d. Gaussian random vector because of the assumption that i.i.d. Gaussian random variables are padded at the receiver instead of zeros. When \mathbf{x} has a Gaussian input alphabet, \mathbf{y} is Gaussian [75] and so is \mathbf{y}_{zp} that yields the following mutual information expression

$$I(\mathbf{x}_{zp}; \mathbf{y}_{zp}) = \log \det(\mathbf{I}_M + \mathbf{H}_{zp} \mathbf{R}_{x_{zp}} \mathbf{H}_{zp}^H) \quad (6.23)$$

where \mathbf{I}_M is an $M \times M$ identity matrix and $\mathbf{R}_{x_{zp}}$ is a diagonal matrix such that $\mathbf{R}_{x_{zp}} = \text{diag}(\mathbf{1}_{1 \times N} \mathbf{0}_{1 \times (M-N)})$. The expression in Eqn. (6.23) can be written by using Sylvester's determinant theorem as

$$I(\mathbf{x}_{zp}; \mathbf{y}_{zp}) = \log \det(\mathbf{I}_M + \mathbf{H}_{zp}^H \mathbf{H}_{zp} \mathbf{R}_{x_{zp}}). \quad (6.24)$$

\mathbf{H}_{zp} can be partitioned as $\begin{bmatrix} \mathbf{A} & \mathbf{B} \\ \mathbf{B} & \mathbf{A} \end{bmatrix}$ where \mathbf{A} is an $N \times N$ upper triangular matrix whose first row is $[h_0 \cdots h_{L-1} 0 \cdots 0]$ and \mathbf{B} is an $N \times N$ lower triangular matrix whose first column is $[0 \cdots 0 h_{L-1} \cdots h_1]$. We give a simple illustrative example for this in Appendix D. Without any loss of generality, it is assumed that $M = 2N$ and $N > L$. Then,

$$I(\mathbf{x}_{zp}; \mathbf{y}_{zp}) = \log \det \left(\begin{bmatrix} \mathbf{I}_N + \mathbf{A}^H \mathbf{A} + \mathbf{B}^H \mathbf{B} & \mathbf{0}_N \\ \mathbf{B}^H \mathbf{A} + \mathbf{A}^H \mathbf{B} & \mathbf{I}_N \end{bmatrix} \right) \quad (6.25)$$

where $\mathbf{0}_N$ is an $N \times N$ zero matrix and \mathbf{I}_N is an $N \times N$ identity matrix. Using the property of block matrices Eqn. (6.25) can be expressed as

$$I(\mathbf{x}_{zp}; \mathbf{y}_{zp}) = \log \det(\mathbf{I}_N + \mathbf{A}^H \mathbf{A} + \mathbf{B}^H \mathbf{B}). \quad (6.26)$$

The proposed model is compared with conventional SC-FDE with CP regarding the outage probability, whose model is

$$\mathbf{y}_{cp} = \mathbf{H}_{cp} \mathbf{x}_{cp} + \mathbf{z}_{cp} \quad (6.27)$$

where \mathbf{x}_{cp} , \mathbf{y}_{cp} and \mathbf{z}_{cp} are $N \times 1$ vectors and \mathbf{H}_{cp} is an $N \times N$ circulant matrix. Based on this model, the outage probability of the conventional SC-FDE can be written as

$$P_{out}^{cp} = P(I(\mathbf{x}_{cp}; \mathbf{y}_{cp}) < R_t) \quad (6.28)$$

where

$$I(\mathbf{x}_{cp}; \mathbf{y}_{cp}) = \log \det(\mathbf{I}_N + \mathbf{H}_{cp} \mathbf{H}_{cp}^H). \quad (6.29)$$

Notice that \mathbf{H}_{cp} can be expressed as $(\mathbf{A} + \mathbf{B})$ which is exemplified in Appendix D.

Then,

$$I(\mathbf{x}_{cp}; \mathbf{y}_{cp}) = \log \det(\mathbf{I}_N + (\mathbf{A} + \mathbf{B})^H (\mathbf{A} + \mathbf{B})) \quad (6.30)$$

which is equal to

$$I(\mathbf{x}_{cp}; \mathbf{y}_{cp}) = \log \det(\mathbf{I}_N + \mathbf{A}^H \mathbf{A} + \mathbf{B}^H \mathbf{B} + \mathbf{A}^H \mathbf{B} + \mathbf{B}^H \mathbf{A}). \quad (6.31)$$

Lemma 6.3.5 $\det(\mathbf{M} + \mathbf{E}) < \det(\mathbf{M})$ where $\mathbf{M} = \mathbf{I}_N + \mathbf{A}^H \mathbf{A} + \mathbf{B}^H \mathbf{B}$ and $\mathbf{E} = \mathbf{A}^H \mathbf{B} + \mathbf{B}^H \mathbf{A}$.

Proof 6.3.6 \mathbf{M} is a banded matrix relying on \mathbf{A} and \mathbf{B} , and can be partitioned as

$\begin{bmatrix} \mathbf{M}_{11} & \mathbf{M}_{12} \\ \mathbf{M}_{12}^H & \mathbf{M}_{22} \end{bmatrix}$ where all submatrices are $\frac{N}{2} \times \frac{N}{2}$ square matrices and \mathbf{M}_{12} is a lower triangular matrix, whose first $(\frac{N}{2} - L)$ entries in the first column are zero. The determinant of \mathbf{M} equals

$$\det(\mathbf{M}) = \det(\mathbf{M}_{11}) \det(\mathbf{M}_{22} - \mathbf{M}_{12}^H \mathbf{M}_{11}^{-1} \mathbf{M}_{12}). \quad (6.32)$$

\mathbf{M} is the summation of an identity and auto-correlation matrix, and hence it is positive definite, so are \mathbf{M}_{22} , $\mathbf{M}_{22} - \mathbf{M}_{12}^H \mathbf{M}_{11}^{-1} \mathbf{M}_{12}$ and $\mathbf{M}_{12}^H \mathbf{M}_{11}^{-1} \mathbf{M}_{12}$ [104].

\mathbf{E} is a special matrix that can be partitioned as $\begin{bmatrix} \mathbf{0} & \mathbf{E}_{12} \\ \mathbf{E}_{12}^H & \mathbf{0} \end{bmatrix}$ such that \mathbf{E}_{12} is an $\frac{N}{2} \times \frac{N}{2}$ upper triangular matrix and only last $(L - 1)$ terms of its first column are non-zero. $\mathbf{P} = \mathbf{M} + \mathbf{E}$ and can be expressed as $\begin{bmatrix} \mathbf{M}_{11} & \mathbf{M}_{12} + \mathbf{E}_{12} \\ \mathbf{M}_{12}^H + \mathbf{E}_{12}^H & \mathbf{M}_{22} \end{bmatrix}$. Similarly, \mathbf{P} is a positive definite matrix, because it is the summation of an identity and auto-correlation matrix. Its determinant is

$$\det(\mathbf{P}) = \det(\mathbf{M}_{11}) \det(\mathbf{M}_{22} - (\mathbf{M}_{12}^H + \mathbf{E}_{12}^H) \mathbf{M}_{11}^{-1} (\mathbf{M}_{12} + \mathbf{E}_{12})). \quad (6.33)$$

Since cross terms are equal to zero due to padding zeros,

$$\det(\mathbf{P}) = \det(\mathbf{M}_{11}) \det(\mathbf{M}_{22} - \mathbf{M}_{12}^H \mathbf{M}_{11}^{-1} \mathbf{M}_{12} - \mathbf{E}_{12}^H \mathbf{E}_{11}^{-1} \mathbf{E}_{12}). \quad (6.34)$$

By the definition of positive semidefinite matrix, when $\mathbf{M}_s = \mathbf{M}_{22} - \mathbf{M}_{12}^H \mathbf{M}_{11}^{-1} \mathbf{M}_{12}$ and $\mathbf{P}_s = \mathbf{M}_{22} - \mathbf{M}_{12}^H \mathbf{M}_{11}^{-1} \mathbf{M}_{12} - \mathbf{E}_{12}^H \mathbf{E}_{11}^{-1} \mathbf{E}_{12}$,

$$\mathbf{a} \mathbf{P}_s \mathbf{a}^H < \mathbf{a} \mathbf{M}_s \mathbf{a}^H \quad (6.35)$$

for $\forall \mathbf{a}$, because $\mathbf{a} (\mathbf{E}_{12}^H \mathbf{E}_{11}^{-1} \mathbf{E}_{12}) \mathbf{a}^H > 0$. Since the matrices on both side are positive definite [104],

$$\det(\mathbf{P}_s) < \det(\mathbf{M}_s) \quad (6.36)$$

and

$$\det(\mathbf{M} + \mathbf{E}) < \det(\mathbf{M}) \quad (6.37)$$

which completes the proof.

Due to Lemma 6.3.5, Eqn. (6.26) is greater than Eqn. (6.31) producing

$$P_{out}^{zp} < P_{out}^{cp} \quad (6.38)$$

which shows the superiority of the proposed model over the conventional one regarding the outage probability. This result is numerically evaluated as well in the subsequent section.

6.4 Simulations

The conventional MMSE SC-FDE that is implemented by appending CP at the transmitter is compared with the proposed MMSE SC-FDE implementation which is based on the idea of ZP at the transmitter and FDO at the receiver. Within this scope, it is assumed that the number of zeros that are padded at the transmitter is equal to the channel memory length and the number of zeros padded at the receiver due to FDO is equal to the transmission block length. We perform Monte Carlo simulations with 10,000 runs. When the block length is 10, there are 2 complex Gaussian channel taps which are equally spaced with symbol period and the target value R_t is 2, ZP with FDO implementation of MMSE SC-FDE is advantageous with respect to CP based structure regarding outage probability as can be observed in Figure 6.3. Furthermore, the lower bound of ZP with FDO is considerably better than the lower bound of conventional CP based implementation for MMSE SC-FDE. This result numerically verifies our outage analysis as well.

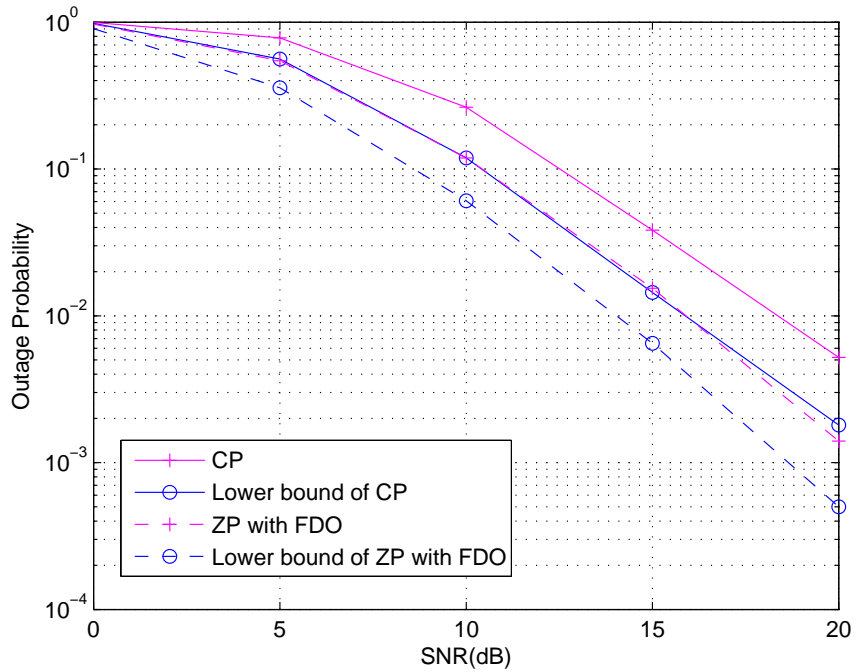


Figure 6.3: Outage probability comparison of SC-FDE for CP and ZP with FDO implementations

Subsequently, the uncoded error performance of MMSE SC-FDE for ZP with FDO is inspected. Similarly, the block length is 10 and there are 2 complex equally spaced Gaussian channel taps. As shown in Figure 6.4, the implementation of SC-FDE by ZP rather than CP does not yield any major improvement for QPSK modulation. Moreover, ZP at the receiver or FDO does not change the performance.

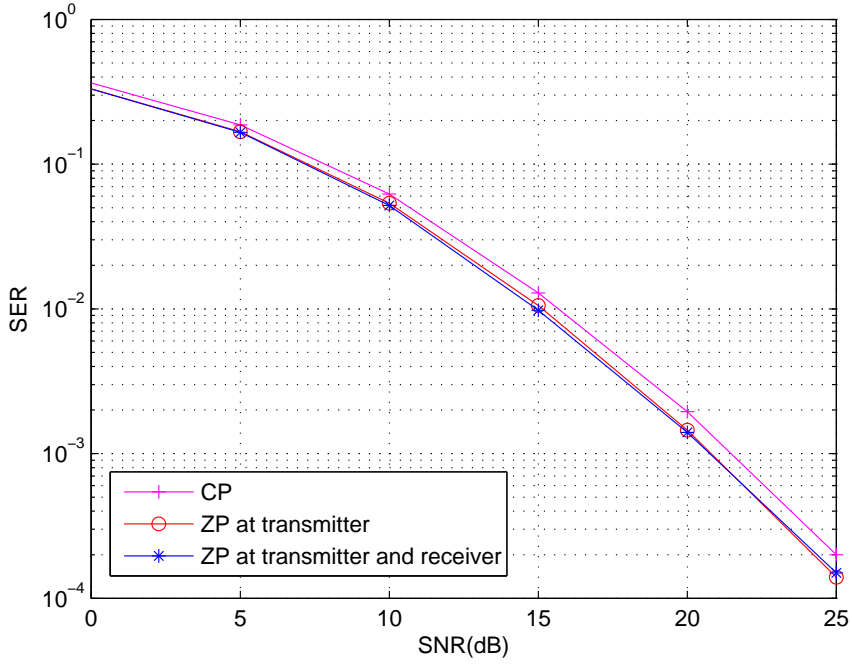


Figure 6.4: MMSE SC-FDE error performance for QPSK when the block length to channel memory length ratio is 5

On the other hand, when there are 5 complex Gaussian channel taps for the same block length and modulation format, the advantage of ZP at the transmitter and the receiver deepens as illustrated in Figure 6.5. Similar results are attained for large block lengths provided that the ratio of block length to channel memory length remains the same. Since frequency domain oversampled SC-FDE leads to equalization over M samples instead of N , it gives relatively good performance. These results are in parallel with the study that explicitly proves that the error performance of MMSE SC-FDE is significantly improved when the ratio of block length to channel memory length increases [58]. Since, DFT corresponds to equally spaced samples of DTFT and more samples are attained due to FDO, it is more likely to sample the signal closer to its peaks so that a larger signal power is accumulated overall.

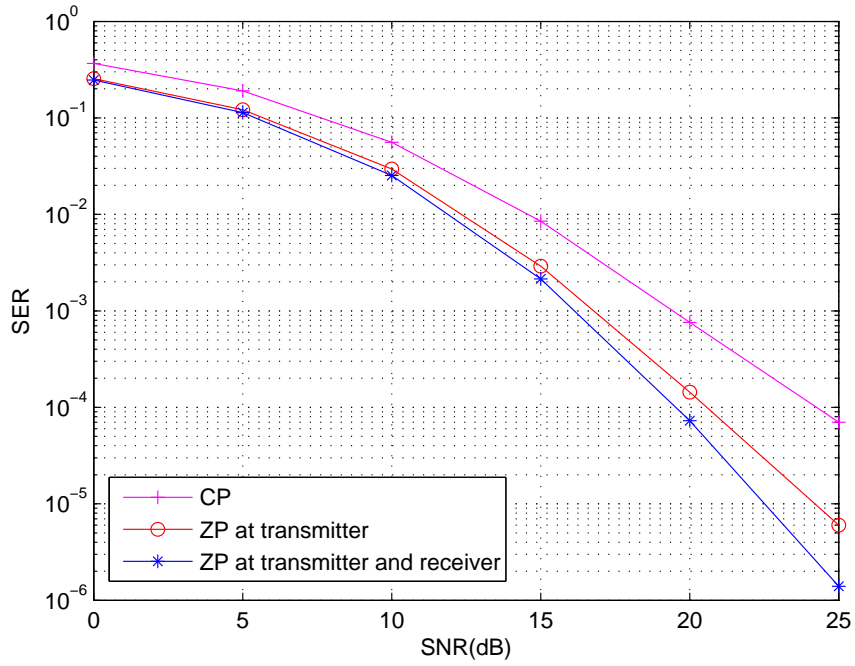


Figure 6.5: MMSE SC-FDE error performance for QPSK when the block length to channel memory length ratio is 2

The error performance of MMSE SC-FDE implementation for ZP with FDO in case of 16-QAM becomes as in Figure 6.6 for the block length to channel memory length ratio of 5. Although the block lengths are different, which are 10 and 25, the advantage of ZP at the transmitter and FDO are observed for both cases.

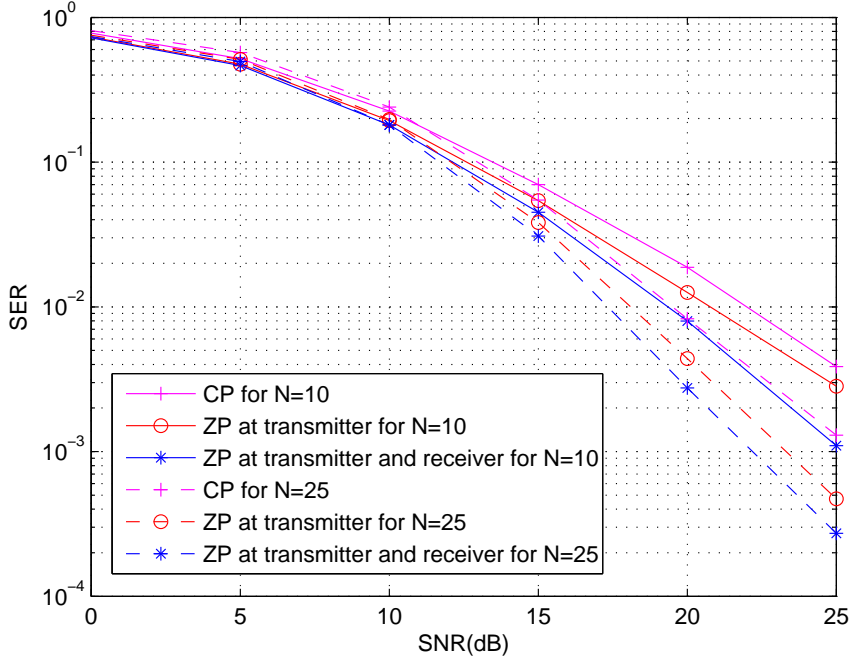


Figure 6.6: MMSE SC-FDE error performance for 16-QAM when the block length to channel memory length ratio is 5

When the block length to channel memory length ratio is decreased to 2 such that the block length is 10 and the number of channel taps are 5, the improvement grows significantly that is given in Figure 6.7. It can be deduced that the enhancement of MMSE SC-FDE due to ZP with FDO grows with incremental constellation sizes for a fixed SER. To illustrate, there is a 2dB SNR gain for QPSK at 10^{-2} SER, whereas it exceeds 5dB for 16-QAM at 10^{-2} SER when the block length to channel memory length ratio is 2. One major drawback of MMSE equalization comes from larger constellation sizes such that the error rate increases excessively with larger constellation sizes [58]. Our proposed MMSE SC-FDE implementation can be a remedy to compensate this negative effect to some extent.

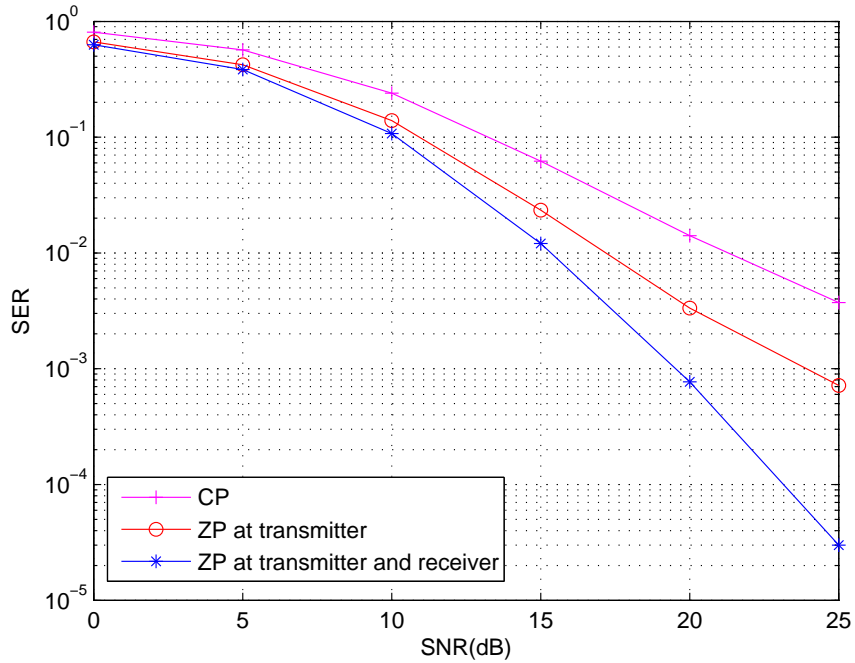


Figure 6.7: MMSE SC-FDE error performance for 16-QAM when the block length to channel memory length ratio is 2

The proposed method is also justified for more practical conditions such that the channel taps are unequally spaced. More clearly, they are uniformly distributed between 0 and a maximum channel delay spread instead of being equally spaced. According to that, the block length is 10, there are 2 complex Gaussian channel taps whose maximum channel delay spread is equal to 2 symbol intervals and the modulation format is QPSK. The performance of MMSE SC-FDE implemented by ZP with FDO under these conditions is given in Figure 6.8. In this case, the proposed implementation of MMSE SC-FDE does not bring any major improvement.

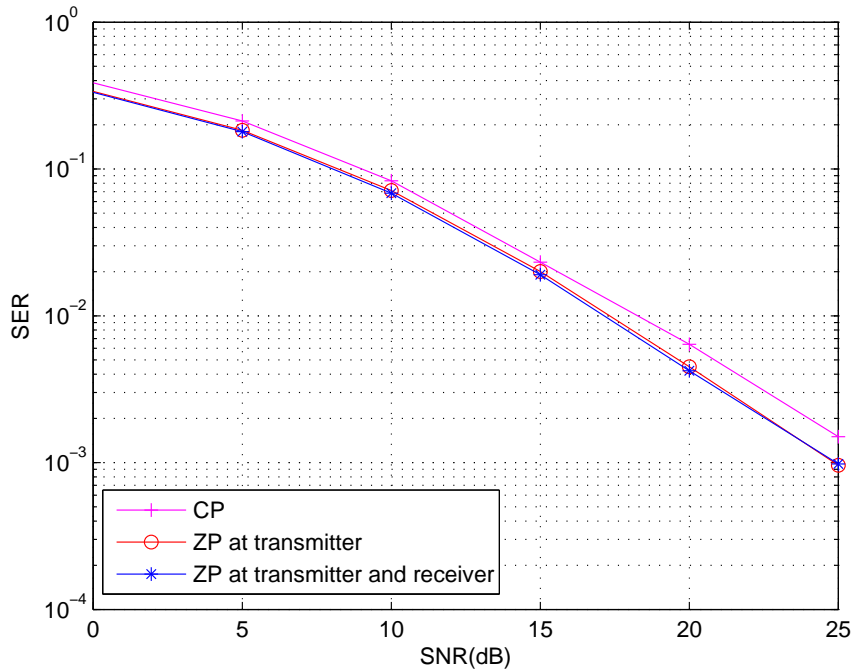


Figure 6.8: MMSE SC-FDE error performance for QPSK when the block length to channel memory length ratio is 5 and there are unequally spaced channel taps

Moreover, the error performance of MMSE SC-FDE implemented by ZP with FDO is generalized to 5 complex Gaussian channel taps which are uniformly distributed in between 0 and 5 symbol intervals in Figure 6.9 for a block length of 10 and QPSK modulation. Hereby, ZP with FDO significantly enhances the performance of MMSE SC-FDE. These results are in parallel with the previous case of equally spaced channel taps.

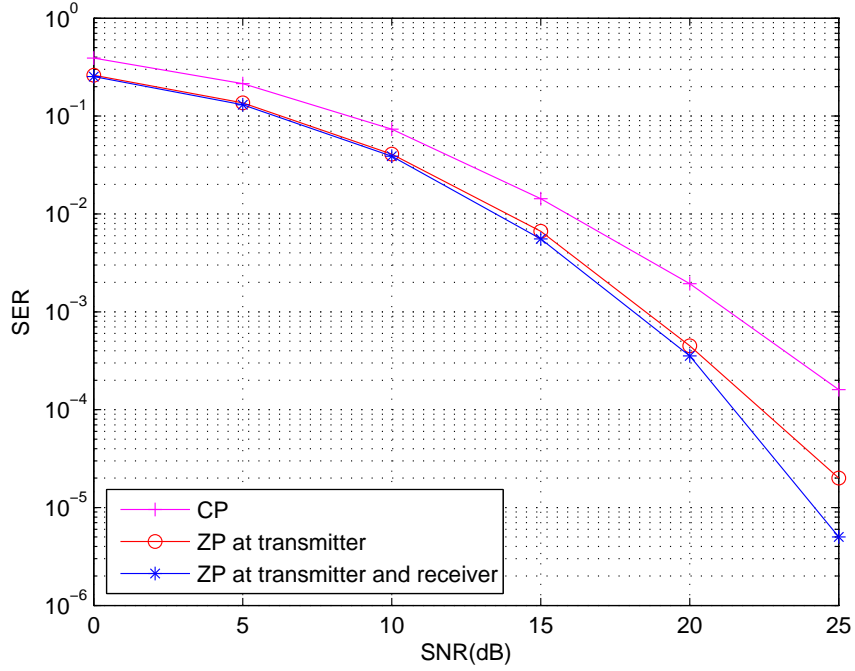


Figure 6.9: MMSE SC-FDE error performance for QPSK when the block length to channel memory length ratio is 2 and there are unequally spaced channel taps

6.5 Conclusions

MMSE SC-FDE implementation by padding zeros at the transmitter and FDO at the receiver is clarified regarding the error performance. The outage probability analysis illustrates that the proposed model is advantageous with respect to the conventional SC-FDE model with CP. The numerical results also show that when the ratio of transmission block length to channel memory is small such as in underwater acoustic channels, the benefit of the proposed model becomes more significant. The advantage of the proposed model over conventional CP based SC-FDE increases for higher constellation sizes as well. Since the proposed model does not disturb the circulant channel matrix structure despite ZP, it has still low complexity equalization operation similar to conventional SC-FDE. Therefore, we suggest to utilize the proposed model in the implementation of MMSE SC-FDE for current communication systems.

CHAPTER 7

CONCLUSIONS AND FUTURE WORKS

Many theoretical findings do not take into account the practical considerations. Therefore, practical applications for the corresponding theoretical results become too complex or even unrealizable, and practical developments do not go parallel with theoretical improvements. The majority of studies in the literature has been mainly focused on theoretical outcomes disregarding practical concerns. This yields a gap between theoretical and practical findings. The ultimate contribution of this thesis is to reduce this gap in the field of interference suppression capability of MMSE detection.

It is crucial to reduce interference while making detection. We aim to mitigate interference with practically implementable solutions, since complexity is the primary impediment in practical applications, and leads to more challenging designs in addition to high power consumption and excessive computation. Throughout the thesis, we avoid high complexity operations so that

- pulse matched filtering is employed instead of channel matched filtering and
- linear MMSE detection is used instead of optimum ML detectors or non-linear detectors.

The proposed FTSR sampling and FDO methods are evaluated in accordance with these choices in which the former method is based on the idea of exploiting the available excess bandwidth in the communication system to obtain more efficient interference suppression schemes. There are not many researches that fully exploit the benefit of excess bandwidth though bandwidth is a valuable commodity and its importance grows day by day due to increasing user demands. The latter method aims

to better utilize the information in the channel.

The contributions of this thesis can be summarized into 4 main parts:

1. The contributions of FTSR sampling in ZP based MMSE equalization for single user communication are given as follows:
 - (a) FTSR sampling yields no advantage for infinite length MMSE equalizers in case of $\text{sinc}(t/T)$ pulse shaping.
 - (b) FTSR sampling produces advantage in case of excess bandwidth even if there is no sampling time errors at the receiver.
 - (c) FTSR sampling compensates the loss due to removal of guard interval.
 - (d) FTSR sampled MMSE equalization is quantified depending on channel characteristics, block length and excess bandwidth.
2. The contributions of FTSR sampling in CP based MMSE equalization for single user communication are given as follows:
 - (a) The closed form expression of MSE is derived in terms of the eigenvalues of the channel and the noise auto-correlation matrix.
 - (b) The average MSE loss due to SR sampling for unequally spaced channel taps is semi-analytically determined related with the derived MSE expression.
 - (c) How excess bandwidth is used more efficiently for the sake of CP based MMSE equalization is studied.
 - (d) A CP based MMSE equalizer implementation is proposed to avoid the complexity increase due to FTSR sampling.
 - (e) More robust CP based MMSE equalization is attained to the shortcoming of CP by using FTSR sampling.
 - (f) The performance of MMSE equalization with CP under 1-bit quantization and FTSR sampling is observed.
3. The contributions of FTSR sampling in multiuser communication are given as follows:

- (a) It is shown that FTSR sampling can exploit the additional DoF due to excess bandwidth gain in multiuser communication, whereas SR sampling cannot.
 - (b) Rank enhancement is presented in multiuser communication due to FTSR sampling in proportion to excess bandwidth when ISI channel taps are unequally spaced.
 - (c) FTSR sampling in multiuser communication is further evaluated by using the findings of MIMO literature.
 - (d) Applications of FTSR sampling are investigated for
 - i. MMSE multiuser detectors
 - ii. Canonical iterative receivers
4. The contributions of FDO technique for the implementation of MMSE SC-FDE are given as follows:
- (a) An MMSE SC-FDE implementation based on FDO is proposed as a low complexity approximation of ZP transmission.
 - (b) A lower bound is found for the outage probability comparison between the proposed and conventional MMSE SC-FDE implementation.
 - (c) A direct outage probability analysis is performed that shows the superiority of the proposed method.
 - (d) The effect of FDO on the MMSE SC-FDE performance is quantified in regard to transmission block length to channel memory length ratio and modulation order.

Some future works are as follows:

1. Generalization of FTSR sampling for non-linear equalizers
2. Communication theoretical analysis of 1 bit quantization including
 - (a) Time synchronization
 - (b) Frequency synchronization
 - (c) Channel estimation

- (d) More efficient equalization
 - (e) Decoding
3. Generalization of FTSR sampling for non-linear multiuser detectors
 4. Derivation of alternative FTSR sampled multiuser receivers for both iterative and non-iterative systems
 5. Application of FTSR sampling to CDMA networks

REFERENCES

- [1] J. G. Proakis, *Digital Communications 4th ed*, New York: McGrawHill, 2001.
- [2] G. D. Forney, "Maximum-likelihood sequence estimation of digital sequences in the presence of intersymbol interference," *IEEE Trans. Inf. Theory*, vol. 18, no. 3, pp. 363-378, May 1972.
- [3] S. U. H. Qureshi and G. D. Jr. Forney, "Performance and properties of a T/2 equalizer," *Natl. Telecom. Conf. Record*, pp. 11.1.1-11.1.14, Los Angeles, CA, Dec. 1977.
- [4] R. D. Gitlin and S. B. Weinstein, "Fractionally-spaced equalization: An improved digital transversal filter," *Bell Syst. Tech. J.*, vol. 60, pp. 275-296, 1981.
- [5] J. R. Barry, E. A. Lee and D. G. Messerschmitt, *Digital Communication*, Springer, 2003.
- [6] G. Ungerboeck, "Fractional tap-spacing equalizer and consequences for clock recovery in data modems," *IEEE Trans. Commun.*, vol. com-24, no. 8, Aug. 1976.
- [7] J. R. Treichler, I. Fijalkow and C. R. Johnson, "Fractionally spaced equalizers," *IEEE Signal Process. Mag.*, vol. 13, no. 3, pp. 65-81, May 1996.
- [8] H. Meyr, M. Oerder and A. Polydoros, "On sampling rate, analog prefiltering, and sufficient statistics for digital receivers," *IEEE Trans. Commun.*, vol. 42, no. 12, pp. 3208-3214, Dec. 1994.
- [9] F. Pancaldi and G. M. Vitetta, "Block channel equalization in the frequency domain," *IEEE Trans. Commun.*, vol. 53, no. 3, pp. 463-471, Mar. 2005.
- [10] C. B. Papadias and D. T. M. Slock, "Fractionally spaced equalization of linear polyphase channels and related blind techniques based on multichannel linear prediction," *IEEE Trans. Signal Process.*, vol. 47, pp. 641-654, 1999.
- [11] P. P. Vaidyanathan and B. Vrcelj, "Theory of fractionally spaced cyclic-prefix equalizers," *Proc. ICASSP*, vol. 2, pp. 1277-1280, 2002.
- [12] M. Huemer, L. Reindl, A. Springer and R. Weigel, "Frequency domain equalization of linear polyphase channels," *Proc. Vehic. Tech. Conf. (VTC)*, vol. 3, pp. 1698-1700, 2000.

- [13] M. V. Clark, "Adaptive frequency-domain equalization and diversity combining for broadband wireless communications," *IEEE JSAC*, vol. 16, no. 8, pp. 1385-95, Oct. 1998.
- [14] D. Falconer and S. L. Ariyavisitakul, "Broadband wireless using single carrier and frequency domain equalization," in *Proc. IEEE 5th Int. Symp. Wireless Personal Multimedia Communication*, vol. 1, pp. 27-36, Oct. 2002.
- [15] T. Obara, H. Tomeba, K. Takeda and F. Adachi, "Oversampling frequency-domain equalization for single-carrier transmission in the presence of timing offset," *IEEE VTS Asia Pacific Wireless Communications Symposium*, 2009.
- [16] M. Luzio, R. Dinis and P. Montezuma, "Pragmatic frequency domain equalization for single carrier with offset modulations," *IEEE Trans. Wireless Commun.*, vol. 12, no. 9, pp. 4496-4505, 2013.
- [17] G. Vachula and F. Hill Jr., "On optimal detection of band-limited PAM signals with excess bandwidth," *IEEE Trans. Commun.*, vol. COM-29, pp. 886-890, 1981.
- [18] C. Tepedelenlioglu and R. Challagulla, "Low-complexity multipath diversity through fractional sampling in OFDM," *IEEE Trans. Signal Process.*, vol. 52, pp. 3104-3116, Nov. 2004.
- [19] T. F. Wong, T. M. Lok, J. S. Lehnert and M. D. Zoltowski, "A linear receiver for direct-sequence spread-spectrum multiple-access systems with antenna arrays and blind adaptation," *IEEE Trans. Inf. Theory*, vol. 44, no. 2, pp. 659-676, Mar. 1998.
- [20] U. Madhow and M. Honig, "MMSE interference suppression for direct-sequence spread spectrum CDMA," *IEEE Trans. Commun.*, vol. 42, pp. 3178-3188, 1994.
- [21] S. Buzzi, M. Lops and A. M. Tulino, "Time-varying narrow-band interference rejection in asynchronous multiuser DS/CDMA systems over frequency-selective fading channels," *IEEE Trans. Commun.*, vol. 47, no. 10, pp. 1523-1536, October 1999.
- [22] S. Buzzi, M. Lops and H. V. Poor, "Code-aided interference suppression for DS/CDMA overlay systems," *Proc. IEEE*, vol. 90, no. 3, pp. 394-435, 2002.
- [23] M. Lops and A. M. Tulino, "Simultaneous suppression of multiaccess and narrow-band interference in asynchronous CDMA networks," *IEEE Trans. Vehicular Technology*, vol. 49, no. 5, Sept. 2000.
- [24] G. B. Giannakis, Z. Wang, A. Scaglione and S. Barbarossa, "AMOUR-generalized multi-carrier transceivers for blind CDMA regardless of multipath," *IEEE Trans. Commun.*, vol. 48, no. 12, pp. 2064-2076, Dec. 2000.

- [25] B. Vrcelj and P. P. Vaidyanathan, "Equalization with oversampling in multiuser CDMA systems," *IEEE Trans. Signal Process.*, vol. 53, no. 5, pp. 1837-1851, 2005.
- [26] M. Luise, M. Marselli and R. Reggiannini, "Low-complexity blind carrier frequency recovery for OFDM signals over frequency-selective radio channels," *IEEE Trans. Commun.*, vol. 50, no. 7, pp. 1182-1188, Jul. 2002.
- [27] Q. Shi, L. Liu, Y. L. Guan and Y. Gong, "Fractionally spaced frequency-domain MMSE receiver for OFDM systems," *IEEE Trans. Veh. Technol.*, vol. 59, no. 9, pp. 4400-4407, Nov. 2010.
- [28] Z. Wang, S. Zhou, G. B. Giannakis, C. R. Berger and J. Huang, "Frequency-domain oversampling for zero-padded OFDM in underwater acoustic communications," *IEEE Journal of Oceanic Engineering*, vol. 37, no. 1, Jan. 2012.
- [29] B. Hombs and J. Lehnert, "Multiple-access interference suppression for MC-CDMA by frequency-domain oversampling," *IEEE Trans. Commun.*, vol. 53, no. 4, pp. 677-686, Apr. 2005.
- [30] X. Zhang, E. Chen and X. Mu, "Single-carrier frequency-domain equalization based on frequency-domain oversampling," *IEEE Commun. Lett.*, vol. 16, no. 1, pp. 24-26, Jan. 2012.
- [31] E. Balevi and A. O. Yilmaz, "Analysis of frequency domain oversampled MMSE SC-FDE," *IEEE Commun. Lett.*, vol. 20, no. 2, pp. 232-235, Feb. 2016.
- [32] G. Ungerboeck, "Adaptive maximum-likelihood receiver for carrier modulated data-transmission systems," *IEEE Trans. Commun.*, vol. 22, no. 5, pp. 624-636, May 1974.
- [33] S. Verdú, *Multiuser Detection*, Cambridge, U.K.: Cambridge Univ. Press, 1998.
- [34] M. Honig, U. Madhow and S. Verdú, "Blind multiuser detection," *IEEE Trans. Inf. Theory*, vol. 41, pp. 944-960, 1995.
- [35] A. Goldsmith, *Wireless Communications*, Cambridge, U.K.: Cambridge Univ. Press, 2004.
- [36] M. M. Moldovan and M. S. Gowda, "Strict diagonal dominance and a Gersgorin type theorem in Euclidean Jordan algebras," *Linear Algebra Appl.*, 431, pp. 148-161, 2009.
- [37] M. H. Hayes, *Statistical Digital Signal Processing and Modeling*, John Wiley, 1996.
- [38] Y. Yang, T. Ihalainen, M. Rinne and M. Renfors, "Frequency-domain equalization in single-carrier transmission: Filter bank approach," *EURASIP J. Advances in Signal Processing*, vol. 2007, Article ID 10438, 16 pages, 2007.

- [39] P. A. Bello, "Characterization of randomly time-invariant linear channels," *IEEE Trans. Commun.*, vol. CS-11, pp. 360-393, Dec. 1963.
- [40] H. Sari, G. Karam and I. Jeanclaude, "Transmission techniques for digital terrestrial TV broadcasting," *IEEE Commun. Mag.*, vol. 33, no. 2, pp. 100-109, Feb. 1995.
- [41] D. Falconer, S. L. Ariyavisitakul, A. Benyamin-Seeyar and B. Eidson, "Frequency domain equalization for single-carrier broadband wireless systems," *IEEE Commun. Mag.*, vol. 40, no. 4, pp. 58-66, Apr. 2002.
- [42] Z. Wang, X. Ma and G. B. Giannakis, "OFDM or single-carrier block transmissions?," *IEEE Trans. Commun.*, vol. 52, no. 3, pp. 380-394, 2004.
- [43] E. Viterbo and K. Fazel, "How to combat long echoes in OFDM transmission schemes: Sub-channel equalization or more powerful channel coding," *Proc. GLOBECOM*, pp. 2069-2074, 1995.
- [44] E. Masry, "The reconstruction of analog signals from the sign of their noisy samples," *IEEE Trans. Inf. Theory*, vol. 27, pp. 735-745, Nov. 1981.
- [45] Z. Cvetkovic and I. Daubechies, "Single-bit oversampled A/D conversion with exponential accuracy in the bit-rate," in *Proc. Data Compression Conf. (DCC)*, Utah, USA, 2000.
- [46] O. Dabeer, J. Singh and U. Madhow, "On the limits of communication performance with one-bit analog-to-digital conversion," *Proc. IEEE Workshop on Signal Processing Advances in Wireless Comm.*, July 2006.
- [47] J. Singh, P. Sandeep and U. Madhow, "Multi-gigabit communication: the ADC bottleneck," *Proc. 2009 IEEE International Conf. Ultra-Wideband (ICUWB)*, 2009.
- [48] J. Singh, O. Dabeer and U. Madhow, "On the limits of communication with low-precision analog-to-digital conversion at the receiver," *IEEE Trans. Commun.*, vol. 57, no. 12, pp. 3629-3639, Dec. 2009.
- [49] T. Koch and A. Lapidoth, "One-bit quantizers for fading channels," *Proc. IZS*, pp. 36-39, 2012.
- [50] E. N. Gilbert, "Increased information rate by oversampling," *IEEE Trans. Inf. Theory*, vol. 39, no. 6, pp. 1973-1976, Nov. 1993.
- [51] S. Shamai (Shitz), "Information rates by oversampling the sign of a bandlimited process," *IEEE Trans. Inf. Theory*, vol. 40, no. 4, pp. 1230-1236, Jul. 1994.
- [52] S. Krone and G. Fettweis, "Achievable rate with 1-bit quantization and oversampling at the receiver," *IEEE Communication Theory Workshop (CTW-10)*, 2010.

- [53] T. Koch and A. Lapidoth, "Increased capacity per unit-cost by oversampling," *IEEE Convention of Electrical and Electronics Engineers in Israel (IEEEI10)*, 2010.
- [54] S. Krone and G. Fettweis, "Capacity of communications channels with 1-bit quantization and oversampling at the receivers," *Proc. of the IEEE Sarnoff Symposium (Sarnoff-12)*, 2012.
- [55] S. Krone and G. Fettweis, "Communications with 1-bit quantization and oversampling at the receiver: Benefiting from inter-symbol-interference," in *Proc. of the IEEE Int. Symposium on Personal, Indoor and Mobile Radio Communications (PIMRC'12)*, Sept. 2012.
- [56] A. Paulraj, R. Nabar and D. Gore, *Introduction to Space-Time Wireless Communications*, Cambridge, U.K.: Cambridge Univ. Press, 2003.
- [57] A. Hedayat, A. Nosratinia and N. Al-Dhahir, "Outage probability and diversity order of linear equalizers in frequency-selective fading channels," in *Proc. 38th Asilomar Conf. on Signals, Systems and Computers*, vol. 2, pp. 2032-2036, Nov. 2004.
- [58] A. Tajer and A. Nosratinia, "Diversity order in ISI channels with single carrier frequency-domain equalizer," *IEEE Trans. Wireless Commun.*, vol. 9, no. 3, pp. 1022-1032, March 2010.
- [59] T. De Mazancourt and D. Gerlic, "The inverse of a block-circulant matrix," *IEEE Trans. Antennas Propagat.*, vol. AP-31, pp. 808-810, Sept. 1983.
- [60] A. P. Liavas and D. Tsipouridou, "On the performance of the mismatched MMSE and the LS linear equalizers," *IEEE Trans. Signal Process.*, vol. 55, no. 7, pp. 3302-3311, 2007.
- [61] D. Kim and G. Stüber, "Residual ISI cancellation for OFDM with applications to HDTV broadcasting," *IEEE J. Sel. Areas Commun.*, vol. 16, no. 8, pp. 1590-1599, Oct. 1998.
- [62] C. Park and G. Im, "Efficient DMT/OFDM transmission with insufficient cyclic prefix," *IEEE Commun. Lett.*, vol. 8, no. 9, pp. 576-578, Sept. 2004.
- [63] T. Hwang and Y. Li, "Iterative cyclic prefix reconstruction for coded single-carrier systems with frequency-domain equalization (SC-FDE)," in *Proc. IEEE Veh. Technol. Conf.*, vol. 3, pp. 1841-1845, Apr. 2003.
- [64] A. Gusmao, P. Torres, R. Dinis and N. Esteves, "A class of iterative FDE techniques for reduced-CP SC-based block transmission," in *Proc. IEEE 4th Int. Symp. Turbo Codes, Related Topics*, Paper 71, Session 13, Apr. 2006.

- [65] A. Gusmao, P. Torres, R. Dinis and N. Esteves, "A reduced-CP approach to SC/FDE block transmission for broadband wireless communications," *IEEE Trans. Commun.*, vol. 55, no. 4, pp. 801-809, 2007.
- [66] H. Lee, Y. Lee and H. Park, "An efficient CP compensation for SC-FDE with insufficient CP symbols," *IEEE Commun. Lett.*, vol. 14, no. 6, pp. 548-550, 2010.
- [67] T. M. Cover and J. A. Thomas, *Elements of Information Theory*, Wiley-Interscience, 2006.
- [68] NTT DOCOMO, "Requirements, candidate solutions & technology roadmap for lte rel-12 onward," in *3GPP Workshop on Release 12 and onwards, RWS-120010*, Ljubljana, Slovenia, June 2012.
- [69] F. Rusek and J. Anderson, "On information rates for faster-than-nyquist signaling," in *Proc. IEEE Global Telecommunications Conf.*, San Francisco, CA, Nov. 2006.
- [70] F. Rusek and J. B. Anderson, "Constrained capacities for faster-than-nyquist signaling," *IEEE Trans. Inf. Theory*, vol. 55, no. 2, Feb. 2009.
- [71] M. El Hefnawy and H. Taoka, "Overview of faster-than-nyquist for future mobile communication systems," in *VTC*, June 2013.
- [72] J. Anderson, F. Rusek and V. Owall, "Faster-than-nyquist signaling," *Proc. IEEE*, vol. 101, no. 8, pp. 1817-1830, 2013.
- [73] A. Barbieri, D. Fertoni and G. Colavolpe, "Time-frequency packing for linear modulations: spectral efficiency and practical detection schemes," *IEEE Trans. Commun.*, vol. 57, no. 10, pp. 2951-2959, Oct. 2009.
- [74] G. J. Foschini, "Layered space-time architecture for wireless communication in fading environments when using multi-element antennas," *Bell Labs Tech. J.*, pp. 41-59, 1996.
- [75] E. Telatar, "Capacity of multi-antenna Gaussian channels," *Eur. Trans. Telecomm. ETT*, vol. 10, no. 6, pp. 585-596, Nov. 1999.
- [76] S. Shamai, L. H. Ozarow and A. D. Wyner, "Information rates for a discrete-time gaussian channel with intersymbol interference and stationary inputs," *IEEE Trans. Inf. Theory*, vol. 37, pp. 1527-1539, Nov. 1991.
- [77] L. Zheng and D. N. C. Tse, "Diversity and multiplexing: A fundamental tradeoff in multiple-antenna channels," *IEEE Trans. Inf. Theory*, vol. 49, pp. 1073-1096, 2003.
- [78] Y. Wu, S. Shamai and S. Verdú, "Degrees of freedom of interference channel: A general formula," *Proc. IEEE ISIT*, pp. 1362-1366, 2011.

- [79] K. Barman and O. Dabeer, "Capacity of MIMO systems with asynchronous PAM," *IEEE Trans. Commun.*, vol. 57, no. 11, Nov. 2009.
- [80] L. Reichel and L. N. Trefethen, "The eigenvalues and pseudo-eigenvalues of toeplitz matrices," *Linear Algebra Appl.*, 162, pp. 153-185, 1992.
- [81] D. N. C. Tse and P. Viswanath, *Fundamentals of Wireless Communications*, Cambridge University Press, 2005.
- [82] J. E. Mazo, "Faster-than-nyquist signaling," *Bell Syst. Tech. J.*, vol. 54, pp. 1451-1462, Oct. 1975.
- [83] A. D. Liveris and C. N. Georghiades, "Exploiting faster-than-nyquist signaling," *IEEE Trans. Commun.*, vol. 51, no. 9, pp. 1502-1511, Sept. 2003.
- [84] H. V. Poor and S. Verdú, "Probability of error in MMSE multiuser detection," *IEEE Trans. Inf. Theory*, vol. 43, no. 3, May 1997.
- [85] R. Lupas and S. Verdú, "Linear multi-user detectors for synchronous code-division multiple-access channels," *IEEE Trans. Inf. Theory*, vol. 35, pp. 123-136, Jan. 1989.
- [86] H. V. Poor and X. Wang, "Code-aided interference suppression for DS/CDMA communications: Interference suppression capability," *IEEE Communications Magazine*, vol. 45, no. 9, pp. 1101-1111, 1997.
- [87] M. L. Honig, P. Crespo and K. Steiglitz, "Suppression of near- and far-end crosstalk by linear pre- and post-filtering," *IEEE JSAC*, vol. 10, pp. 614-629, Apr. 1992.
- [88] M. V. Clark, L. J. Greenstein, W. K. Kennedy and M. Shafi, "MMSE diversity combining for wide-band digital cellular radio," *IEEE Trans. Commun.*, vol. 40, no. 6, June 1992.
- [89] D. Shiu, G. J. Foschini, M. J. Gans and J. M. Kahn, "Fading correlation and its effect on the capacity of multielement antenna systems," *IEEE Trans. Commun.*, vol. 48, pp. 502-513, Mar. 2000.
- [90] X. Wang and H. V. Poor, "Iterative (Turbo) soft interference cancellation and decoding for coded CDMA," *IEEE Trans. Commun.*, vol. 47, no. 7, July 1999.
- [91] D. Reynolds and X. Wang, "Low-complexity turbo-equalization for diversity channels," *Signal Process.*, vol. 81, no. 5, pp. 989-995, May 2001.
- [92] X. Wautelet, A. Dejonghe and L. Vandendorpe, "MMSE-based fractional turbo receiver for space-time BICM over frequency-selective MIMO fading channels," *IEEE Trans. Signal Process.*, vol. 52, no. 6, pp. 1804-1809, June 2004.

- [93] J. Hagenauer, "The turbo principle: Tutorial introduction and state of the art," *Proc. 1st Int. Symp. Turbo Codes*, pp. 1-12, Sept. 1997.
- [94] L. R. Bahl, J. Cocke, F. Jelinek and J. Raviv, "Optimal decoding of linear codes for minimizing symbol error rate," *IEEE Trans. Inf. Theory*, vol. IT-20, pp. 284-287, Mar. 1974.
- [95] M. Tüchler, R. Koetter and A. C. Singer, "Turbo equalization: Principles and new results," *IEEE Trans. Commun.*, vol. 50, no. 5, May 2002.
- [96] B. Muquet, Z. Wang, G. B. Giannakis, M. de Courville and P. Duhamel, "Cyclic prefixing or zero padding for wireless multicarrier transmissions?," *IEEE Trans. Commun.*, vol. 50, no. 12, pp. 2136-2148, Dec. 2002.
- [97] Z. Wang and G. B. Giannakis, "Wireless multicarrier communications where Fourier meets Shannon," *IEEE Signal Process. Mag.*, vol. 17, no. 3, May 2000.
- [98] L. H. Grokop and D. N. C. Tse, "Diversity multiplexing tradeoff in ISI channels," *IEEE Trans. Inf. Theory*, vol. 55, no. 1, pp. 109-135, Jan. 2009.
- [99] S. H. Song and K. B. Letaief, "Diversity analysis for linear equalizers over ISI channels," *IEEE Trans. Commun.*, vol. 59, no. 9, Sept. 2011.
- [100] A. Hedayat and A. Nosratinia, "Outage and diversity of linear receivers in flat-fading MIMO channels," *IEEE Trans. Signal Process.*, vol. 55, no. 12, pp. 5868-5873, Dec. 2007.
- [101] B. Peng, P. Salvo Rossi, H. Dong and K. Kansanen, "Time-domain oversampled OFDM communication in doubly-selective underwater acoustic channels," *IEEE Commun. Lett.*, vol. 19, no. 6, pp. 1081-1084, June 2015.
- [102] D. Guo, S. Shamai and S. Verdú, "Mutual information and minimum mean-square error in Gaussian channels," *IEEE Trans. Inf. Theory*, vol. 51, no. 4, pp. 1261-1282, Apr. 2005.
- [103] D. Guo, Y. Wu, S. Shamai (Shitz) and S. Verdú, "Estimation in Gaussian noise: Properties of the minimum mean-square error," *IEEE Trans. Inf. Theory*, vol. 51, no. 4, Apr. 2011.
- [104] R. Horn and C. Johnson, *Matrix Analysis*, Cambridge University Press, Cambridge, 1985.

APPENDIX A

POTENTIAL OF EXCESS BANDWIDTH IN SINGLE USER COMMUNICATION

The capacity of a communication system over a bandlimited channel is expressed in terms of the average power P , N_0 and bandwidth W as

$$C = W \log_2 \left(1 + \frac{P}{N_0 W} \right) \text{ bits/sec} \quad (\text{A.1})$$

and more generally as

$$C = \int_0^{\frac{1}{2T}} \log_2 \left(1 + \frac{P |P_c(f)|^2}{N_0} \right) df \text{ bits/sec} \quad (\text{A.2})$$

where $P_c(f)$ is the Fourier transform of $p_c(t)$. When excess bandwidth is employed,

$$C_{exc} = \int_0^{\frac{1+r}{2T}} \log_2 \left(1 + \frac{P |P_c(f)|^2}{N_0} \right) df \text{ bits/sec}. \quad (\text{A.3})$$

For large $\frac{P}{N_0}$,

$$C_{exc} \approx \frac{1+r}{T} \log \left(\frac{P}{N_0} \right) \quad (\text{A.4})$$

and

$$C \approx \frac{1}{T} \log \left(\frac{P}{N_0} \right). \quad (\text{A.5})$$

Then,

$$\lim_{\frac{P}{N_0} \rightarrow \infty} \frac{C_{exc}}{C} = 1 + r. \quad (\text{A.6})$$

As shown in Eqn. (A.6), there is a potential capacity gain due to excess bandwidth.

APPENDIX B

MMSE FILTERING COMPARISON FOR TIME AND FREQUENCY DOMAIN

The MMSE filter in time domain corresponding to the model in Eqn. (4.6) is stated in Eqn. (4.10) and the filtered signal becomes

$$\mathbf{W}_{mmse} \mathbf{y}_{ftsr} = \mathbf{H}_{ftsr}^H (\mathbf{H}_{ftsr} \mathbf{H}_{ftsr}^H + \mathbf{R}_z)^{-1} \mathbf{y}_{ftsr}. \quad (\text{B.1})$$

When MMSE filter is applied in frequency domain, the MMSE filter is equal to

$$\mathbf{W}_{mmse}^f = \mathbf{H}_{ftsr}^H \mathbf{Q}^H (\mathbf{Q} \mathbf{H}_{ftsr} \mathbf{H}_{ftsr}^H \mathbf{Q}^H + \mathbf{Q} \mathbf{R}_z \mathbf{Q}^H)^{-1} \quad (\text{B.2})$$

where \mathbf{Q} is the DFT matrix and

$$\mathbf{W}_{mmse}^f = \mathbf{H}_{ftsr}^H \mathbf{Q}^H (\mathbf{Q} (\mathbf{H}_{ftsr} \mathbf{H}_{ftsr}^H + \mathbf{R}_z) \mathbf{Q}^H)^{-1} \quad (\text{B.3})$$

that is equivalent to

$$\mathbf{W}_{mmse}^f = \mathbf{H}_{ftsr}^H (\mathbf{H}_{ftsr} \mathbf{H}_{ftsr}^H + \mathbf{R}_z)^{-1} \mathbf{Q}^H. \quad (\text{B.4})$$

MMSE filtering the received signal in frequency domain gives

$$\mathbf{W}_{mmse}^f \mathbf{Q} \mathbf{y}_{ftsr} = \mathbf{H}_{ftsr}^H (\mathbf{H}_{ftsr} \mathbf{H}_{ftsr}^H + \mathbf{R}_z)^{-1} \mathbf{y}_{ftsr}. \quad (\text{B.5})$$

Eqn. (B.1) and Eqn. (B.5) show that the MMSE filtering in frequency domain produces the same vector with time domain MMSE filtering.

APPENDIX C

CIRCULANT MATRIX INTERPRETATION OF \mathbf{H}_{ZP}

\mathbf{H}_{zp} can be partitioned into

$$\mathbf{H}_{zp} = \begin{pmatrix} \mathbf{H}_{11} & \mathbf{H}_{12} \\ \mathbf{H}_{21} & \mathbf{H}_{22} \end{pmatrix} \quad (\text{C.1})$$

where \mathbf{H}_{11} is a Toeplitz matrix with dimension $(N + L) \times N$, and \mathbf{H}_{12} , \mathbf{H}_{21} , \mathbf{H}_{22} are $(N + L) \times (M - N)$, $(M - N - L) \times N$, $(M - N - L) \times (M - N)$ zero matrices respectively. Since the last $(M - N)$ entries of \mathbf{x}_{zp} are zero, we can write any value to \mathbf{H}_{12} and \mathbf{H}_{22} without any change in \mathbf{y}_{zp} though it is not possible to modify \mathbf{H}_{21} . Hence, one can implement \mathbf{H}_{zp} as a circulant matrix.

APPENDIX D

AN ILLUSTRATIVE MATRIX EXAMPLE FOR OUTAGE PROBABILITY ANALYSIS

Consider an illustrative example for \mathbf{H}_{zp} matrix whose dimension is $M \times M$ such that $M = 6$ and $L = 1$. Then, \mathbf{H}_{zp} becomes

$$\mathbf{H}_{zp} = \begin{pmatrix} h_0 & h_1 & 0 & 0 & 0 & 0 \\ 0 & h_0 & h_1 & 0 & 0 & 0 \\ 0 & 0 & h_0 & h_1 & 0 & 0 \\ 0 & 0 & 0 & h_0 & h_1 & 0 \\ 0 & 0 & 0 & 0 & h_0 & h_1 \\ h_1 & 0 & 0 & 0 & 0 & h_0 \end{pmatrix} \quad (\text{D.1})$$

which can be written as

$$\mathbf{H}_{zp} = \begin{pmatrix} \mathbf{A} & \mathbf{B} \\ \mathbf{B} & \mathbf{A} \end{pmatrix} \quad (\text{D.2})$$

where

$$\mathbf{A} = \begin{pmatrix} h_0 & h_1 & 0 \\ 0 & h_0 & h_1 \\ 0 & 0 & h_0 \end{pmatrix} \quad (\text{D.3})$$

and

$$\mathbf{B} = \begin{pmatrix} 0 & 0 & 0 \\ 0 & 0 & 0 \\ h_1 & 0 & 0 \end{pmatrix}. \quad (\text{D.4})$$

Moreover, this implies that \mathbf{H}_{cp} matrix with dimension $N \times N$ in which $N = 3$ is equal to

$$\mathbf{H}_{cp} = \mathbf{A} + \mathbf{B} \quad (\text{D.5})$$

due to the fact that

$$\mathbf{H}_{cp} = \begin{pmatrix} h_0 & h_1 & 0 \\ 0 & h_0 & h_1 \\ h_1 & 0 & h_0 \end{pmatrix}. \quad (\text{D.6})$$

CURRICULUM VITAE

PERSONAL INFORMATION

Surname, Name: Balevi, Eren

Nationality: Turkish (TC)

Date and Place of Birth: 04.09.1984, Konya

Marital Status: Single

Phone: 0 536 7917079

EDUCATION

Degree	Institution	Year of Graduation
M.S.	Middle East Technical University	2010
B.S.	Middle East Technical University	2008
High School	Meram Anatolian High School	2002

PROFESSIONAL EXPERIENCE

Year	Place	Enrollment
2008-2013	ASELSAN/HBT	System Engineer
2013-	ASELSAN/MGEO	Software Engineer

PUBLICATIONS

E. Balevi and A. O. Yılmaz, "Analysis of frequency domain oversampled MMSE SC-FDE," IEEE Communications Letters, vol. 20, pp. 232-235, February 2016.

E. Balevi and O. B. Akan, "A physical channel model for nanoscale neuro-spike communication," IEEE Transactions on Communications, vol. 61, no. 3, pp. 1178-1187, March 2013.

Submitted Publications

E. Balevi and A. O. Yılmaz, "Interference mitigation in multiuser communication by faster than symbol rate sampling," IEEE Transactions on Wireless Communications, 2016.

E. Balevi and A. O. Yılmaz, "Performance limits of CP based MMSE equalization against practical problems," IEEE Transactions on Communications, 2016.